The American Mineralogist

Journal of the Mineralogical Society of America

Vol. 35 NOVEMBER-DECEMBER, 1950 Nos. 11 and 12

Contents

Published bi-monthly by the Society

The enlarged issues of this journal for 1950 are made possible by a grant from the Penrose Fund of the Geological Society of America.

The American Mineralogist—Journal of the Mineralogical Society of America

A journal containing articles on mineralogy, crystallography, petrography, and allied sciences, issued every two months. Contributions are invited from everyone.

Office of Publication, Mineralogical Laboratory, Ann Arbor, Mich.

The general conduct of the journal is in the hands of the Editor, **Walter F. Hunt**, Ann Arbor, Michigan. The council of the Mineralogical Society has appointed the following board of associate editors, to whom should be sent articles dealing with the special subjects indicated:

Michael Fleischer, U. S. Geological Survey, Washington, D.C., *New minerals.*
Esper S. Larsen, U. S. Geological Survey, Washington, D.C., *Optical crystallography.*
Austin F. Rogers, Stanford University, California, *Geometrical crystallography.*
M. N. Short, University of Arizona, Tucson, Arizona, *Mineralography.*
George Tunell, University of California at Los Angeles, *Structural crystallography.*

Contributors of leading articles are given without charge 100 reprints (without covers) of their article. If additional reprints are desired these can be purchased at the following rates:

Pages	*1–4*	*5–8*	*9–12*	*13–16*	*17–20*	*21–24*	*25–28*	*29–32*	*Covers*
Copies									
25	$3.50	$5.00	$ 8.00	$ 9.50	$11.00	$13.00	$15.00	$16.00	$4.90
50	3.80	5.55	8.80	10.40	12.10	14.20	16.40	17.50	5.50
75	4.10	6.10	9.60	11.30	13.20	15.40	17.80	19.00	6.10
100	4.40	6.65	10.40	12.20	14.30	16.60	19.20	20.50	6.70
Addl. C's	1.20	2.20	3.20	3.60	4.40	4.80	5.60	6.00	2.40

Cover Composition $1.55.

Sent to all members and fellows of the Mineralogical Society of America. Subscription price, $4.00 per year (single copies of normal issues, $1.00 plus postage).

Entered as second class matter at the post office at Menasha, Wis., under Act of March 3, 1879. Acceptance for mailing at the special rate of postage provided for in section 1103, Act of Oct. 3, 1917, paragraph 4 section 429 P. L. & R. authorized March 13, 1922.

Notices of change of address, orders, and remittances should be sent to Dr. Earl Ingerson, U.S. Geological Survey, Washington 25, D. C.

Printed by the George Banta Publishing Company, Menasha, Wisconsin

THE AMERICAN MINERALOGIST

JOURNAL OF THE MINERALOGICAL SOCIETY OF AMERICA

Vol. 35 NOVEMBER-DECEMBER, 1950 Nos. 11 and 12

THE ATOMIC ARRANGEMENT AND CHEMICAL COMPOSITION OF KRENNERITE[1]

GEORGE TUNELL[2] AND K. J. MURATA[3]

ABSTRACT

The crystal structure of krennerite has been analyzed by means of Weissenberg photographs and powder diffraction photographs. The dimensions of the unit cell, all determined röntgenographically, are $a_0=16.54$ Å, $b_0=8.82$ Å, $c_0=4.46$ Å, all ± 0.03 Å. The density determined pycnometrically on five single crystals from Cripple Creek, Colorado, crushed into fragments is 8.63; the x-ray density is 8.86. The unit cell contains 8(Au, Ag) Te_2; the ratio of Au to Ag was found by analyses of crystals from Cripple Creek to be close to 4 to 1. The space-group is C_{2v}^4-Pma. The eighteen parameters defining the atomic positions were determined by calculation of the intensities of the diffraction lines of a powder photograph (which had been rigorously indexed from the single crystal data), and of the diffraction spots of Weissenberg equator photographs of crystals rotating about the c- and b-axes; the positions of the atoms were confirmed by a Fourier projection of the structure on the plane 001 made from a Weissenberg equator photograph taken with the crystal rotating about the c-axis. The gold (or silver) atoms are situated in (a) with $z=0$ (arbitrary), in (c) with $y_1=0.319$, $z_1=0.014$, and in (d) with $x_2=0.124$, $y_2=0.666$, $z_2=0.500$; the tellurium atoms are situated in (c) with $y_3=0.018$, $z_3=0.042$ and $y_4=0.617$, $z_4=0.042$ and in (d) with $x_5=0.003$, $y_5=0.699$, $z_5=0.042$, and $x_6=0.132$, $y_6=0.364$, $z_6=0.500$, and $x_7=0.119$, $y_7=0.964$, $z_7=0.500$. Each gold (or silver) atom is surrounded by six tellurium atoms, and each tellurium atom is surrounded by three gold (or silver) atoms and three tellurium atoms, or by five gold (or silver) atoms and one tellurium atom, or by one gold (or silver) atom and five tellurium atoms.

INTRODUCTION

The atomic arrangement of krennerite has been determined in the present investigation[4] by x-ray analysis of euhedral crystals from Cripple Creek, Colorado. The crystals had a metallic luster and pale yellowish white color; their identity was confirmed by measurement on the two-

[1] A report on research carried out under the auspices of the Geophysical Laboratory of the Carnegie Institution of Washington, the U. S. Geological Survey, and the Office of Naval Research. Published by permission of the Director of the U. S. Geological Survey.

[2] Department of Geology, University of California at Los Angeles.

[3] U. S. Geological Survey, Washington, D. C.

[4] The work of the senior author was carried out mainly at the Geophysical Laboratory of the Carnegie Institution of Washington while he was a member of the staff.

circle reflection goniometer. Euhedral crystals of krennerite have been measured previously with the reflection goniometer by Krenner,[5] vom Rath,[6] Schrauf,[7] Miers,[8] and Smith.[9] They found the symmetry of the crystals to be that of the orthorhombic system. The values of the axial elements calculated by the various authors are given in Table 1. Krenner did not calculate axial elements, but his indices and angles imply the same choice of axes, unit forms, and orientation as that of vom Rath. Schrauf and Smith followed vom Rath's choice of axes and unit forms.

TABLE 1. AXIAL ELEMENTS OF KRENNERITE DETERMINED BY PREVIOUS INVESTIGATORS

	a	*b*	*c*
vom Rath	0.9407	1	0.5045
Schrauf	0.9396	1	0.5073
Miers*	0.9389	1	0.5059
Smith	0.9369	1	0.5068

* Miers' values are here recalculated to conform with the orientation of vom Rath, Schrauf, and Smith.

Miers followed vom Rath's choice of unit forms, but interchanged the *a*- and *b*-axes. The present *x*-ray analysis leads to unit cell dimensions from which the following axial elements have been calculated

$$a:b:c=1.875:1:0.506,$$

and these agree well with the morphological elements if the value of *a* in the morphological elements be multiplied by 2. Thus the following transformation is obtained:

vom Rath to Tunell and Murata 200/010/001.

Rotation and Weissenberg equator and equi-inclination layer-line photographs of krennerite were made with crystals rotating about the *a*- and *c*-axes and rotation and Weissenberg equator photographs with a crystal rotating about the *b*-axis. Copper K-radiation was used. Powder photographs were made with filtered cobalt K-radiation and with filtered and unfiltered copper K-radiation. A crystal[10] from Cripple Creek measured previously on the two-circle reflection goniometer by Professor M. A. Peacock, was rotated about the *c*-axis and a rotation photograph was made. It was then oscillated 180° about the *c*-axis and equator and

[5] Krenner, J. A.: *Ann. d. Phys. u. Chem.*, **1**, 636–640 (1877).
[6] vom Rath, G.: *Z. Kryst. Mineral.*, **1**, 614–617 (1877).
[7] Schrauf, A.: *Z. Kryst. Mineral.*, **2**, 235–239 (1878).
[8] Miers, H. A.: *Mineralog. Mag.*, **9**, 184–186 (1890).
[9] Smith, G. F. H.: *Mineralog. Mag.*, **13**, 264–267 (1903).
[10] Kindly supplied by Professors Palache and Peacock.

equi-inclination layer-line Weissenberg photographs were made. The crystal was developed prismatically and terminated by a cleavage face 001; it was roughly rectangular in cross-section with dimensions 0.36 mm. and 0.60 mm. in the plane 001. A second crystal from Cripple Creek, also measured previously on the two-circle reflection goniometer by Professor Peacock, was rotated about the *c*-axis and an equator Weissenberg photograph was made. This crystal was then remounted and rotated about the *b*-axis and a rotation photograph and an equator Weissenberg photograph were made. It was remounted again and rotated about the *a*-axis and a rotation photograph and Weissenberg equator and equi-inclination layer-line photographs were made. This crystal was bounded by a large basal cleavage at one end of the *c*-axis and predominantly by large faces of the pyramid *u* at the other end of the *c*-axis; the prism *l* was dominant in the vertical zone. The approximate dimensions of the crystal in the *a*-, *b*-, and *c*-directions were 0.90 mm., 0.90 mm., and 0.50 mm. A crystal[11] from the Vindicator Mine, Cripple Creek, Colorado (U. S. National Museum No. 96647), measured on the two-circle reflection goniometer by Tunell was oscillated 180° around the *c*-axis and Weissenberg equator and equi-inclination layer-line photographs were made. This crystal was elongated parallel to the *c*-axis and the diameters of its cross-section were approximately 0.04 mm. and 0.08 mm. Powder photographs were made with unfiltered copper K-radiation of one of the crystals supplied by Professors Palache and Peacock. A powder photograph was made with filtered copper K-radiation of crystals from the Vindicator Mine (U. S. National Museum No. 96647). A powder photograph of euhedral crystals from the Moose Mine, Cripple Creek, Colorado, was made with filtered cobalt K-radiation.

Chemical Composition and Density

No complete chemical analysis or determination of the density of crystallographically studied krennerite free from admixed impurities had been made previously. Five euhedral crystals of krennerite from the Moose Mine were therefore freed from adhering gangue in order to obtain these data. One of these crystals had been measured on the two-circle reflection goniometer; the other four had been observed to have exactly the same habit. A few very minute crystals of pyrite attached to these krennerite crystals could not be completely removed since they were partly embedded in the krennerite crystals; the pyrite left in the sample was believed to be insignificant in amount, however, and this was confirmed by the analysis which shows only 0.05 per cent of iron.

The density of the five crystals (total weight of crystals, 0.9476 g.)

[11] Kindly lent by Dr. W. F. Foshag of the U. S. National Museum.

was measured by means of the pycnometer described by Johnston and Adams.[12] Since krennerite characteristically shows minute voids under the binocular microscope on cleavage surfaces, the crystals were crushed and their density was measured with specially purified toluene as pycnometer fluid, the pycnometer being filled under reduced pressure to promote entrance of the fluid into the voids. All weights were reduced to a vacuum. The value of the density found, corrected for the 0.05 per cent of iron present as pyrite, is 8.63.

The crushed sample was analyzed by the following method. It was dissolved in a minimum amount of aqua regia; the resulting solution

TABLE 2. ANALYSIS OF KRENNERITE FROM MOOSE MINE, CRIPPLE CREEK, COLORADO

	Per Cent	Atomic Ratios
Au	36.19	0.1835 } 0.2286 or 1.000
Ag	4.87	0.0451 }
Te	58.50	0.4584 0.4584 or 2.005
Fe*	.05	
Insoluble	.09	
	99.70	

* The iron was derived from a small amount of pyrite that was present as a contaminant.

was diluted until its acidity was about one normal and allowed to stand overnight. Throughout the analysis a record was kept of the amounts of acids used so that rough adjustments of the acidity could readily be made.

Silver chloride, together with any residue unattacked by aqua regia, was caught and weighed on a sintered glass filtering crucible. Its correct weight was obtained by dissolving it from the crucible with warm dilute ammonium hydroxide and reweighing, and the amount of insoluble residue was obtained by subtracting from this second weight the known weight of the crucible itself.

The filtrate containing gold, tellurium, and other constituents was digested on the steam bath with hydrochloric acid to free it from nitric acid. Gold and tellurium were precipitated together in a hot solution, which was about three-normal with respect to hydrochloric acid, by means of sulphurous acid and hydrazine, as described by Lenher and Homberger.[13] The precipitate was washed as rapidly as possible with a

[12] Johnston, J., and Adams, L. H.: *Jour. Am. Chem. Soc.*, **34,** 566–568 (1912).

[13] Lenher, Victor, and Homberger, A. W.: *Jour. Am. Chem. Soc.*, **30,** 387–391 (1908).

very dilute solution of sulphurous acid until free from chloride. It was treated in a beaker with a minimum amount of cold dilute nitric acid to dissolve tellurium, leaving gold to be filtered off, ignited, and weighed.

The nitric acid solution of tellurium was evaporated to dryness on the steam bath and then digested with dilute hydrochloric acid. The element was reprecipitated as before in three-normal hydrochloric acid solution, caught, and weighed on a sintered glass crucible. The filtrate from this precipitation was reduced in volume and treated further with sulphurous acid to recover any tellurium that passed through the filter. The final filtrate was added to that from the combined precipitate of gold and tellurium, treated with nitric acid, and placed on the steam bath to evaporate. The difficulty arising from the tendency of precipitated tellurium to oxidize and pass through the filter might perhaps be overcome by determining the small amounts found in the filtrate by a colorimetric method like that described by Pierson.[14]

The filtrate from the combined precipitate of gold and tellurium was evaporated to dryness on the steam bath. The small amounts of silver chloride and tellurous acid, which were apparent in the evaporated residue, were determined after separation by means of dilute nitric acid. The filtrate from the final recovery of tellurium was reduced to a small volume, boiled with a few drops of nitric acid, and iron precipitated with ammonium hydroxide, to be subsequently estimated as the thiocyanate. The ammoniacal filtrate from the separation of iron gave no precipitate upon being treated with hydrogen sulphide.

A partial analysis of krennerite crystals from a different specimen from Cripple Creek (U. S. National Museum No. 96647) was also made (weight of sample 0.1678 g.). One crystal from this specimen had been measured on the two-circle reflection goniometer. The crystals analyzed were hand-picked under the binocular microscope and identified by the perfect cleavage perpendicular to the striated zone. The sample was believed to be very pure and this was confirmed by the analysis, no iron or insoluble impurity being found.

The values of the atomic ratio of gold to silver determined by us, namely, 4.07:1 and 3.56:1, are rather close to that obtained by Sipöcz[15] for krennerite from Săcărâmbu (Nagy-Ág), namely, 3.26:1. Sipöcz also determined the densities of two samples of krennerite from Săcărâmbu (Nagy-Ág)to be 8.63 and 8.18. The analysis of Sipöcz shows that his material contained the following percentages of impurities: quartz 2.29, copper 0.33, iron 0.58, antimony 0.64; hence it is not surprising that while one of his density values agrees with ours the other is considerably too

[14] Pierson, G. G.: *Ind. Eng. Chem.*, Anal. Ed., **6**, 437–439 (1934).

[15] Sipöcz, L.: *Math. és Term. Tud. Köz.*, **20**, 174–176 (1885).

low. The incomplete analysis of krennerite from Cripple Creek made by Myers[16] yielded only 0.45 per cent of silver. Since our two analyses of krennerite from different mines in the Cripple Creek district and the analysis of Sipöcz of krennerite from Săcărâmbu (Nagy-Ág) all yielded a silver content of approximately 5 per cent, the existence of krennerite at Cripple Creek of such low silver content seems doubtful.

TABLE 3. ANALYSIS OF KRENNERITE FROM VINDICATOR MINE, CRIPPLE CREEK, COLORADO

(U. S. National Museum No. 96647)

	Per Cent
Au	35.1
Ag	5.4
Te	Not determined
Fe	None
Insoluble	None

DETERMINATION OF THE UNIT CELL AND SPACE-GROUP

The dimensions of the structural unit cell, all determined by purely röntgenographic measurements, are $a_0 = 16.54$ Å, $b_0 = 8.82$ Å, $c_0 = 4.46$ Å, all ± 0.03 Å.[17] The volume of the unit cell is accordingly 650.6 Å^3. The density computed from the x-ray measurements with use of the average of our two chemical analyses of krennerite from Cripple Creek is 8.86.[18] This is in reasonable agreement with the density determined by us with the pycnometer, namely, 8.63, and establishes the content of the unit cell as $8(Au,Ag)Te_2$.

Diffraction effects were obtained on the Weissenberg photographs from the following planes: $g00$, $0u0$, $0g0$, $00u$, $00g$, $0uu$, $0ug$, $0gu$, $0gg$, $g0u$, $g0g$, $uu0$, $ug0$, $gu0$, $gg0$, uuu, uug, ugu, ugg, guu, gug, ggu, ggg, where u denotes any odd number and g denotes any even number. No diffraction effects were obtained from the following: $u00$, $u0u$, $u0g$, although representatives of each were in a position to diffract. Thus krennerite belongs to one of

[16] Myers, W. S., (in) Chester, A. H.: *Am. Jour. Sci.*, (4) **5**, 376 (1898).

[17] Based on the wave-lengths: copper $K\alpha_1$, $\lambda = 1.5405$ Å, copper $K\alpha_2$, $\lambda = 1.5443$ Å; copper $K\beta_1$, $\lambda = 1.3922$ Å. (In a preliminary report on the crystal structure of krennerite by Tunell and Ksanda (*Jour. Wash. Acad. Sci.*, **26**, 507–509 (1936)), the dimensions of the unit cell were given in kX units.)

[18] The density ρ was calculated by the use of the equation

$$\rho = 1.660 \Sigma A / V,$$

where ΣA is the sum of the atomic weights of the atoms in the unit cell and V is the volume of the unit cell in Å^3.

the following space-groups: C_{2v}^2-$P2am$, C_{2v}^4-Pma, D_{2h}^5-Pmam, which are characterized by the absence of diffraction effects from $u00$, $u0u$, $u0g$, owing to the presence of a glide plane parallel to 010 with a glide component of $a/2$.

Determination of the Atomic Arrangement

In his morphologic study of sylvanite and krennerite Schrauf[19] noted that the angles in one zone of sylvanite including its cleavage are closely similar to the angles in one zone of krennerite including its cleavage. The angles[20] in these zones are as follows according to Schrauf:

Sylvanite $mt = 31° 38'$, $mr = 42° 44'$, $ms = 61° 35'$, m: cleavage $= 90°$,
Krennerite $a\tau = 31° 41'$, $a\rho = 42° 48'$, $ah = 61° 38'$, a:cleavage $= 90°$;

the forms in Schrauf's table have the following indices referred to the sylvanite axes of Tunell[21] and the krennerite axes of Tunell and Murata:

Sylvanite m-{001}, t-{013}, r-{012}, s-{011}, and
Krennerite a-{100}, τ-{601}, ρ-{401}, h-{201}.

X-ray measurements by the authors have confirmed this analogy and shown that it is even closer than Schrauf supposed. Thus the spacing of the cleavage plane of sylvanite is $d_{010} = 4.49$ Å[22] and that of the cleavage plane of krennerite is $d_{001} = 4.46$ Å. The plane 001 of sylvanite has the spacing $d_{001} = 8.30$ Å; Schrauf showed that the analogous plane of krennerite is 100, and we have found that the spacing $d_{100} = 16.54$ Å, very nearly twice the spacing of the plane 001 of sylvanite. The a-axis of sylvanite has an identity period $a_0 = 8.96$ Å, and the analogous direction of krennerite, the b-axis, has an identity period $b_0 = 8.82$ Å. Moreover, the intensities of the diffraction effects from the analogous pairs of planes 001 of sylvanite and 100 of krennerite, and 010 of sylvanite and 001 of krennerite are similar, as shown in Table 4. These facts strongly suggest a basic similarity in the structures of the two minerals. The structure of sylvanite can be described as consisting of lines of atoms parallel to the a-axis lying alternately in or near the plane $y = 0$ and near the plane $y = \frac{1}{2}$. Along these lines the gold (or silver) atoms are separated by pairs of tellurium atoms. Similar lines of atoms should therefore exist in krennerite parallel to the b-axis and should lie alternately in or near the plane

[19] Schrauf, A.: *Z. Kryst. Mineral.*, **2**, 209–252 (1878).

[20] G. F. H. Smith found for these angles of krennerite $a\tau = 31° 38\frac{1}{2}'$, $a\rho = 42° 45'$, $ah = 61° 35\frac{1}{2}'$, thus confirming the close similarity with the angles mt, mr, and ms of sylvanite. *Mineralog. Mag.* **13**, 267 (1903).

[21] Tunell, George: *Am. Mineral.*, **26**, 457–477 (1941).

[22] The dimensions of the unit cell of sylvanite reported by Tunell (op. cit.) were in kX units, although they were given in Å units in accordance with custom at that time.

$z=0$ and in or near the plane $z=\frac{1}{2}$. Such a structure for krennerite would be possible in the space-groups C_{2v}^2-*P2am* and D_{2h}^5-*Pmam* only if the atoms lay exactly in the planes $z=0$ and $z=\frac{1}{2}$. The planes $z=0$ and $z=\frac{1}{2}$

TABLE 4. COMPARISON OF INTENSITIES OF ANALOGOUS PLANES IN SYLVANITE AND KRENNERITE

Sylvanite				Krennerite			
hkl	Spacing	Intensity	Cu K-Radiation	*hkl*	Spacing	Intensity	Cu K-Radiation
				100	16.54 Å	0	$\alpha_1+\alpha_2$
001	8.30 Å	0	$\alpha_1+\alpha_2$	200	8.27	0	$\alpha_1+\alpha_2$
				300	5.51	0	$\alpha_1+\alpha_2$
002	4.15	0	$\alpha_1+\alpha_2$	400	4.14	0	$\alpha_1+\alpha_2$
				500	3.31	0	$\alpha_1+\alpha_2$
003	2.77	0	$\alpha_1+\alpha_2$	600	2.76	0	$\alpha_1+\alpha_2$
				700	2.36	0	$\alpha_1+\alpha_2$
004	2.08	s	$\alpha_1+\alpha_2$	800	2.07	s	$\alpha_1+\alpha_2$
				900	1.84	0	$\alpha_1+\alpha_2$
005	1.66	0	$\alpha_1+\alpha_2$	10.0.0	1.65	0	$\alpha_1+\alpha_2$
				11.0.0	1.50	0	$\alpha_1+\alpha_2$
006	1.38	0	$\alpha_1+\alpha_2$	12.0.0	1.38	0	$\alpha_1+\alpha_2$
				13.0.0	1.27	0	$\alpha_1+\alpha_2$
007	1.19	0	$\alpha_1+\alpha_2$	14.0.0	1.18	0	$\alpha_1+\alpha_2$
				15.0.0	1.10	0	$\alpha_1+\alpha_2$
008	1.04	m	α_1	16.0.0	1.03	m	$\alpha_1+\alpha_2$
				17.0.0	0.97	0	$\alpha_1+\alpha_2$
009	0.92	0	α_1	18.0.0	0.92	0	α_1
				19.0.0	0.87	0	α_1
0.0.10	0.83	w	α_1	20.0.0	0.83	w	α_1
010	4.49	w	$\alpha_1+\alpha_2$	001	4.46	w	$\alpha_1+\alpha_2$
020	2.25	s	$\alpha_1+\alpha_2$	002	2.23	s	$\alpha_1+\alpha_2$
030	1.49	m	$\alpha_1+\alpha_2$	003	1.49	m	$\alpha_1+\alpha_2$
040	1.12	w	$\alpha_1+\alpha_2$	004	1.11	m	$\alpha_1+\alpha_2$
050	0.90	m	α_1	005	0.89	w	α_1

are reflection planes in these space-groups and a slight displacement of any atom from one of the planes $z=0$ or $z=\frac{1}{2}$ would require the presence of an additional atom on the other side of the reflection plane. If the atoms were situated in the planes $z=0$ and $z=\frac{1}{2}$ in a structure of this type no odd order reflections should be present from the plane 001. Such reflections are present, however, and therefore the space-groups C_{2v}^2-*P2am* and D_{2h}^5-*Pmam* may be left out of consideration.

Such a structure differs from that of sylvanite in one respect: in sylvanite the gold (or silver) atoms lie in a single series of parallel planes that are perpendicular to 010 and parallel to the c-axis; in krennerite the gold (or silver) atoms do not lie in a series of parallel planes but instead lie in or near a series of corrugated sheets. These corrugated sheets are made up of two sets of parallel planes, both sets perpendicular to 001

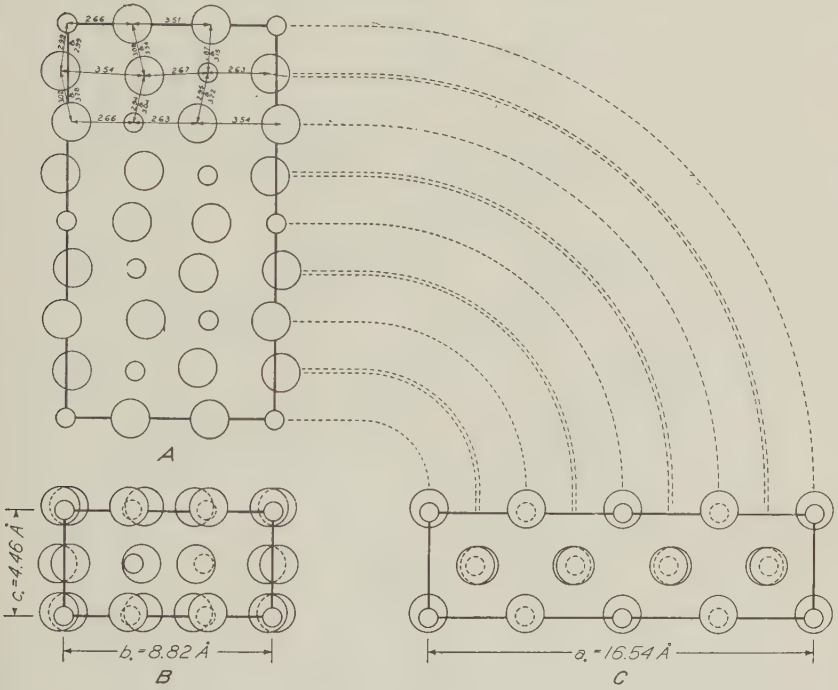

FIG. 1. Orthographic projections of the unit cell of krennerite. *A*. Top view. *B*. Front view. *C*. Side view. Small circles—gold (or silver) atoms. Large circles—tellurium atoms.

and inclined at an angle of 35° to the b-axis, one set lying in the angle between the positive end of the b-axis and the positive end of the a-axis and the other set lying in the angle between the positive end of the b-axis and the negative end of the a-axis. The corrugation of the sheets of gold (or silver) atoms is caused by the presence of the reflection planes $x = \frac{1}{4}$ and $x = \frac{3}{4}$. The zigzag pattern of the corrugated sheets is clearly evident in projection in Fig. 1*A* and Fig. 3.

There are eight gold (or silver) and sixteen tellurium atoms to be located in the unit cell. The space-group C_{2v}^4-Pma furnishes the following sets of equivalent positions:

(a) $00z$; $\frac{1}{2}0z$, (b) $0\frac{1}{2}z$; $\frac{1}{2}\frac{1}{2}z$, (c) $\frac{1}{4}yz$; $\frac{3}{4}\bar{y}z$, (d) xyz; $\bar{x}\bar{y}z$; $\frac{1}{2}-x, y, z$; $\frac{1}{2}+x, \bar{y}, z$,[23]

of which (a) and (b) have the symmetry C_2-2, (c) the symmetry C_s-m, and (d) the symmetry C_1-1. In krennerite gold (or silver) atoms are situated in (a) with $z=0$ (arbitrary), in (c) with $y_1=0.319$, $z_1=0.014$, and

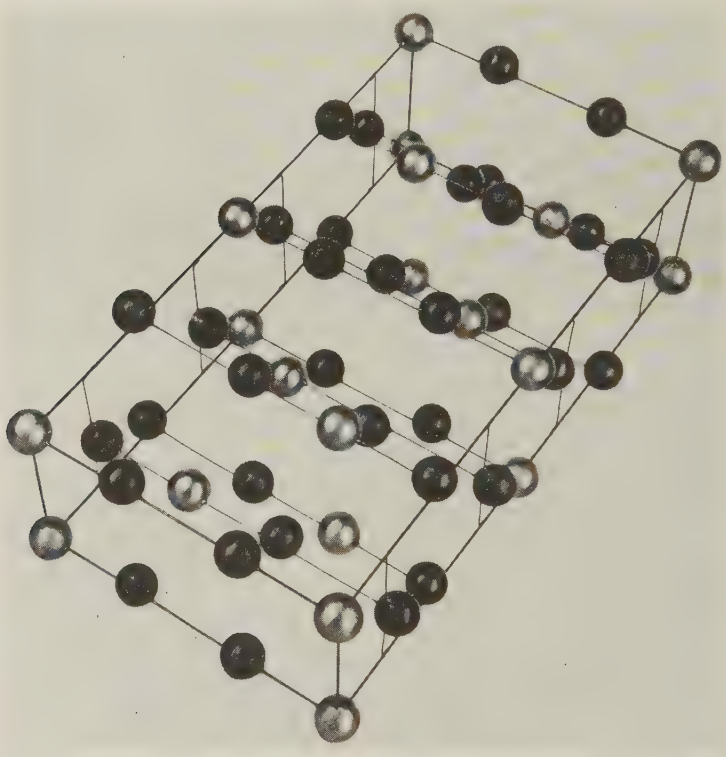

FIG. 2. Model showing the arrangement of the atoms in krennerite. The parallelepiped represented by the outside wires is the unit cell. The longest edge represents the a-axis, the edge intermediate in length represents the b-axis, the shortest edge represents the c-axis. The grey spheres represent gold (or silver) atoms; the black spheres represent tellurium atoms.

in (d) with $x_2=0.124$, $y_2=0.666$, $z_2=0.500$; tellurium atoms are situated in (c) with $y_3=0.018$, $z_3=0.042$, and $y_4=0.617$, $z_4=0.042$ and in (d) with $x_5=0.003$, $y_5=0.699$, $z_5=0.042$, and $x_6=0.132$, $y_6=0.364$, $z_6=0.500$, and $x_7=0.119$, $y_7=0.964$, $z_7=0.500$. Orthographic projections of this struc-

[23] As is customary, x denotes an atomic coordinate along the a-axis expressed as a fraction of a_0; y denotes an atomic coordinate along the b-axis expressed as a fraction of b_0; z denotes an atomic coordinate along the c-axis expressed as a fraction of c_0.

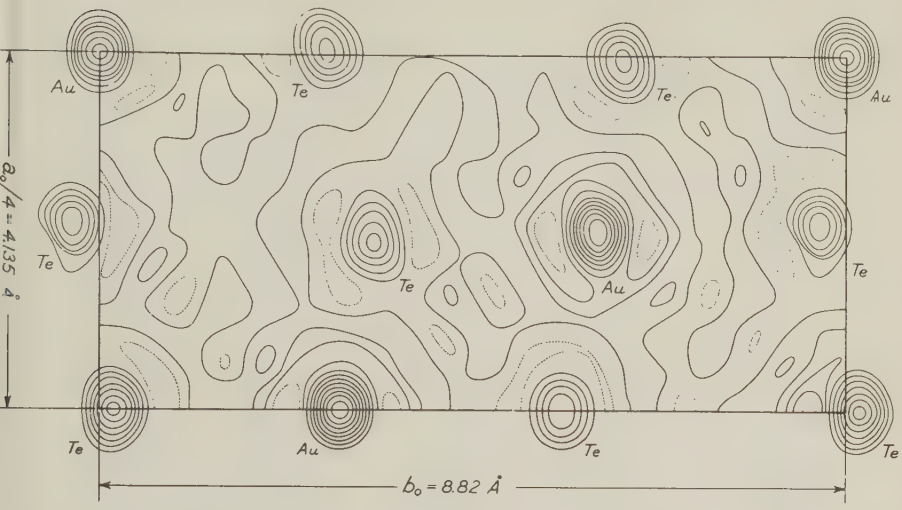

FIG. 3. Fourier projection along the *c*-axis of the structure of krennerite. The contour map within the rectangle represents the projection on the plane 001 of one-fourth of the unit cell. The peaks lettered Au represent gold (or silver) atoms; those lettered Te represent tellurium atoms. Dotted lines are depression contours. The origin is in the upper left-hand corner of the rectangle. The positive direction of the *a*-axis is from top to bottom of the drawing; the positive direction of the *b*-axis is from left to right; the positive direction of the *c*-axis (which is perpendicular to the plane of the paper) is upward from the plane of the paper.

ture are given in Fig. 1, and a model of the structure is shown in Fig. 2. The intensities calculated from this structure are compared with those observed in Tables 5, 6 and 7. Table 5 contains the observed and calculated intensities of diffraction lines in a powder photograph taken with Co K-radiation filtered through iron foil. The indexing of the powder photograph was carried out rigorously by use of the unit cell dimensions obtained from the single crystal Weissenberg photographs. Table 5 lists in decreasing order the calculated and observed spacings and intensities of all planes the spacings of which are greater than 1.28 Å, together with the observed spacings and intensities of the remaining lines of the powder photographs. The intensities I_p of the lines on the powder diffraction film taken with filtered radiation were calculated from the formula

$$I_p = \frac{1 + \cos^2 2\theta}{\sin 2\theta \sin \theta} j |F|^2,$$

where 2θ denotes the angle between the incident and diffracted beams, F the structure factor, and j the number of cooperating planes. On the powder photograph the α_1 and α_2 lines were not resolved. Tables 6 and 7 contain the observed and calculated intensities of diffraction spots in

TABLE 5. RELATIVE INTENSITIES* OF THE *X*-RAY DIFFRACTION LINES OF KRENNERITE FROM A POWDER PHOTOGRAPH TAKEN WITH FILTERED COBALT K-RADIATION

Indices (*hkl*)	Spacing (calculated)	Relative intensity (calculated)	Spacing (measured)	Relative intensity (observed)
100	16.54 Å	0.00		
010	8.82	.03		
200	8.27	.00		
110	7.79	.02		
210	6.04	.61	6.08 Å	½
300	5.51	.00		
310	4.69	.68	4.69	1
001	4.46	.10	4.47	½
020	4.41	.00		
101	4.31	.00		
120	4.26	.01		
400	4.14	.00		
011	3.98	.18	3.94	2
201	3.93	.00		
220	3.89	.00	3.88	2
111	3.87	.55		
410	3.75	.14		
211	3.59	.15		
301	3.47	.00		
320	3.44	.00		
500	3.31	.00		
311	3.23	.02		
021	3.14	.00		
510	3.10	.09		
121	3.08	.02		
401	3.03	10.00	3.03	10
420	3.02	.00		
030	2.94	3.62	2.94	6
221	2.93	.03		
130	2.89	.04		
411	2.87	.02		
230	2.76	.00		
600	2.76	.00		
321	2.73	.00		
501	2.66	.00		
520	2.65	.02		
610	2.63	.00		
330	2.59	.01		
511	2.54	.00		
421	2.50	.00		
031	2.45	.03		
131	2.43	.04		
430	2.39	.00		

TABLE 5—*Continued*

Indices (*hkl*)	Spacing (calculated)	Relative intensity (calculated)	Spacing (measured)	Relative intensity (observed)
700	2.36	.00		
231	2.35	.00	2.35	½
601	2.35	.00		
620	2.34	.02		
710	2.28	.01		
521	2.28	.01		
611	2.27	.19		
331	2.24	.07	2.23	5
002	2.23	1.97		
102	2.21	.00		
040	2.20	.00		
530	2.19	.02		
140	2.18	.00		
012	2.16	.00	2.16	1
202	2.15	.00		
112	2.14	.00		
240	2.13	.14		
431	2.11	5.42	2.11	7
212	2.09	.09		
701	2.09	.00		
720	2.08	.00		
621	2.07	.02	2.07	4
800	2.07	1.59		
302	2.07	.00		
340	2.04	.39		
711	2.03	.21		
810	2.01	.00		
312	2.01	.15	2.01	1
630	2.00	.00		
022	1.99	.00		
041	1.98	.23		
122	1.98	.01		
531	1.97	.01	1.97	2
402	1.96	.08		
141	1.96	.57		
440	1.94	.21		
222	1.93	.04		
241	1.92	.10	1.92	2
412	1.92	.05		
721	1.89	.00		
801	1.88	.02		
322	1.87	.00		
820	1.87	.00		
341	1.86	.01		

TABLE 5—*Continued*

Indices (*hkl*)	Spacing (calculated)	Relative intensity (calculated)	Spacing (measured)	Relative intensity (observed)
502	1.85	.00		
900	1.84	.00		
730	1.84	.03	1.84	1
811	1.84	.04		
631	1.83	.00		
540	1.83	.24		
512	1.81	.04		
910	1.80	.00		
422	1.79	.00		
441	1.78	.00		
032	1.78	1.52	1.78	4
132	1.77	.02		
050	1.76	.00		
150	1.75	.00		
232	1.74	.00		
602	1.73	.00	1.74	1
821	1.73	.00		
250	1.72	.01		
640	1.72	.02		
522	1.71	.01		
731	1.70	.01		
612	1.70	.01		
901	1.70	.00		
541	1.70	.00		
920	1.70	.00	1.69	4
332	1.69	.01		
830	1.69	1.28		
350	1.68	.01		
911	1.67	.02		
10.0.0	1.65	.00		
051	1.64	.00		
432	1.63	.06		
151	1.63	.02		
10.1.0	1.63	.05		
702	1.62	.00		
450	1.62	.00		
622	1.61	.02		
740	1.61	.00		
251	1.61	.02		
641	1.61	.16		
712	1.60	.00		
921	1.59	.01		
831	1.58	.01		
351	1.57	.00		

TABLE 5—*Continued*

Indices (*hkl*)	Spacing (calculated)	Relative intensity (calculated)	Spacing (measured)	Relative intensity (observed)
042	1.57	.00		
532	1.57	.01		
142	1.56	.01		
930	1.56	.00		
550	1.55	.01		
10.0.1	1.55	.00		
10.2.0	1.55	.00		
242	1.54	.09		
10.1.1	1.53	.00		
451	1.52	.00		
722	1.52	.00	1.52	4
802	1.52	1.11		
741	1.52	.34		
342	1.51	.28		
840	1.51	.00		
11.0.0	1.50	.00		
812	1.49	.00	1.50	½
632	1.49	.00		
003	1.49	.03		
650	1.48	.01		
11.1.0	1.48	.05		
103	1.48	.00		
931	1.47	.02		
551	1.47	.01		
442	1.47	.17		
013	1.47	.01	1.47	3
10.2.1	1.46	.01		
060	1.47	.19		
203	1.46	.00		
160	1.46	.01		
113	1.46	.04		
260	1.45	.00		
213	1.44	.02		
10.3.0	1.44	.00		
303	1.44	.00		
822	1.43	.00		
841	1.43	.08		
11.0.1	1.43	.00		
11.2.0	1.42	.00		
732	1.42	.03		
360	1.42	.00		
902	1.42	.00		
542	1.42	.17		
313	1.42	.00		

TABLE 5—*Continued*

Indices (*hkl*)	Spacing (calculated)	Relative intensity (calculated)	Spacing (measured)	Relative intensity (observed)
750	1.41	.00		
651	1.41	.02		
940	1.41	.00		
023	1.41	.00		
11.1.1	1.41	.01		
123	1.40	.00	1.40	2
912	1.40	.00		
403	1.40	.83		
061	1.40	.01		
161	1.39	.01		
223	1.39	.03		
052	1.38	.00		
460	1.38	.00		
413	1.38	.00		
12.0.0	1.38	.00		
152	1.38	.01		
261	1.38	.00		
10.3.1	1.37	.00		
323	1.37	.00		
252	1.36	.03		
642	1.36	.02		
12.1.0	1.36	.01		
11.2.1	1.36	.00		
503	1.36	.00		
361	1.35	.02		
922	1.35	.00		
832	1.35	1.18	1.35	4
751	1.35	.01		
941	1.35	.13		
352	1.34	.01		
560	1.34	.01		
850	1.34	.00		
513	1.34	.00		
11.3.0	1.34	.00		
423	1.33	.00		
10.0.2	1.33	.00		
033	1.33	.03		
461	1.32	.34	1.33	2
133	1.32	.01		
10.4.0	1.32	.06		
12.0.1	1.32	.70	1.32	3
12.2.0	1.32	.00		
10.1.2	1.31	.06		
452	1.31	.00		

TABLE 5—*Continued*

Indices (*hkl*)	Spacing (calculated)	Relative intensity (calculated)	Spacing (measured)	Relative intensity (observed)
233	1.31	.00		
603	1.31	.00		
742	1.31	.01		
12.1.1	1.30	.00		
523	1.30	.01		
660	1.30	.00		
613	1.30	.04		
333	1.29	.01		
561	1.29	.00		
851	1.29	.00		
11.3.1	1.28	.03		
			1.268	3
			1.251	½
			1.232	2
			1.212	2
			1.202	4
			1.179	½
			1.165	½
			1.120	1
			1.089	½
			1.082	2
			1.074	1
			1.061	1 Broad
			1.048	2
			1.036	1
			1.015	3
			.999	½
			.983	2
			.977	1
			.971	½
			.965	1
			.959	2
			.941	2
			.935	1

* The intensities were estimated visually on a scale of ten, where ten represents the intensity of the strongest line.

two Weissenberg equator photographs with the crystals rotating about the *b*- and *c*-axes. The intensities I_w of the α_1 spots (where the α_1 and α_2 spots were resolved) on the Weissenberg equator films were calculated from the formula

$$I_w = \frac{1 + \cos^2 2\theta}{\sin 2\theta} |F|^2$$

TABLE 6. RELATIVE INTENSITIES OF *X*-RAY DIFFRACTION SPOTS FROM A WEISSENBERG EQUATOR PHOTOGRAPH OF KRENNERITE TAKEN WITH THE CRYSTAL ROTATING AROUND THE *b*-AXIS

Indices (*hkl*)	Spacing (calculated)	Relative intensity (Observed)*	Relative intensity (Calculated)	CuK-radiation†
005	0.89Å	w	.15	α_1
205	0.89	w	.00	α_1
405	0.87	w	.61	α_1
605	0.85	w	.00	α_1
805	0.82	m	.22	α_1
004	1.11	m	.72	α_1
204	1.10	w	.00	α_1
404	1.08	w	.08	α_1
604	1.03	w	.00	α_1
804	0.98	w	.62	α_1
10.0.4	0.93	w	.00	α_1
12.0.4	0.87	w	.10	α_1
14.0.4	0.81	w	.00	α_1
003	1.49	m	.14	$\alpha_1+\alpha_2$
203	1.46	w	.00	$\alpha_1+\alpha_2$
403	1.40	m	1.77	$\alpha_1+\alpha_2$
603	1.31	w	.00	$\alpha_1+\alpha_2$
803	1.21	w	.08	$\alpha_1+\alpha_2$
10.0.3	1.11	w	.00	$\alpha_1+\alpha_2$
12.0.3	1.01	w	.65	α_1
14.0.3	0.93	w	.00	α_1
16.0.3	0.85	w	.06	α_1
002	2.23	s	5.53	$\alpha_1+\alpha_2$
202	2.15	w	.00	$\alpha_1+\alpha_2$
402	1.96	w	.13	$\alpha_1+\alpha_2$
602	1.73	w	.00	$\alpha_1+\alpha_2$
802	1.52	w	2.26	$\alpha_1+\alpha_2$
10.0.2	1.33	w	.00	$\alpha_1+\alpha_2$
12.0.2	1.17	w	.04	$\alpha_1+\alpha_2$
14.0.2	1.04	w	.00	$\alpha_1+\alpha_2$
16.0.2	0.94	m	.68	α_1
18.0.2	0.85	w	.00	α_1
001	4.46	w	.13	$\alpha_1+\alpha_2$
201	3.93	0	.00	$\alpha_1+\alpha_2$
401	3.03	m	10.00	$\alpha_1+\alpha_2$
601	2.35	0	.00	$\alpha_1+\alpha_2$
801	1.88	0	.03	$\alpha_1+\alpha_2$
10.0.1	1.55	w	.00	$\alpha_1+\alpha_2$
12.0.1	1.32	m	1.57	$\alpha_1+\alpha_2$
14.0.1	1.14	w	.00	$\alpha_1+\alpha_2$
16.0.1	1.01	0	.01	$\alpha_1+\alpha_2$
18.0.1	0.90	0	.00	α_1
20.0.1	0.81	s	1.23	α_1
200	8.27	0	.00	$\alpha_1+\alpha_2$
400	4.14	0	.00	$\alpha_1+\alpha_2$
600	2.76	0	.00	$\alpha_1+\alpha_2$
800	2.07	s	4.81	$\alpha_1+\alpha_2$
10.0.0	1.65	0	.00	$\alpha_1+\alpha_2$
12.0.0	1.38	0	.00	$\alpha_1+\alpha_2$
14.0.0	1.18	0	.00	$\alpha_1+\alpha_2$
16.0.0	1.03	m	1.03	$\alpha_1+\alpha_2$
18.0.0	0.92	0	.00	α_1
20.0.0	0.83	w	.01	α_1

* Denotation of symbols: s, strong; m, medium; w, weak.

† The symbol $\alpha_1+\alpha_2$ denotes an unresolved spot resulting from α_1 and α_2 rays together; the symbol α_1 denotes a spot resulting from α_1 rays alone.

TABLE 7. RELATIVE INTENSITIES OF X-RAY DIFFRACTION SPOTS FROM A WEISSENBERG EQUATOR PHOTOGRAPH OF KRENNERITE TAKEN WITH THE CRYSTAL ROTATING AROUND THE c-AXIS

Indices (*hkl*)	Spacing (calculated)	Relative intensity		CuK-radiation†
		(Observed)*	(Calculated)	
0.11.0	0.80 Å	w	.03	α_1
1.11.0	0.80	w	.01	α_1
2.11.0	0.80	w	.03	α_1
3.11.0	0.79	w	.01	α_1
4.11.0	0.79	w	.02	α_1
0.10.0	0.88	0	.01	α_1
1.10.0	0.88	w	.01	α_1
2.10.0	0.88	w	.03	α_1
3.10.0	0.87	s	.36	α_1
4.10.0	0.86	s	.60	α_1
5.10.0	0.85	s	.41	α_1
6.10.0	0.84	m	.03	α_1
7.10.0	0.83	w	.00	α_1
8.10.0	0.81	0	.01	α_1
9.10.0	0.79	w	.01	α_1
090	0.98	m	.06	α_1
190	0.98	0	.00	α_1
290	0.97	0	.00	α_1
390	0.96	0	.00	α_1
490	0.95	0	.00	α_1
590	0.94	0	.00	α_1
690	0.92	0	.00	α_1
790	0.90	w	.01	α_1
890	0.88	m	.18	α_1
990	0.86	0	.02	α_1
10.9.0	0.84	0	.00	α_1
11.9.0	0.82	0	.00	α_1
12.9.0	0.80	w	.00	α_1
080	1.10	0	.00	$\alpha_1+\alpha_2$
180	1.10	0	.00	$\alpha_1+\alpha_2$
280	1.09	w	.00	$\alpha_1+\alpha_2$
380	1.08	w	.00	$\alpha_1+\alpha_2$
480	1.06	0	.00	$\alpha_1+\alpha_2$
580	1.04	0	.00	$\alpha_1+\alpha_2$
680	1.02	0	.00	$\alpha_1+\alpha_2$
780	1.00	0	.00	$\alpha_1+\alpha_2$
880	0.97	0	.00	$\alpha_1+\alpha_2$
980	0.94	0	.00	$\alpha_1+\alpha_2$
10.8.0	0.92	0	.01	α_1
11.8.0	0.89	w	.00	α_1
12.8.0	0.86	0	.00	α_1
13.8.0	0.83	w	.00	α_1
14.8.0	0.80	0	.02	α_1
070	1.26	0	.00	$\alpha_1+\alpha_2$

TABLE 7—*Continued*

Indices (*hkl*)	Spacing (calculated)	Relative intensity		CuK-radiation
		(Observed)	(Calculated)	
170	1.26	0	.00	$\alpha_1+\alpha_2$
270	1.24	w	.08	$\alpha_1+\alpha_2$
370	1.23	m	.48	$\alpha_1+\alpha_2$
470	1.20	m	.48	$\alpha_1+\alpha_2$
570	1.18	m	.40	$\alpha_1+\alpha_2$
670	1.14	w	.04	$\alpha_1+\alpha_2$
770	1.11	0	.00	$\alpha_1+\alpha_2$
870	1.07	0	.00	$\alpha_1+\alpha_2$
970	1.04	w	.01	$\alpha_1+\alpha_2$
10.7.0	1.00	w	.10	$\alpha_1+\alpha_2$
11.7.0	0.96	m	.28	α_1
12.7.0	0.93	m	.26	α_1
13.7.0	0.89	m	.22	α_1
14.7.0	0.86	w	.01	α_1
15.7.0	0.83	0	.00	α_1
16.7.0	0.80	w	.01	α_1
060	1.47	s	1.02	$\alpha_1+\alpha_2$
160	1.46	w	.02	$\alpha_1+\alpha_2$
260	1.45	0	.00	$\alpha_1+\alpha_2$
360	1.42	w	.01	$\alpha_1+\alpha_2$
460	1.38	w	.00	$\alpha_1+\alpha_2$
560	1.34	w	.02	$\alpha_1+\alpha_2$
660	1.30	w	.00	$\alpha_1+\alpha_2$
760	1.25	w	.05	$\alpha_1+\alpha_2$
860	1.20	m	.63	$\alpha_1+\alpha_2$
960	1.15	0	.00	$\alpha_1+\alpha_2$
10.6.0	1.10	0	.00	$\alpha_1+\alpha_2$
11.6.0	1.05	w	.00	$\alpha_1+\alpha_2$
12.6.0	1.00	w	.00	$\alpha_1+\alpha_2$
13.6.0	0.96	0	.03	$\alpha_1+\alpha_2$
14.6.0	0.92	0	.00	α_1
15.6.0	0.88	m	.08	α_1
16.6.0	0.84	m	.50	α_1
17.6.0	0.81	w	.01	α_1
050	1.76	0	.00	$\alpha_1+\alpha_2$
150	1.75	0	.01	$\alpha_1+\alpha_2$
250	1.72	w	.03	$\alpha_1+\alpha_2$
350	1.68	w	.02	$\alpha_1+\alpha_2$
450	1.62	0	.00	$\alpha_1+\alpha_2$
550	1.55	w	.02	$\alpha_1+\alpha_2$
650	1.48	w	.01	$\alpha_1+\alpha_2$
750	1.41	w	.00	$\alpha_1+\alpha_2$
850	1.34	w	.00	$\alpha_1+\alpha_2$
950	1.27	0	.00	$\alpha_1+\alpha_2$

TABLE 7—*Continued*

Indices (*hkl*)	Spacing (calculated)	Relative intensity		CuK-radiation
		(Observed)	(Calculated)	
10.5.0	1.20	w	.01	$\alpha_1+\alpha_2$
11.5.0	1.14	w	.02	$\alpha_1+\alpha_2$
12.5.0	1.08	0	.00	$\alpha_1+\alpha_2$
13.5.0	1.03	w	.00	$\alpha_1+\alpha_2$
14.5.0	0.98	w	.01	$\alpha_1+\alpha_2$
15.5.0	0.93	w	.00	$\alpha_1+\alpha_2$
16.5.0	0.89	w	.00	$\alpha_1+\alpha_2$
17.5.0	0.85	0	.00	α_1
18.5.0	0.81	0	.01	α_1
040	2.20	0	.01	$\alpha_1+\alpha_2$
140	2.18	w	.01	$\alpha_1+\alpha_2$
240	2.13	w	.26	$\alpha_1+\alpha_2$
340	2.04	m	.80	$\alpha_1+\alpha_2$
440	1.94	m	.48	$\alpha_1+\alpha_2$
540	1.83	m	.54	$\alpha_1+\alpha_2$
640	1.72	w	.06	$\alpha_1+\alpha_2$
740	1.61	0	.01	$\alpha_1+\alpha_2$
840	1.51	w	.00	$\alpha_1+\alpha_2$
940	1.41	w	.00	$\alpha_1+\alpha_2$
10.4.0	1.32	m	.17	$\alpha_1+\alpha_2$
11.4.0	1.24	m	.32	$\alpha_1+\alpha_2$
12.4.0	1.17	m	.13	$\alpha_1+\alpha_2$
13.4.0	1.10	w	.10	$\alpha_1+\alpha_2$
14.4.0	1.04	w	.00	$\alpha_1+\alpha_2$
15.4.0	0.98	0	.00	$\alpha_1+\alpha_2$
16.4.0	0.93	w	.00	$\alpha_1+\alpha_2$
17.4.0	0.89	w	.00	$\alpha_1+\alpha_2$
18.4.0	0.85	m	.18	α_1
19.4.0	0.81	m	.46	α_1
030	2.94	s	10.00	$\alpha_1+\alpha_2$
130	2.89	w	.05	$\alpha_1+\alpha_2$
230	2.76	0	.00	$\alpha_1+\alpha_2$
330	2.59	0	.02	$\alpha_1+\alpha_2$
430	2.39	0	.00	$\alpha_1+\alpha_2$
530	2.19	w	.04	$\alpha_1+\alpha_2$
630	2.01	0	.00	$\alpha_1+\alpha_2$
730	1.84	w	.07	$\alpha_1+\alpha_2$
830	1.69	s	3.21	$\alpha_1+\alpha_2$
930	1.56	0	.01	$\alpha_1+\alpha_2$
10.3.0	1.44	0	.00	$\alpha_1+\alpha_2$
11.3.0	1.34	w	.00	$\alpha_1+\alpha_2$
12.3.0	1.24	w	.00	$\alpha_1+\alpha_2$
13.3.0	1.16	0	.02	$\alpha_1+\alpha_2$
14.3.0	1.09	0	.00	$\alpha_1+\alpha_2$

TABLE 7—*Continued*

Indices (*hkl*)	Spacing (calculated)	Relative intensity (Observed)	Relative intensity (Calculated)	CuK-radiation
15.3.0	1.03	w	.05	$\alpha_1+\alpha_2$
16.3.0	0.97	s	1.09	$\alpha_1+\alpha_2$
17.3.0	0.92	0	.00	$\alpha_1+\alpha_2$
18.3.0	0.87	w	.00	$\alpha_1+\alpha_2$
19.3.0	0.83	w	.00	α_1
20.3.0	0.79	w	.02	α_1
020	4.41	0	.00	$\alpha_1+\alpha_2$
120	4.26	0	.00	$\alpha_1+\alpha_2$
220	3.89	0	.00	$\alpha_1+\alpha_2$
320	3.44	0	.00	$\alpha_1+\alpha_2$
420	3.02	0	.00	$\alpha_1+\alpha_2$
520	2.65	w	.03	$\alpha_1+\alpha_2$
620	2.34	w	.03	$\alpha_1+\alpha_2$
720	2.08	0	.00	$\alpha_1+\alpha_2$
820	1.87	0	.00	$\alpha_1+\alpha_2$
920	1.70	w	.00	$\alpha_1+\alpha_2$
10.2.0	1.55	0	.00	$\alpha_1+\alpha_2$
11.2.0	1.42	0	.01	$\alpha_1+\alpha_2$
12.2.0	1.32	0	.01	$\alpha_1+\alpha_2$
13.2.0	1.22	w	.01	$\alpha_1+\alpha_2$
14.2.0	1.14	w	.01	$\alpha_1+\alpha_2$
15.2.0	1.07	w	.00	$\alpha_1+\alpha_2$
16.2.0	1.00	0	.00	$\alpha_1+\alpha_2$
17.2.0	0.95	w	.00	$\alpha_1+\alpha_2$
18.2.0	0.90	w	.01	$\alpha_1+\alpha_2$
19.2.0	0.85	0	.02	α_1
20.2.0	0.81	w	.00	α_1
010	8.82	0	.03	$\alpha_1+\alpha_2$
110	7.79	0	.01	$\alpha_1+\alpha_2$
210	6.04	w	.40	$\alpha_1+\alpha_2$
310	4.69	w	.57	$\alpha_1+\alpha_2$
410	3.75	w	.16	$\alpha_1+\alpha_2$
510	3.10	w	.12	$\alpha_1+\alpha_2$
610	2.63	0	.01	$\alpha_1+\alpha_2$
710	2.28	0	.01	$\alpha_1+\alpha_2$
810	2.01	0	.00	$\alpha_1+\alpha_2$
910	1.80	w	.00	$\alpha_1+\alpha_2$
10.1.0	1.63	w	.13	$\alpha_1+\alpha_2$
11.1.0	1.48	w	.15	$\alpha_1+\alpha_2$
12.1.0	1.36	w	.02	$\alpha_1+\alpha_2$
13.1.0	1.26	0	.01	$\alpha_1+\alpha_2$
14.1.0	1.17	0	.00	$\alpha_1+\alpha_2$
15.1.0	1.09	0	.01	$\alpha_1+\alpha_2$
16.1.0	1.03	0	.00	$\alpha_1+\alpha_2$
17.1.0	0.97	w	.00	$\alpha_1+\alpha_2$
18.1.0	0.91	w	.11	$\alpha_1+\alpha_2$

TABLE 7—*Continued*

Indices (*hkl*)	Spacing (calculated)	Relative intensity		CuK-radiation
		(Observed)	(Calculated)	
19.1.0	0.87	m	.12	α_1
20.1.0	0.82	w	.01	α_1
100	16.54	0	.01	$\alpha_1+\alpha_2$
200	8.27	0	.00	$\alpha_1+\alpha_2$
300	5.51	0	.00	$\alpha_1+\alpha_2$
400	4.14	0	.00	$\alpha_1+\alpha_2$
500	3.31	0	.00	$\alpha_1+\alpha_2$
600	2.76	0	.00	$\alpha_1+\alpha_2$
700	2.36	0	.00	$\alpha_1+\alpha_2$
800	2.07	m	6.43	$\alpha_1+\alpha_2$
900	1.84	0	.00	$\alpha_1+\alpha_2$
10.0.0	1.65	0	.00	$\alpha_1+\alpha_2$
11.0.0	1.50	0	.00	$\alpha_1+\alpha_2$
12.0.0	1.38	0	.00	$\alpha_1+\alpha_2$
13.0.0	1.27	0	.00	$\alpha_1+\alpha_2$
14.0.0	1.18	0	.00	$\alpha_1+\alpha_2$
15.0.0	1.10	0	.00	$\alpha_1+\alpha_2$
16.0.0	1.03	s	1.38	$\alpha_1+\alpha_2$
17.0.0	0.97	0	.00	$\alpha_1+\alpha_2$
18.0.0	0.92	0	.00	$\alpha_1+\alpha_2$
19.0.0	0.87	0	.00	α_1
20.0.0	0.83	w	.02	α_1

* Denotation of symbols: s, strong; m, medium; w, weak.

† The symbol $\alpha_1+\alpha_2$ denotes an unresolved spot resulting from α_1 and α_2 rays together; the symbol α_1 denotes a spot resulting from α_1 rays alone.

and the intensities I_w of the unresolved α_1 and α_2 spots on the same films from the formula

$$I_w = 1.5 \frac{1 + \cos^2 2\theta}{\sin 2\theta} |F|^2.$$

The atomic *f*-values of James and Brindley[24] were used except that in view of the substitution of silver atoms for some of the gold atoms, a composite value made up of 79 per cent of the *f*-value of gold and 21 per cent of the *f*-value of silver was used in place of the *f*-value of gold. No correction was made for absorption. However, it was observed that an equator Weissenberg photograph of a very small crystal (of cross section 0.04 mm. by 0.08 mm.) exhibited relative intensities closely similar to those of a considerably larger one (of cross section 0.36 mm. by 0.60 mm.), both crystals being oscillated about the *c*-axis. The intensities used are relative and were estimated visually. For computation of a Fourier series leading to the construction of the projection of the struc-

[24] James, R. W., and Brindley, G. W.: *Z. Krist.*, **78**, 475 (1931).

ture on the plane 001, the intensities on the Weissenberg equator photograph taken with the crystal rotating around the c-axis were used, and these were obtained by visual comparison of the diffraction spots on the film with a standard scale of spots prepared in the Department of Chemistry of The Johns Hopkins University.[25] On this standard scale the intensities are taken to be proportional to the exposure times of the spots to a beam of constant energy output. The observed intensities obtained by comparison with the standard scale were multiplied by 2/3 for the spots in which the $\alpha_1\alpha_2$-doublet is not resolved to reduce them to the same basis as the spots due to α_1-radiation alone. The resulting values divided by the Lorentz and polarization factors yielded numbers proportional to the squares of the absolute values of the structure factors. The square roots of these numbers were extracted and positive and negative signs were affixed in accordance with the signs of the F's obtained from the structure arrived at by comparison of observed and calculated intensities. The experimental F-values are listed in Table 8, along with the calculated F-values, which are given for comparison. The synthesis of the two-dimensional Fourier series was carried out by the method divised by Patterson[26] and improved by Patterson and Tunell.[27] The values of $A(x, y)=\rho(x, y)+K$, where $\rho(x, y)$ denotes the projected electron density and K denotes a constant, were computed at 900 points in the quarter projection, corresponding to division of each of the unit cell edges into 60 parts. Vertical sections were drawn along the lines of the grid work parallel to the b-axis, and from them a contour map of $A(x, y)$ was plotted (Fig. 3). The positions of the atoms found from the contour map are as given at the beginning of this section.

Discussion of the Atomic Arrangement

In the krennerite structure each gold (or silver) atom is surrounded by six tellurium atoms. The orientation of the distorted octahedra is most easily seen from Fig. 1A. Two neighbors of each gold (or silver) atom have their centers situated nearly on a line passing through the center of the gold (or silver) atom parallel to the b-axis; the other four neighbors have their centers not far from a plane passing through the center of the gold (or silver) atom perpendicular to the b-axis. The tellurium atoms also are surrounded by six neighbors, in some cases by three gold (or silver) atoms and three tellurium atoms, in others by five gold (or silver) atoms and one tellurium atom, and in still others by one

[25] The writers are indebted to Dr. David Harker for the use of this scale.

[26] Patterson, A. L.: *Phil. Mag.* (7), **22,** 753–754 (1936).

[27] Patterson, A. L., and Tunell, G.: *Am. Mineral.*, **27,** 655–679 (1942).

TABLE 8. OBSERVED AND CALCULATED VALUES OF THE STRUCTURE FACTOR F (The upper figure in each square is the observed value; the lower figure in each square is the calculated value.)

k \ h	0	1	2	3	4	5	6	7	8	9	10	11	12	13	14	15	16	17	18	19	20
11	−8. −8.7	−8. −4.7	+13. +8.2	−7. −5.1	+6. +6.4																
10	0. +5.7	+11. +5.3	+23. +12.3	+105. +42.6	+128. +54.2	−110. −42.7	+27. +10.9	−9. −3.7	0. +6.3	+7. +4.8											
9	+22. +21.4	0. +1.7	0. +1.0	0. −2.7	0. −1.3	0. −2.9	0. +2.3	−23. −9.3	+66. +31.4	0. −9.3	0. +0.2	0. +1.8	−7. −1.9								
8	0. −1.5	0. +3.3	−8. −3.6	+8. +1.4	0. +2.5	0. +0.4	0. +2.1	0. −2.0	0. −2.2	0. +2.7	0. −8.1	+12. +1.4	0. +3.9	+9. +3.4	0. +6.4						
7	0. +0.9	0. +4.3	+21. +20.9	+98. +50.2	+98. +49.6	−99. −20.3	+20. +14.5	0. −3.9	0. +2.0	+8. +8.4	+21. +23.3	+115. +45.4	+110. +41.5	−102. −24.8	+11. +8.0	0. −2.3	+7. +4.1				
6	+106. +65.2	−10. +8.5	0. +2.1	−7. −6.0	+7. −2.3	+8. +9.2	−8. +3.6	−21. −16.8	+103. +58.0	0. −0.3	0. +0.3	+8. +4.6	+8. −0.9	0. +11.9	0. +4.1	−31. −21.2	+92. +46.0	−8. −5.1			
5	0. +2.0	0. +5.6	−9. −9.6	+6. +7.3	0. −1.7	−7. −8.1	−10. −7.8	+7. −2.6	−8. +1.0	0. +4.3	−8. −8.2	+8. +2.6	0. +0.5	−8. −4.8	−11. −5.2	+7. +1.4	−7. −0.8	0. +1.0	0. −6.3		
4	0. −3.8	+5. +3.7	+14. +25.5	+22. +45.4	+22. +35.7	−47. −40.8	+17. +13.5	0. −5.4	−7. −2.3	+10. +1.8	+29. +29.1	+72. +41.2	+31. +26.4	−22. −23.8	+8. +3.6	0. −5.0	−7. +0.2	−10. +0.3	+28. +27.8	+71. +35.9	
3	+74. +127.3	−4. +9.4	0. +0.6	0. −6.1	0. −0.8	+5. +9.6	0. +2.9	−16. −14.9	+106. +103.9	0. +1.9	0. −1.6	+8. −1.4	+8. +2.2	0. +6.5	0. +3.3	−21. −16.0	+104. +73.7	0. −1.9	+6. −3.9	+10. +1.2	+13. +5.7
2	0. +0.8	0. +2.2	0. −2.4	0. +1.6	0. −1.1	−5. −6.8	−5. −7.7	0. +1.6	0. +0.2	+6. +2.7	0. +4.1	0. −5.9	0. +0.7	−8. −5.6	−8. −8.8	+8. +5.0	0. −0.6	−11. −0.6	+10. +6.8	0. −10.1	+8. +2.1
1	0. −3.9	0. +2.8	+8. +17.1	+9. +23.3	+5. +13.7	−6. −13.5	0. +3.7	0. −5.5	0. −2.8	−9. +0.9	+9. +21.7	+19. +24.8	+11. +9.8	0. −6.1	0. −3.8	0. −6.8	0. −1.3	−11. +1.2	+19. +21.7	+30. +24.3	+17. +7.0
0		0. 0.	0. −0.9	0. 0.	0. +0.7	0. 0.	0. +2.0	0. 0.	+68. +128.0	0. 0.	0. −3.0	0. 0.	0. +4.0	0. 0.	0. +4.8	0. 0.	+107. +86.2	0. 0.	0. −3.4	0. 0.	+9. +7.5

gold (or silver) atom and five tellurium atoms. In all cases two neighbors of each tellurium atom have their centers situated nearly on a line through the center of the tellurium atom parallel to the *b*-axis; the other four neighbors have their centers not far from a plane through the center of the tellurium atom perpendicular to the *b*-axis. The distances between the gold (or silver) and the tellurium atoms are 2.66, 2.99, 2.99, 2.67, 2.63, 2.87, 3.15, 2.95, 3.22, 2.66, 2.63, 2.94, and 3.04 Å. The distances between the tellurium atoms are 3.51, 3.08, 3.34, 3.54, 3.02, 3.28, and 3.54 Å. All these distances are shown in Fig. 1*A*. The structure can be described as consisting of lines of atoms parallel to the *b*-axis. These lines are at $x=0$, $z=0$, at $x=0.124$, $z=0.500$, and at $x=0.250$, $z=0.014$. Along each of these lines gold (or silver) atoms are separated by pairs of tellurium atoms, the gold (or silver) atoms lying exactly on the line and the tellurium atoms close to it. The gold (or silver) atoms also lie in corrugated sheets with two layers of tellurium atoms, in similar corrugated sheets, between successive corrugated sheets of gold (or silver) atoms. The zigzag pattern of the corrugated sheets is clearly shown in projection on the basal plane in Fig. 1*A*.

Acknowledgment

The authors are greatly indebted to Mrs. Ruth P. Tunell for carrying out many of the calculations and for making the drawing of Fig. 1. We also wish to express our appreciation to Professor Charles Palache, Professor M. A. Peacock, Dr. W. F. Foshag, and Dr. A. H. Koschmann for supplying the crystals investigated, to Mrs. Edward Teller for translating the article by Sipöcz from the Hungarian, to the late Dr. R. C. Wells for facilitating the chemical analysis of the krennerite crystals in the Chemical Laboratory of the Geological Survey, to Mr. H. A. Schmidt, Jr., for skillfully constructing the model, and to Mr. J. Harper Snapp for photographing the model.

DIFFERENTIAL THERMAL ANALYSIS CURVES OF CARBONATE MINERALS*

Carl W. Beck, *University of New Mexico, Albuquerque, New Mexico.*

Abstract

Fifty-one differential thermal analysis curves are presented and interpreted. These curves are of forty-eight carbonate minerals, one artificial carbonate, one oxide mineral, and one artificial oxide.

Introduction

Differential thermal analysis studies were made on forty-eight carbonate minerals, one artificial carbonate, one oxide mineral, and one artificial oxide. The differential thermal analysis curves resulting from these studies are shown in Figs. 1–9. The discussion of the carbonates will follow the proposed classification to be used in Volume 2 of the 7th edition of Dana's *System of Mineralogy* now in preparation at Harvard University. A description of the apparatus used in the present study has been given in an earlier publication (Beck, 1950).

Usually the compounds were heated from room temperature to 1000° C. When this gave a curve that was difficult to interpret because of more than one reaction phase, additional runs were made on the original compounds. These additional runs were stopped at appropriate intermediate reaction phases as indicated by the thermal peaks. Optical and powder *x*-ray studies were made on these phases to aid in the interpretation of the thermal curves.

Chemical analyses were made on some of the minerals, but for the most part the identification of the minerals was established by optical and *x*-ray data. The chemical analyses appear in Table 7.

The numbers in parentheses after mineral names represent the minerals in the Harvard collection from which the samples were taken.

The abbreviation "DTA" should be read "differential thermal analysis."

The temperatures are in degrees Centigrade.

Procedure

The heating portion of the apparatus used by the author is modelled after that of Berkelhamer (1945). The recording portion of the apparatus

* Abridged from a Ph.D. thesis, "An Improved Method of Differential Thermal Analysis and Its Use in the study of Natural Carbonates", Harvard University, 1946. Contribution from the Department of Mineralogy and Petrography, Harvard University No. 322.

is an Esterline-Angus Graphic Ammeter, appropriately amplified. Briefly, the basic principle of the amplifier is: the direct voltage generated in the thermocouple by a thermal reaction is changed to alternating voltage; the alternating voltage is then amplified to a desired amount; and, finally, the amplified alternating voltage is rectified to direct voltage in order to operate the Esterline-Angus recorder. The amplifier has a selector switch designed to pick off five different portions of the output voltage to give sensitivity Scales 1, 2, 3, 4, and 5. A comparison of the sensitivity of the different scales is shown in Table 1. The thermal changes are recorded equally well by the pen and ink recorder as by the more conventional photographic method. In addition, the author believes the pen and ink recorder, because of continual visual observation of the curve, is superior in the precision with which a thermal run may be stopped at any desired phase. The author's method of making a differential thermal analysis run is comparable to that used by other investigators.

Table 1. Comparison of the Sensitivity of the Different Scales of the Non-Photographic Recorder

Scale	Average value of ΔT for 1 cm. deflection, °C.
1	4.1
2	2.4
3	0.85
4	0.21
5	0.10

Experimental Results

Acid Carbonates

The differential thermal analysis curves of the acid carbonates are shown in Fig. 1.

Nahcolite, $HNaCO_3$ (92481) ($\alpha = 1.380$, $\beta = 1.500$, $\gamma = 1.585$). The specimen is from Searles Lake, California. The DTA curve shows an endothermic reaction beginning at 135°, reaching a peak at 205°, and ending at 225°. The endothermic reaction is the loss of H_2O and CO_2.

The small peak at 630° is due to an admixture of magnesite. The area under this curve corresponds to 5.55% magnesite. A quantitative analysis by the author for magnesium shows 6.71% magnesite. The random deflections around 750° are due to fusing of the Na_2CO_3 at a temperature lower than the recorded fusing point of Na_2CO_3, namely 851° (Handbook of Chemistry and Physics).

Trona, $HNaCO_3 \cdot Na_2CO_3 \cdot 2H_2O$ (84568) ($\alpha = 1.414$, $\beta = 1.495$, $\gamma = 1.541$). The specimen is from an unknown locality. The DTA curve shows an endothermic reaction beginning at slightly below 100°, reaching a peak at 170°, and ending at 185°. The decomposition product is Na_2CO_3, hygroscopic in nature. The break in the curve is due to the loss of the two molecules of water of crystallization and the decomposition of the acid sodium carbonate part of the trona structure. The latter decomposition reaches

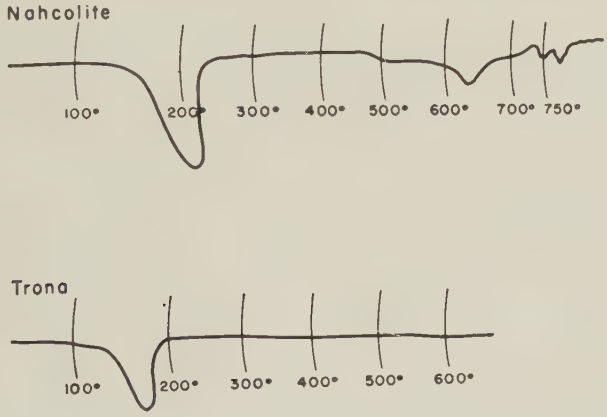

FIG. 1. Differential thermal analysis curves of the acid carbonates.

a peak at a lower temperature than the nahcolite decomposition. Two factors contribute to this: (1) the loss of the water of crystallization partially destroys the compound, increases the surface area, and makes further thermal decomposition easier; and (2) the acid carbonate makes up only 37.2% by weight of the trona structure.

TABLE 2. CHARACTERISTIC THERMAL PEAKS AND AREAS OF THE ACID CARBONATES

Mineral	Reaction product	Peak temperature, ° C.	Area, mm.²	Weight, gm.	Scale
Nahcolite	H_2O, CO_2	205	400	0.330	2
Trona	H_2O, CO_2	170	195	0.250	3

Anhydrous Normal Carbonates

I. *Calcite Group.*

A. Calcite series. The DTA curves of the calcite series are shown in Fig. 2.

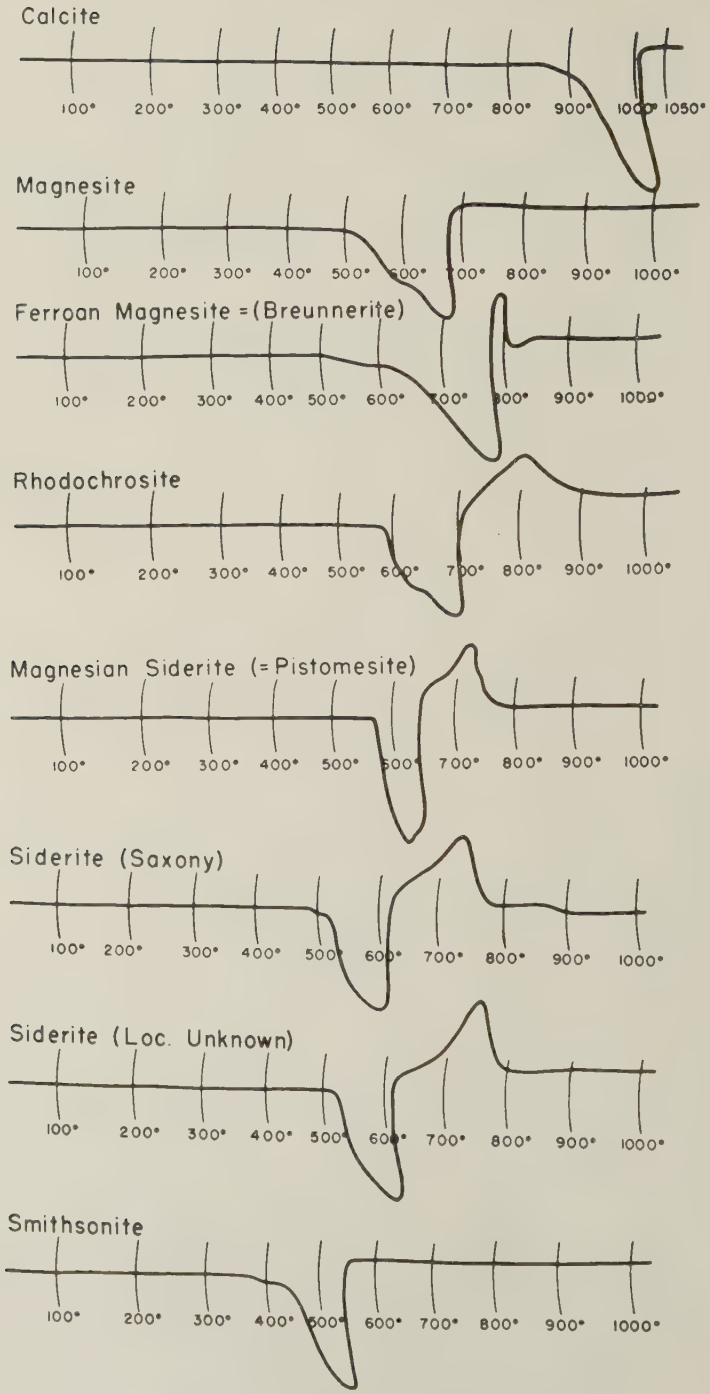

FIG. 2. Differential thermal analysis curves of the calcite series.

1. Calcite, $CaCO_3$, ($\omega = 1.658$, $\epsilon = 1.486$). The specimen is from Canada, a clear cleavage fragment of Iceland Spar. The endothermic decomposition begins at 850°, reaches a peak at 990°, and ends rapidly at 1005°.
2. Magnesite, $MgCO_3$ ($\omega = 1.703$, $\epsilon = 1.511$). The specimen is from Styria, Austria. The decomposition begins slowly at 470°, reaches a peak at 660°, and ends rapidly at 685°. The curve flattens out from approximately 570° to 600°, then the slope increases to the peak at 660°. Brill (1905) studied the dissociation of artificial normal magnesium carbonate and reported a series of small breaks corresponding to many intermediate magnesium oxy-carbonates, and one large break corresponding to $MgO \cdot MgCO_3$. Davis (1906) and Friedrich and Smith (1912) dispute the findings of Brill because neither of their investigations revealed any discontinuities in the decomposition of artificial normal magnesium carbonate. Similarly, Šplíchal, Škramovský, and Goll (1936) detected no oxy-carbonates during the decomposition of magnesium carbonate. In an effort to determine if the change in slope of the DTA curve of magnesite is due to the formation of an intermediate oxy-carbonate, optical and powder *x*-ray studies were made on the starting magnesite, on the decomposition product formed when magnesite is heated to 1000°, and on the decomposition product formed when magnesite is heated to 575°. The 1000° product is periclase, $n = 1.736$. The 575° product gives the same *x*-ray lines as the starting magnesite but the spacings are slightly different. This difference becomes greater with smaller *d's*. Optically the grains are cloudy due to decomposition; they are composed of a very fine-grained aggregate so that a grain does not show extinction between crossed nicols. The average $n =$ about 1.72. The evidence for the formation of an intermediate oxy-carbonate is, therefore, inconclusive.
3. Ferroan Magnesite (= breunnerite), $(Mg, Fe)CO_3$, ($\omega = 1.726$, $\epsilon = 1.528$). The specimen is from Gustine, Stanislaus County, California. The chemical analysis shows 15.31% $FeCO_3$ (Table 7). The decomposition is slow from 500° to 590°, then proceeds more rapidly to the peak at 755°, and overlaps the exothermic peak representing the oxidation of ferrous oxide to ferric oxide. The latter reaches a peak at 785°. The area of the exothermic peak corresponds to 19.3% $FeCO_3$ (compare siderite), a good check with the chemical analysis. Powder

x-ray pictures show the breunnerite has the spacing of magnesite, and the decomposition product has the spacing of periclase.

4. Rhodochrosite, $MnCO_3$. The specimen is from Butte, Montana. The decomposition begins rapidly at 580°, proceeds more slowly from 615° to 625°, reaches a peak at 680°, and immediately overlaps the exothermic peak representing the oxidation of the decomposition product to Mn_3O_4. The exothermic peak is at 795°. Mn_3O_4 is the stable oxide of manganese at elevated temperatures (Pavlovitch, 1935; Mellor, Vol. XII). The curve in the region of 580-680° is probably the resultant of the decomposition of $MnCO_3$ to MnO, oxidation of MnO to Mn_2O_3, and decomposition of Mn_2O_3 to Mn_3O_4.
5. Siderite, $FeCO_3$, ($\omega = 1.869$, $\epsilon = 1.628$). The specimen is from Lodenstein, Saxony. The curve is characterized by the endothermic decomposition followed by the exothermic oxidation of ferrous oxide to ferric oxide. That the oxidation product was ferric oxide was determined by a powder x-ray picture. The endothermic reaction begins at 500–525°, reaches a peak at 585°, and ends at 605°. The oxidation takes place at 625°, reaches a peak at 735°, and ends at 765°.
6. Siderite, $FeCO_3$, ($\omega = 1.871$, $\epsilon = 1.630$). The specimen is from an unknown locality. The endothermic break is at 515°, reaches a peak at 590°, and ends at 615°. The exothermic break begins at 650°, reaches a peak at 740°, and ends at 790°.
7. Magnesian Siderite (=pistomesite), $(Fe,Mg)CO_3$ (73911), ($\omega = 1.814$, $\epsilon = 1.588$). The specimen is from Traversella, Piedmont, Italy. The decomposition begins very rapidly at 575°, reaches a peak at 580°, and merges with an exothermic curve. The exothermic curve reaches a peak at 725° and ends at 770°. The endothermic break is due to the decomposition of the $FeCO_3$ and $MgCO_3$, and the exothermic curve is due to the oxidation of ferrous oxide to ferric oxide. The area under the exothermic peak corresponds to about 65% $FeCO_3$, a close check with the chemical analysis (Table 7). The decomposition product is the compound magnesio-ferrite, $MgO \cdot Fe_2O_3$, identified by a powder x-ray picture.
8. Smithsonite, $ZnCO_3$, ($\omega = 1.851$, $\epsilon = 1.620$). The specimen is from Magdalena, New Mexico. The decomposition begins slowly at 425°, reaches a peak at 525°, and ends at 550°. The decomposition product is ZnO.

B. *Dolomite series.* The DTA curves for the dolomite series are shown in Fig. 3.

1. Dolomite, $CaMg(CO_3)_2$, ($\omega = 1.684$, $\epsilon = 1.502$). The specimen is from West Roxbury, Vermont. The DTA curve has two endothermic breaks: the first begins at 750°, reaches a peak at 815°, and ends at 845°; the second begins at 855°, reaches a peak at 965°, and ends at 985°. The first peak is due to the decomposition of the $MgCO_3$ part of the dolomite structure and takes place at a temperature 155 degrees higher than the peak temperature for magnesite. The second peak is due to the complete decomposition of the dolomite structure and takes place at a temperature 25 degrees lower than the decomposition peak of calcite. A powder *x*-ray picture of a sample heated to 850° shows lines of calcite and MgO. The final decomposition product is a mixture of MgO and CaO.
2. Ferroan Dolomite (=ankerite), $Ca(Mg,Fe)(CO_3)_2$ (80383), ($\omega = 1.700$, $\epsilon = 1.519$). The specimen is from Phoenixville, Pennsylvania. The DTA curve is characterized by three endothermic peaks and one exothermic peak. The first endothermic peak is due to the decomposition of the $FeCO_3$ part of the structure; this reaction begins rapidly at 725°, reaches a peak of 740°, an ends at an indeterminate temperature because this curve merges with the exothermic curve due to the oxidation of ferrous oxide to ferric oxide. The exothermic peak is at 785°. The exothermic peak merges slowly with the endothermic peak due to the decomposition of the $MgCO_3$ part of the ankerite structure. This second endothermic peak is at 890°, and this second curve merges with the final endothermic peak due to the complete decomposition of the carbonate. The final curve reaches a peak at 960°. Powder *x*-ray pictures show the starting ankerite has the same spacing as dolomite, and the final decomposition product is a mixture of CaO and $MgO \cdot Fe_2O_3$ (magnesio-ferrite).
3. Ferroan Dolomite (=ankerite), $Ca(Mg, Fe)(CO_3)_2$, ($\omega = 1.716$, $\epsilon = 1.527$). The specimen is from the Tri-State District. This curve is similar to the ankerite curve discussed above. The differences may be explained by differences in chemical composition. No chemical analysis was made for the Phoenixville ankerite, but the indices of refraction indicate it is lower in $FeCO_3$ than is this Tri-State ankerite specimen. This is reflected in the areas of the iron oxidation break. The final decomposition product is again a mixture of CaO and $MgO \cdot Fe_2O_3$.

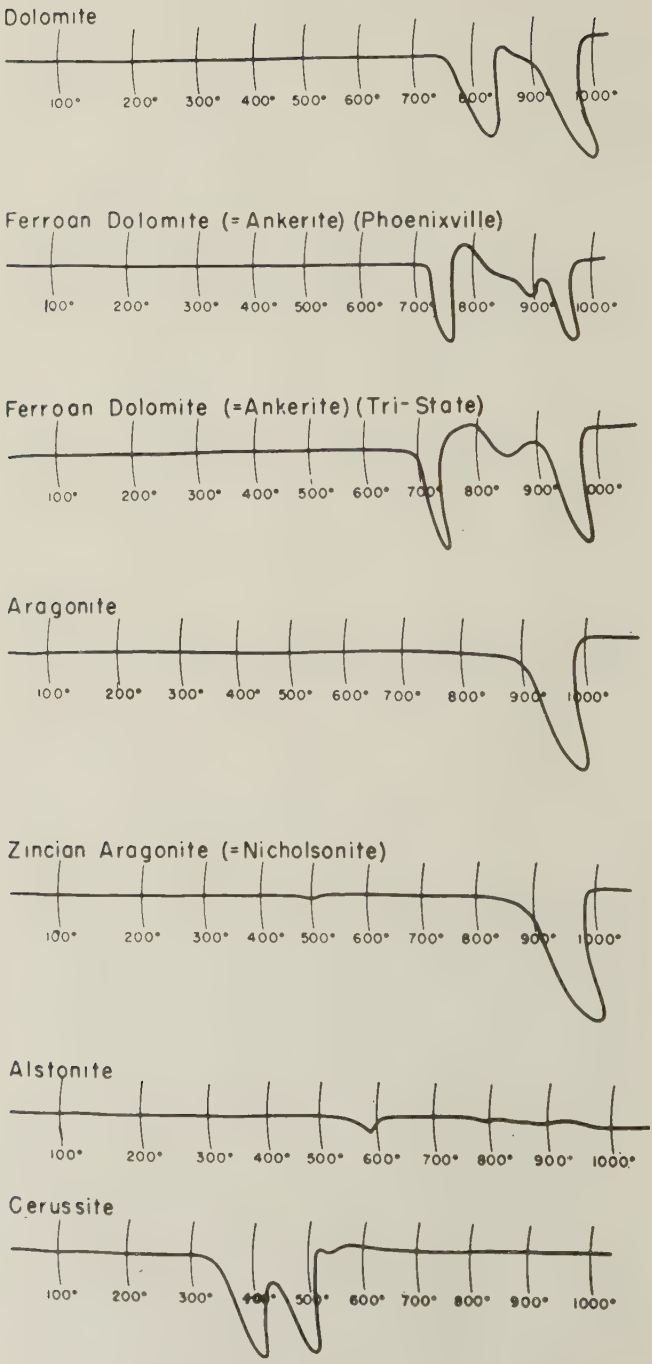

FIG. 3. Differential thermal analysis curves of the dolomite series and the aragonite group.

A powder x-ray picture of the product formed when this ankerite is heated to 790° checks no listed compound.

II. *Aragonite Group*. The DTA curves for the aragonite group are shown in Fig. 3.

A. Aragonite, $CaCO_3$, ($\alpha = 1.530$, $\beta = 1.680$, $\gamma = 1.685$). The specimen is from Staditz, Bohemia. The decomposition begins at 850°, reaches a peak at 965°, and returns to the line of zero deflection at 980°. Argonite changes into calcite when heated above 450°. In this study there was no break in the DTA curve to show this transformation. Cuthbert and Rowland (1947) likewise show no inversion point in their aragonite curve. However, recently Faust (1949) reported a small endothermic break in the aragonite curve at 447°.

B. Zincian Aragonite (=nicholsonite), $(Ca,Zn)CO_3$ (90299), ($\alpha = 1.532$, $\beta = 1.680$, $\gamma = 1.688$). The specimen is from Tsumeb, S. W. Africa. The tiny endothermic break at 500° is probably due to the small amount of $ZnCO_3$ in this specimen. A quantitative analysis by the author for $ZnCO_3$ revealed 1.24%. The analysis is not very accurate because of the small amount of sample available, but it reveals the extent of isomorphous substitution of Zn for Ca. The large endothermic break is due to the decomposition of the $CaCO_3$. It begins at 840°, reaches a peak at 970°, and ends at 985°, a close check with pure aragonite.

C. Alstonite (=bromlite), $(Ba,Ca)CO_3$ (80396). The specimen is from Cumberland, England. The DTA curve shows that alstonite is not susceptible to differential thermal treatment with the apparatus used in this investigation because the decomposition of the compound is above the temperature range which can be detected using chromel-alumel differential thermocouples.

The small endothermic break at 585° probably represents a substitution of Mg for Ca and/or Ba. The area corresponds to about 3% $MgCO_3$. Analyses of alstonite reported in Dana's *System of Mineralogy* (Sixth edition, 1892, p. 284) show that Mn is the common substitute for Ca and Ba. However, the break at 585° does not represent the decomposition of $MnCO_3$ because it is not followed by the characteristic exothermic peak (compare rhodochrosite, Fig. 2).

D. Cerussite, $PbCO_3$. The specimen is from Wallace, Idaho. The DTA curve is characterized by a double endothermic break, each part representing approximately the same thermal energy. The decomposition begins at 320°, reaches a peak at 395°, merges

TABLE 3. CHARACTERISTIC THERMAL PEAKS AND AREAS OF THE ANHYDROUS NORMAL CARBONATES

Mineral	Reaction product	Peak temperature, ° C.		Area, mm.²	Weight, gm.	Scale
		Endothermic	Exothermic			
Calcite	CO_2	990		740	0.500	2
Magnesite	CO_2	660		900	0.500	2
Breunnerite	CO_2, MgO	755		860	0.530	2
	Fe_2O_3		785	62		
Rhodochrosite	CO_2	680		595	0.470	2
	Mn_3O_4		795	315		
Siderite (Lodenstein)	CO_2	585		615	0.540	2
	Fe_2O_3		735	320		
Siderite (Loc. unkn.)	CO_2	590		605	0.520	2
	Fe_2O_3		740	295		
Pistomesite	CO_2	580		510	0.580	2
	$MgO \cdot Fe_2O_3$		725	200		
Smithsonite	CO_2	525		495	0.500	2
Dolomite	CO_2	815		315	0.500	2
	CO_2	965		435		
Ankerite (Phoenixville)	CO_2	740		160	0.505	2
	Fe_2O_3		785	45		
	CO_2	890		355		
	CO_2	960				
Ankerite (Tri-State)	CO_2	720		305	0.465	2
	Fe_2O_3		795	20		
	CO_2	850		130		
	CO_2	965		330		
Aragonite	CO_2	965		475	0.410	2
Nicholsonite	CO_2	500		small	0.510	2
	CO_2	970		625		
Cerussite	CO_2	395		810	1.050	2
	CO_2	490				

with the second curve which reaches a peak at 490°, and ends at 510°. The decomposition may take place according to:

$$2PbCO_3 + \text{heat} = PbO \cdot PbCO_3 + CO_2$$
$$PbO \cdot PbCO_3 + \text{heat} = 2PbO + CO_2$$

To test this theory a powder *x*-ray study was made of decomposition samples taken at 425° and 550°. The sample heated to 550° showed the $PbCO_3$ had decomposed entirely to PbO (litharge). However, the sample heated to 425° gave *x*-ray lines which were not those of $PbCO_3$, PbO, nor a mixture of $PbCO_3$ and PbO. This gives support to the belief that an oxy-carbonate is formed during the decomposition of cerussite.

Cuthbert and Rowland (1947) report a third endothermic peak at about 860°. They suggest, following Tzentnershver, that the decomposition of cerussite is in three stages: $3PbO \cdot 5PbCO_3$, $2PbO \cdot PbCO_3$, and $PbO \cdot PbCO_3$. The author did not get the third peak; furthermore, the *x*-ray picture at 550° shows complete decomposition to PbO.

Hydrous Normal Carbonates

The DTA curves of the hydrous normal carbonates are shown in Fig. 4.

Gay-Lussite, $CaCO_3 \cdot Na_2CO_3 \cdot 5H_2O$ (76971), ($\alpha = 1.445$, $\beta = 1.515$, $\gamma = 1.522$). The specimen is from Lagunillo, Maracaibo, Venezuela. The DTA curve shows an overlapping endothermic doublet at 145° and 175° due to the loss of the water of crystallization in two distinct stages. The remainder of the curve is highly irregular due to the slow fusing of the mineral.

Nesquehonite, $MgCO_3 \cdot 3H_2O$ (77292), ($\alpha = 1.412$, $\beta = 1.501$, $\gamma = 1.526$). The specimen is from No. 2 Tunnel, Nesquehoning Carbon Company, Nesquehoning, Pennsylvania. The doublet endothermic curve is due to the loss of two molecules of water of crystallization. This reaction begins at 140°, reaches a double peak at 210–235°, and ends at 300°. The second endothermic curve is due to the loss of a third molecule of water. This reaction begins at 380°, reaches a peak at 425°, and ends at 475°. Powder *x*-ray studies indicate that this second reaction results in a seemingly amorphous MgO decomposition product. The decomposition of the remaining carbonate begins at 480°, reaches a doublet peak at 535° and 585°, and ends at 620°. The inversion of the amorphous (?) MgO to cubic MgO is superimposed upon the last endothermic reaction and is shown by the exothermic peak at 510°. By analogy with hydromagnesite and artinite (Fig. 6), the loss of the third molecule of water is like the loss of

basic water. The formula, therefore, might better be written $Mg(HCO_3)(OH)\cdot 2H_2O$, which would make the intermediate decomposition $Mg(HCO_3)(OH)$. Davis (1906) confirms this on artificial $MgCO_3\cdot 3H_2O$. He reports that the third molecule of water comes off with the evolution of CO_2.

Optical and powder x-ray studies were made on the decomposition

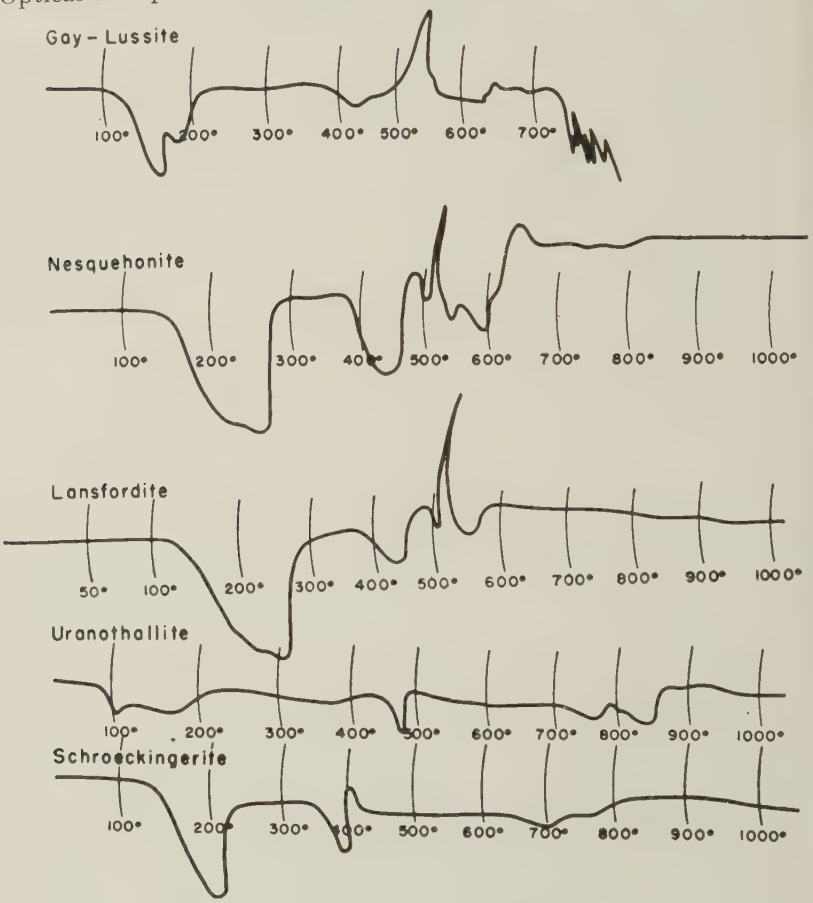

FIG. 4 Differential thermal analysis curves of the hydrous normal carbonates.

products when nesquehonite was heated to 325°, 470°, 515°, and 1000° The 325° product gives the spacing of no listed compound. Most of th grains retain an orthorhombic external shape. They are diffused, but n amorphous material is present. A few of the grains are still nesquehonite some are mostly decomposed but retain a little nesquehonite, but mos are entirely decomposed. Average $n = 1.425$. The 470° product gives th

spacing of no listed compound. There is a broad, amorphous band at $d = 2.45$ Å. Optically the product appears isotropic with $n =$ about 1.545. The 515° product shows periclase lines. The 1000° product is periclase.

Table 4. Characteristic Thermal Peaks and Areas of the Hydrous Normal Carbonates

Mineral	Reaction product	Peak temperature, °C.		Area, mm.²	Weight, gm.	Scale
		Endothermic	Exothermic			
Gay-Lussite	H_2O	145		400	0.250	3
	H_2O	175				
Nesquehonite	H_2O	210–235		865	0.280	3
	OH^-	425		355		
	MgO?		510	small		
	CO_2	535–585		355		
Lansfordite	H_2O	210–235		760	unknown	3
	OH^-	440		155		
	MgO?		510	small		
	CO_2	555		100		
Uranothallite	?	110		170	0.140	3
	?	175				
	?	475		65		
	?	750		140		
	?	890				
Schroeckingerite	?	190		400	0.295	3
	?	385		75		
	?		410	15		
	?	700		indefinite		

Lansfordite, $MgCO_3 \cdot 5H_2O$ (77072). The specimen is from the No. 2 Tunnel, Nesquehoning Carbon Company, Nesquehoning, Pennsylvania. The sample required special treatment to make the run. Lansfordite rapidly loses two molecules of water on standing at room temperature to form nesquehonite. The mineral specimen at Harvard had been kept under oil. To ready it for a differential thermal analysis run the specimen was cleaned with ether and kept under ether. The run was started from room temperature instead of 50°. Because only enough sample was available to fill about $\frac{1}{5}$ of the sample hole, the hole was partly filled with inert alumina, then the lansfordite was packed around the thermojunction, and the remainder of the hole was filled with more alumina.

The reaction begins at 115°, reaches a doublet peak at 210–230°, and ends at 275°. This curve is due to the volatilization of four molecules of water. The second endothermic curve, due to the loss of a fifth molecule of water, begins at 375°, reaches a peak at 440°, and ends at 480°. The exothermic peak at 510°, by analogy with nesquehonite, is the inversion of amorphous (?) MgO to cubic MgO. The third endothermic curve is due to the loss of CO_2. It begins at 490°, reaches a peak at 555°, and ends at 575°. Unlike nesquehonite, this latter deflection has but one peak.

Uranothallite, $Ca_2U(CO_3)_4 \cdot 10H_2O$ (?) (94861). The specimen is from Joachimsthal, Bohemia. Any interpretation of the DTA curve would be speculative because (1) not enough material was available to permit the stopping of a run at different phases, and (2) the composition of this, and other uranium carbonates is not definitely determined.

Schroeckingerite, $NaCa_3(UO_2)(CO_3)_3(SO_4)F \cdot 10H_2O$. The specimen is from near Wamsutter, Wyoming, and is Larsen's (Larsen and Gonyer, 1937) type material. Again the interpretation of the DTA curve is difficult and is presented without comment. The above formula was assigned to schroeckingerite by Jaffe, Sherwood, and Peterson (1948), and verified in the laboratory of the U. S. Geological Survey by F. S. Grimaldi (in press). A powder *x*-ray picture of the final decomposition product is the same as the end product of the decomposition of uranothallite.

Carbonates Containing Hydroxyl or Halogen

Bastnäsite Group. The DTA curves of the bastnäsite group are shown in Fig. 5.

I. Bastnäsite, $CeFCO_3$ (88742), ($\omega = 1.719$, $\epsilon = 1.820$). The specimen is from Ampanbabe, Madagascar. The DTA curve shows that the loss of CO_2 begins slowly at 350°, has a characteristic shoulder at 470°, and reaches a peak at 625°. The endothermic curve merges with an exothermic curve. The latter reaches a peak at 650° and is due to the oxidation of cerous oxide to ceric oxide. Fluorine is lost during the run as shown by a slight attack on the nickel cover.

An *x*-ray picture of the final decomposition product gives the structure of CeO_2, but other lines suggest the presence of isostructural RO_2, where R = other rare earth elements.

II. Bastnäsite, $CeFCO_3$ (84440), ($\omega = 1.719$, $\epsilon = 1.820$). The specimen is from St. Peter's Dome, El Paso County, Colorado. The DTA curve is practically identical with that of the Madagascar bastnäsite.

III. "Tysonite," $(Ce,La,Di)F_3$ (82848), ($\omega = 1.718$, $\epsilon = 1.818$). The specimen, labeled "tysonite," is from Colorado. The DTA curve shows that the specimen is bastnäsite. The curve is practically identical with those of the two foregoing bastnäsite samples. Most bastnäsite is pseudomorphic after tysonite; therefore, the error in identification is not unnatural.

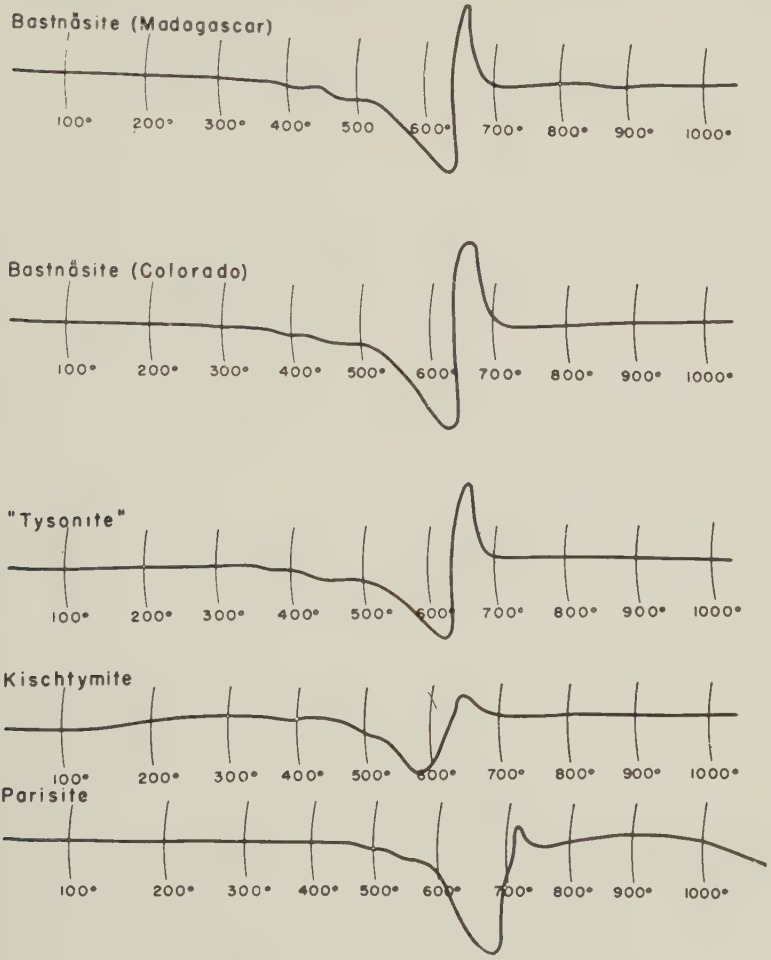

FIG. 5. Differential thermal analysis curves of the bastnäsite group.

IV. Kischtymite (= hydroxyl bastnäsite?) (84435), ($\omega = 1.711$, $\epsilon = 1.812$). The specimen is from Kischtymsk, U.S.S.R. The kischtymite DTA curve is similar to the bastnäsite curves. The smaller areas under the curves probably are due to the smaller amount of the mineral

that was available for analysis. Decomposition begins slowly about 360°, and reaches a peak at 580°. This peak is 40–45° lower than the corresponding bastnäsite peak; this may be partly, or entirely due to the smaller charge, or it may reflect a characteristic difference between kischtymite and bastnäsite. The end of the reaction is slower than in the case of the bastnäsites, and as a result the peak of the exothermic curve due to the oxidation of cerous to ceric oxide comes at the characteristic temperature, namely, 650°. From DTA alone kischtymite would be classified as bastnäsite.

V. Parisite, $2CeFCO_3 \cdot CaCO_3$ (11019), ($\omega = 1.675$, $\epsilon = 1.755$). The specimen is from Muso, Colombia. The decomposition begins at 470°, and reaches a peak at 660°. This endothermic curve merges with an exothermic curve that reaches a peak at 720°. The exothermic peak again represents the oxidation of cerous to ceric oxide. At 975° an endothermic break begins slowly; the run was stopped at 1100° and before the peak was reached.

The DTA curves for the remainder of the carbonates containing hydroxyl or halogen are shown in Figs. 6, 7, and 8.

Hydromagnesite, $3MgCO_3 \cdot Mg(OH)_2 \cdot 3H_2O$ (84570), ($\alpha = 1.522$, $\beta = 1.528$, $\gamma = 1.545$). The specimen is from Alameda, California. The decomposition begins slowly at 275–325° with the loss of the water of crystallization, reaches a peak at 375°, and merges with the curve representing the loss of basic water. The latter curve reaches a peak at 440°. These reactions result in the formation of amorphous (?) MgO which inverts to cubic MgO at 510° as shown by the exothermic curve. The loss of CO_2 begins at 485°, reaches a doublet peak at 565° and 600°, and ends at 610°. This curve is similar to the curves discussed above for nesquehonite and lansfordite save in this case the water of crystallization comes off at a higher temperature, high enough to overlap the loss of hydroxyl water.

Artinite, $MgCO_3 \cdot Mg(OH)_2 \cdot 2H_2O$, ($\alpha = 1.489$, $\beta = 1.534$, $\gamma = 1.556$). The specimen is from Luning, Nevada. The decomposition begins at 230° with the loss of the water of crystallization, reaches a peak at 280°, and ends at 305°. The loss of hydroxyl water begins at 385°, reaches a peak at 440°, and merges with the curve due to the loss of CO_2. This latter reaction has a peak at 540°, a characteristic shoulder at 575°, and ends at 585°. Superimposed upon this latter curve is an exothermic reaction which is of smaller magnitude than those recognized in nesquehonite, lansfordite, and hydromagnesite. However, this exothermic curve reaches a peak at 510°, and it is believed that it represents an inversion of amorphous (?) MgO to cubic MgO. The loss of the water of crystal-

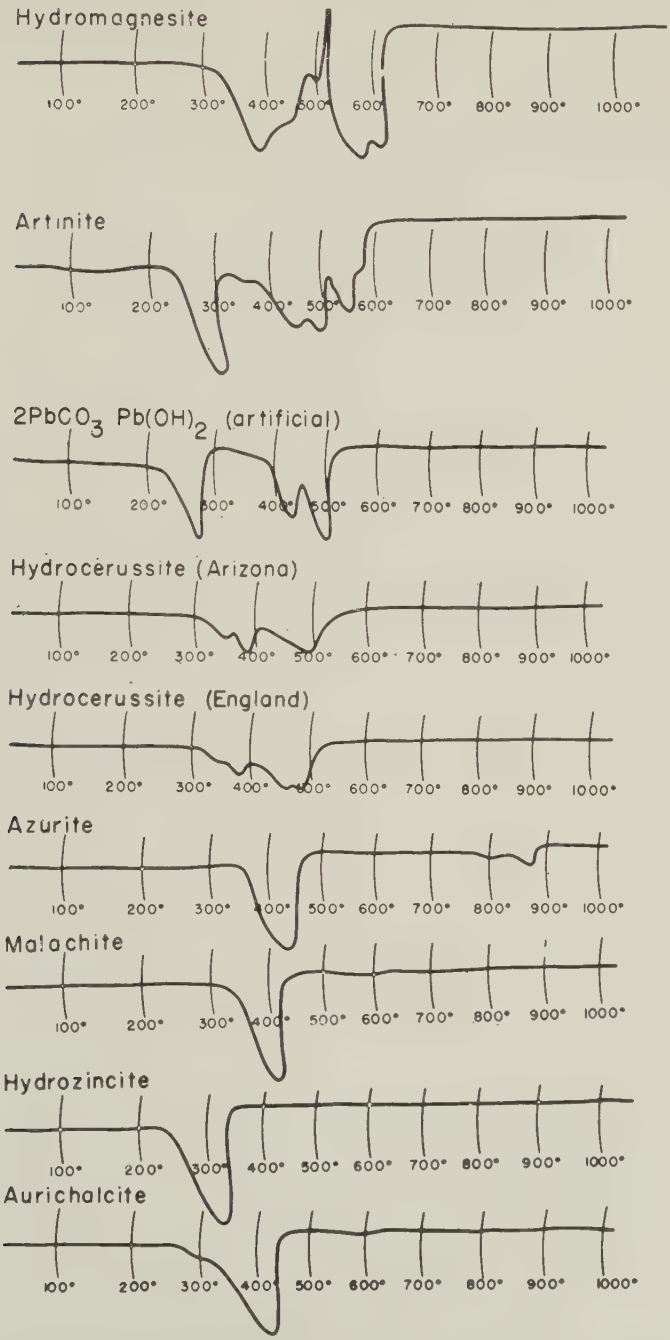

FIG. 6. Differential thermal analysis curves of carbonates containing hydroxyl.

lization is at a lower temperature than the corresponding reaction in hydromagnesite.

Hydrocerussite (artificial), $2PbCO_3 \cdot Pb(OH)_2$. The loss of hydroxyl water begins at 235°, reaches a peak at 270°, and ends at 290°. The decomposition of the carbonate is shown by the double endothermic break beginning at 380°, reaching peaks at 430° and 490°, and ending at 505°. This doublet peak is analogous to the decomposition of cerussite, and is likewise probably due to the formation of an intermediate oxy-carbonate before complete decomposition.

Hydrocerussite, $2PbCO_3 \cdot Pb(OH)_2$. The specimen is from Mammoth Mine, Arizona. The loss of hydroxyl water begins at 280–300°, reaches a peak at 345°, and merges with the double peak due to the loss of CO_2. This doublet reaches peaks at 385° and 500°, and ends at 550°. The natural hydrocerussite, therefore, loses its water at a temperature 75° higher than the artificial compound. On the other hand the first peak of the loss of CO_2 in the natural compound is at a temperature 45° lower than in the artificial compound, while the peak of the final decomposition is at approximately the same temperature for both.

Hydrocerussite, $2PbCO_3 \cdot Pb(OH)_2$. The specimen is from Mendip Hills, Somerset, England. The loss of hydroxyl water begins at 295° and merges completely with the first curve of the decomposition of the carbonate part of the structure. This latter reaction reaches a peak at 380° and merges with the second characteristic peak of the decomposition of $PbCO_3$. This second curve reaches a peak at 485°. The DTA curve for this specimen of hydrocerussite agrees very well with the run for the Arizona hydrocerussite.

Azurite, $2CuCO_3 \cdot Cu(OH)_2$, ($\alpha = 1.730$, $\beta = 1.758$, $\gamma = 1.838$). The specimen is from Tsumeb, S. W. Africa. The loss of hydroxyl water and CO_2 takes place in one endothermic break. The decomposition begins at 350°, reaches a peak at 430°, and ends at 475°. The decomposition product is tenorite, CuO, identified by a powder *x*-ray picture. The endothermic doublet at 850° and 930° is due to an admixture of dolomite.

Malachite, $CuCO_3 \cdot Cu(OH)_2$, ($\alpha = 1.655$). The specimen is from Tsumeb, S. W. Africa. The loss of water and CO_2 takes place in one endothermic break. The decomposition begins at 315°, reaches a peak at 385°, and ends at 420°. This decomposition takes place at a temperature 45 degrees lower than does the decomposition of azurite. The loss of hydroxyl water occurs at a lower temperature than does the loss of CO_2 in most compounds; and, since there is more hydroxyl water in malachite than in azurite, it is to be expected that the former would decompose at a lower

temperature than the latter. The decomposition product is again tenorite.

Hydrozincite, $2ZnCO_3 \cdot 3Zn(OH)_2$ (85740), ($\alpha = 1.636$, $\beta = 1.728$, $\gamma = 1.740$). The specimen is from Cumillas, Spain. The loss of hydroxyl water and CO_2 takes place in one endothermic break. The decomposition begins at 230°, reaches a peak at 310°, and ends at 340°. The decomposition product is zincite, ZnO.

Aurichalcite, $2(Zn,Cu)CO_3 \cdot 3(Zn,Cu)(OH)_2$ (80960). The specimen is from the Big Cottonwood District, Utah. The loss of hydroxyl water and CO_2 takes place in one endothermic break. The decomposition begins at 275°, has a characteristic shoulder at 300°, reaches a peak at 415°, and ends at 445°. The final decomposition product is a mixture of tenorite and zincite, with zincite dominating.

Bismutite, Bi_2CO_5 (84598). The specimen is from Engle Station,* New Mexico. The decomposition curve consists of a large endothermic break and a small endothermic break. The decomposition begins at 420°, reaches a peak at 495°, and ends at 520°. The smaller break begins immediately, reaches a peak at 605°, and ends at 640°. The third endothermic peak is due to the inversion of Bi_2O_3; it begins at 640° and reaches a peak at 710°. A powder *x*-ray picture shows the final decomposition product to be γ-Bi_2O_3, the body-centered cubic polymorph (Schumb and Rittner, 1943).

Bismutite, Bi_2CO_5 (90756). The specimen is from Petaca, New Mexico. The decomposition curve consists of two merging endothermic breaks. The decomposition begins at 400°, reaches a peak at 530°, merges with the second curve which reaches a peak at 625°, and ends at 695°. These temperatures are 20–50 degrees higher than the corresponding reactions in the Engle Station bismutite. The small endothermic peak at 730° is due to the inversion of the decomposition product, Bi_2O_3. That this is an inversion is shown by a cooling curve which gives the reinversion at about 715°.

Powder *x*-ray pictures of samples heated to 560° and 640° are identical with β-Bi_2O_3, the tetragonal or pseudocubic high temperature polymorph (Schumb and Rittner, 1943). Therefore, the second endothermic break is believed to be an inversion of β-Bi_2O_3 to an undetermined polymorph which changes back to β-Bi_2O_3 on cooling to room temperature.

Powder *x*-ray pictures of samples heated to 700° and 750° are identical and consist of a mixture of β-Bi_2O_3 and the simple cubic polymorph. The

* Presumably from the Grandview Canyon district, San Andres Mountains, New Mexico.

lines check very well with the spacing reported by Sillén (1938). Sillén reports that β-Bi_2O_3 kept molten several hours changes to a simple cubic polymorph. This transformation takes place only if impurities, such as silica, are present.

Bismutite, Bi_2CO_5. The specimen is from Willimantic, Connecticut. The DTA curve is similar to the DTA curve for the Engle Station, New Mexico bismutite. The decomposition begins at 400°, reaches a peak at 480°, and ends at 530°. The second endothermic curve begins at 135°, reaches a peak at 600°, and ends at 650°.

Powder x-ray pictures of samples heated to 525° and 700° are identical with γ-Bi_2O_3, the body-centered cubic polymorph. Again, the second endothermic break seems to represent an inversion which reinverts on cooling.

DTA curves were run on artificial Bi_2O_3 and bismite (Fig. 7). Powder x-ray pictures of both, before and after heating, give the spacing of α-Bi_2O_3, the monoclinic polymorph (Sillén, 1938; Schumb and Rittner, 1943). The inversion and reinversion of artificial Bi_2O_3 are shown on the DTA curve.

In summary, the first endothermic break in the DTA runs of the bismutite minerals is due to the loss of CO_2. The smaller second endothermic break probably represents an undetermined inversion. Sillén (1938) reports that such inversions are facilitated by the presence of silica impurities. A DTA run on C.P. artificial Bi_2CO_5 did not show the second endothermic break; presumably it is free of any impurities. All the bismutites show another inversion around 725° to form β-Bi_2O_3, a mixture of β-Bi_2O_3 and the simple cubic polymorph, or γ-Bi_2O_3.

Beyerite, $(Ca,Pb)Bi_2(CO_3)_2O_2$. The specimen is from Fremont County, Colorado, and was supplied by E. Wm. Heinrich (Heinrich, 1947). The DTA curve shows a large endothermic break which begins at 485°, reaches a peak at 570°, and ends at 625°. A second endothermic curve begins at 660°, reaches a peak at 675°, and ends at 700°. The DTA curve shows the start of another endothermic break at 725°; this is the start of the inversion of Bi_2O_3. A powder x-ray picture of the final product shows that it is β-Bi_2O_3.

The beyerite curve is similar to the bismutite curves, but the peaks are 50–75 degrees higher for the beyerite breaks. The energy associated with the first endothermic break is greater for beyerite than for bismutite. Again, it is believed that the first endothermic break is due to the loss of CO_2, and the second endothermic break is an undetermined inversion.

Rutherfordine, UO_2CO_3 (?) (89472). The specimen is from Morogoro, Tanganyika Territory, Africa. The formula of rutherfordine is open to question, and any interpretation of the DTA curve would be speculative.

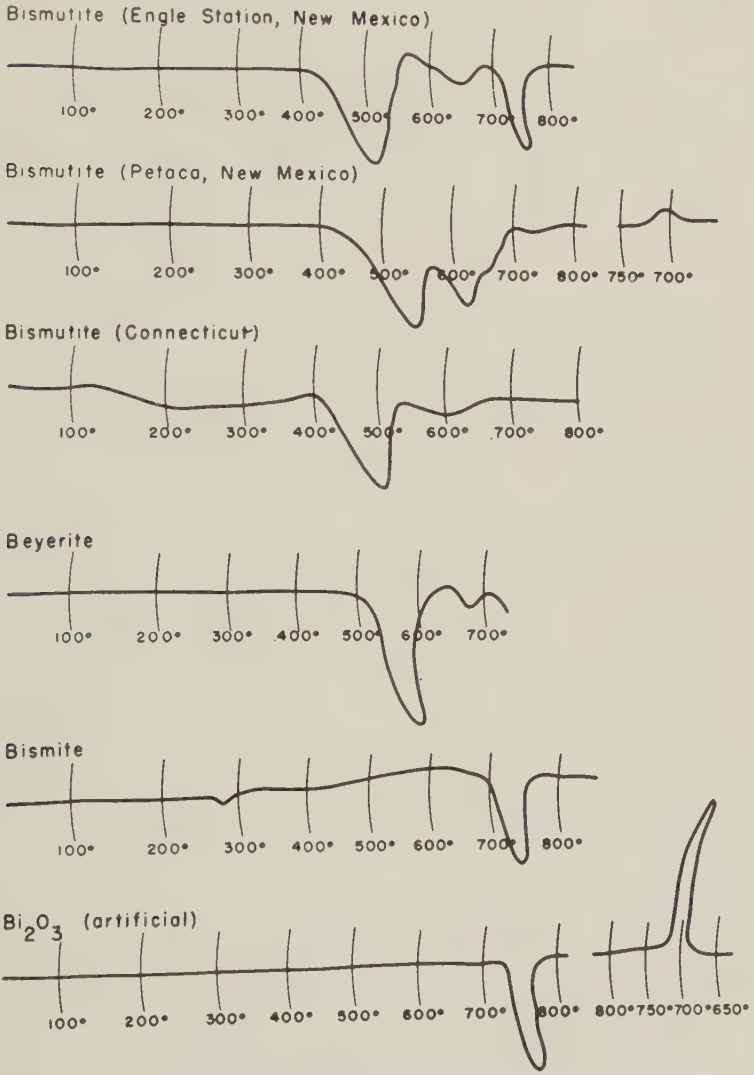

FIG. 7. Differential thermal analysis curves of some bismuth minerals.

Powder *x*-ray pictures of the final decomposition product show the same lines as the decomposition products of uranothallite and schroeckingerite, but with slightly different spacings.

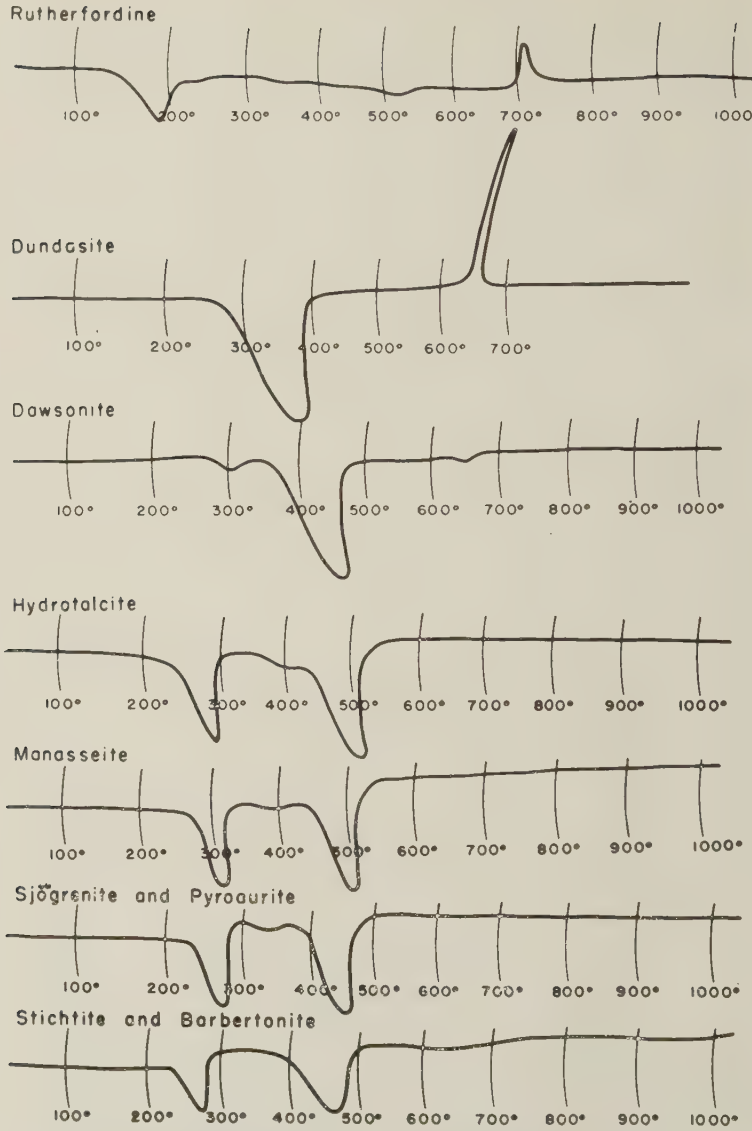

FIG. 8. Differential thermal analysis curves of rutherfordine, dundasite, dawsonite, the pyroaurite group, and the sjögrenite group.

Dundasite, $Pb(AlO)_2(CO_3)_2 \cdot 4H_2O$ (84578). The specimen is from Dundas, Tasmania. The loss of water of crystallization and CO_2 takes place in one endothermic reaction. This reaction begins at 250°, reaches a peak at 350°, and ends at 400°. A powder *x*-ray picture of the decomposition

product at 500° shows it to be amorphous. A probable inversion is shown by the exothermic peak at 660°. The run was stopped at 700° to avoid fusing the PbO. A powder x-ray picture of the mineral heated to 700° gives lines corresponding to neither Al_2O_3 nor PbO.

Dawsonite, $Na_3Al(CO_3)_3 \cdot 2Al(OH)_3$ (91177), ($\alpha = 1.465$, $\beta = 1.540$, $\gamma = 1.598$). The specimen is from Montreal, Canada. The small endothermic break which begins at 275°, reaches a peak at 300°, and ends at 315° is due to the loss of non-essential water from the structure. The optics and powder x-ray picture of a sample heated to 325° are identical with the starting mineral. The large endothermic break is the loss of hydroxyl water and CO_2. This reaction begins at 345°, reaches a peak at 440°, and ends at 470°.

Hydrotalcite, $MgCO_3 \cdot 5Mg(OH)_2 \cdot 2Al(OH)_3 \cdot 4H_2O$, ($\omega = 1.512$, $\epsilon = 1.498$). The specimen is from Snarum, Norway. The first endothermic reaction might be the loss of the four molecules of water of crystallization. This reaction begins slowly from 200–240°, reaches a peak at 285°, and ends at 300°. A small endothermic reaction begins at 350°, reaches a peak at 405°, and overlaps a large endothermic reaction which reaches a peak at 495°, and ends at 520°. The 405° peak is believed to be the loss of basic water from $Al(OH)_3$, and the 495° peak is believed to be the loss of basic water and CO_2 from $Mg(OH)_2$ and $MgCO_3$.

A powder x-ray picture of the 1000° decomposition product gives the spacing of periclase with no evidence of alumina.

Manasseite, $MgCO_3 \cdot 5Mg(OH)_2 \cdot 2Al(OH)_3 \cdot 4H_2O$ (87211), ($\omega = 1.524$, $\epsilon = 1.510$). The specimen is from Snarum, Norway. The first endothermic reaction might be the loss of four molecules of water of crystallization. This reaction begins at 275°, reaches a peak at 315°, and ends at 340°. A small endothermic reaction begins at 360°, reaches a peak at 400°, and overlaps a large endothermic reaction which reaches a peak at 495°, and ends at 535°.

Manasseite and hydrotalcite are polymorphs and their differential thermal curves are similar. The main difference is in the temperature at which the water of crystallization is lost; the manasseite peak is 30° higher than the hydrotalcite peak. The other two endothermic peaks are practically identical for the two minerals.

Pyroaurite and Sjögrenite, $MgCO_3 \cdot 5Mg(OH)_2 \cdot 2Fe(OH)_3 \cdot 4H_2O$ (83907), ($\omega = 1.572$, $\epsilon = 1.549$). These two polymorphous minerals occur in a specimen from Långban, Sweden. They are isostructural with hydrotalcite and manasseite respectively (Frondel, 1941). The estimated ratio of pyroaurite:sjögrenite in the specimen is 1:9.

The DTA curve is a combination of the curves of pyroaurite and sjögrenite. The same three endothermic curves which were characteristic of hydrotalcite and manasseite are also characteristic of the pyroaurite-sjögrenite mixture, but they reach peaks at different temperatures. The loss of the four molecules of water of crystallization begins at 215°, reaches a peak at 270°, and ends at 290°. The small endothermic break begins at 295°, reaches a peak at 350°, and overlaps the large endothermic break which reaches a peak at 455°, and ends at 500°. This DTA curve is dominated by sjögrenite. By analogy with hydrotalcite and manasseite, a curve of pyroaurite would lose the water of crystallization at a temperature slightly lower than the curve of the pyroaurite-sjögrenite mixture.

Stichtite and Barbertonite, $MgCO_3 \cdot 5Mg(OH)_2 \cdot 2Cr(OH)_3 \cdot 4H_2O$ (92549), ($\omega = 1.551$, $\epsilon = 1.523$). These two polymorphous minerals are from the Transvaal, South Africa. Stichtite is isostructural with hydrotalcite and pyroaurite; barbertonite, with manasseite and sjögrenite (Frondel, 1941). The estimated ratio of stichtite:barbertonite is 1:1. Unlike the DTA curves of the other minerals of this group, this DTA curve shows only two endothermic breaks—the small one is absent. The loss of the four molecules of water of crystallization begins at 235°, reaches a peak at 275°, and ends at 290°. The second endothermic curve begins slowly at 360°, reaches a peak at 455°, and ends at 500°. These two peaks, therefore, correspond closely with the hydrotalcite, manasseite, and pyroaurite-sjögrenite curves. By analogy with hydrotalcite it would be expected that stichtite would lose its water of crystallization at a peak slightly below 275°.

This DTA curve enables one to interpret the three preceding curves, especially the small endothermic break. The first break in all cases is believed to be the loss of four molecules of water of crystallization. The small endothermic reaction represents the loss of hydroxyl water from the trivalent cation; in the case of stichtite-barbertonite this break is either higher or lower and overlaps the last or first endothermic break; that is, the loss of hydroxyl water from $Cr(OH)_3$ is at a higher or lower temperature than the corresponding loss in $Al(OH)_3$ and $Fe(OH)_3$. The last endothermic reaction is the loss of hydroxyl water from the $Mg(OH)_2$ plus the loss of CO_2 from $MgCO_3$.

Frondel (1941) discusses the constitution and polymorphism of the pyroaurite and sjögrenite groups. Pyroaurite, stichtite, and hydrotalcite belong to the rhombohedral or pyroaurite group. The cell dimensions and the indices of refraction decrease from pyroaurite to hydrotalcite. Sjögrenite, barbertonite, and manasseite belong to the hexagonal or sjögrenite group. The cell dimensions and indices of refraction decrease

TABLE 5. CHARACTERISTIC THERMAL PEAKS AND AREAS OF THE CARBONATES CONTAINING HYDROXYL OR HALOGEN

Mineral	Reaction product	Peak temperature, °C.		Area, mm.²	Weight, gm.	Scale
		Endothermic	Exothermic			
Bastnäsite, Ampanbabe	CO_2, F_2	625		500	0.800	2
	CeO_2		650	110		
Bastnäsite Colorado	CO_2, F_2	620		530	0.810	2
	CeO_2		655	190		
"Tysonite" (Bastnäsite)	CO_2, F_2	625		460	0.795	2
	CeO_2		650	140		
Kischtymite	CO_2, F_2	580		275	0.630	2
	CeO_2		650	30		
Parisite	CO_2, F_2	660		530	0.770	2
	CeO_2		720	20		
Hydromagnesite	H_2O	375			0.325	3
	OH^-	440		595		
	MgO		510	small		
	CO_2	565		710		
	CO_2	600				
Artinite	H_2O	280		340	0.265	3
	OH^-	440				
	CO_2	480		675		
	MgO		510	small		
	CO_2	540				
$2PbCO_3 \cdot Pb(OH)_2$ (artificial)	H_2O	270		215	0.680	2
	CO_2	430		395		
	CO_2	490				
Hydrocerussite (Arizona)	H_2O	345			0.960	2
	CO_2	385		420		
	CO_2	500				
Hydrocerussite (England)	H_2O	345			0.575	2
	CO_2	380		350		
	CO_2	485				
Azurite	H_2O, CO_2	430		440	0.550	2
Malachite	H_2O, CO_2	385		380	0.580	2

TABLE 5. *Continued*

Mineral	Reaction product	Peak temperature, °C.		Area, mm.²	Weight, gm.	Scale
		Endothermic	Exothermic			
Hydrozincite	H_2O, CO_2	310		535	0.355	2
Aurichalcite	H_2O, CO_2	415		540	0.315	2
Bismutite (Engle Station)	CO_2 Inversion? γ-Bi_2O_3	495 605 710		440 80 ?	0.875	3
Bismutite (Pectaca)	CO_2 Inversion? Simple cubic and β-Bi_2O_3	530 625 730		820	0.960	3
Bismutite (Willimantic)	CO_2 Inversion?	480 600		340 60	1.000	3
Beyerite	CO_2 Inversion? β-Bi_2O_3	570 675 725		380 35 ?	0.490	3
Rutherfordine	? ?	190	715	130 20	0.225	3
Dundasite	H_2O, CO_2 ?	350	660	620 75	0.340	2
Dawsonite	H_2O OH^-, CO_2	300 440		20 415	0.390	2
Hydrotalcite	H_2O OH^- OH^-, CO_2	285 405 495		235 385	0.285	2
Manasseite	H_2O OH^- OH^-, CO_2	315 400 495		180 330	0.325	2
Pyroaurite & Sjögrenite	H_2O OH^- OH^-, CO_2	270 350 455		195 325	0.295	2
Stichtite & Barbertonite	H_2O OH^-, CO_2	275 455		110 215	0.210	2

Table 6. Characteristic Thermal Peaks and Areas of the Compound Carbonates, with Sulfates, Halides

Mineral	Reaction product	Peak temperature, °C. endothermic	Area, mm.²	Weight, gm.	Scale
Phosgenite	CO_2	435	175	0.930	2
Leadhillite	H_2O, CO_2	345	150	0.850	2
	CO_2	485	65		

Table 7. Chemical Analyses of Some of the Carbonate Minerals

Mineral	Locality	% metallic oxide	% CO_2	% H_2O	Analyst
Calcite	Canada	CaO —56.17	43.72		Carl W. Beck
Magnesite	Austria	MgO—46.91 CaO—0.58	52.13		Carl W. Beck
Breunnerite	California	MgO—39.62 FeO — 9.51 CaO — 0.43	49.74		Carl W. Beck
Rhodochrosite	Montana	MnO—56.98 FeO — 0.34	38.78		F. A. Gonyer
Siderite	Saxony	FeO —52.6 MnO—10.4	38.5		H. R. Shell
Pistomesite	Italy	FeO —42.58 MgO—14.18 MnO— 0.39	41.75		F. A. Gonyer
Ankerite	Tri-State	CaO —30.68 FeO —11.64 MgO—10.80 MnO— 1.71	44.28		F. A. Gonyer
Artinite	Nevada	MgO—41.81	22.82	35.46	F. A. Gonyer
Beyerite	Colorado	Bi_2O_3—73.65 CaO — 8.85 PbO — 1.73 CuO — 1.10 MnO— 0.12	13.59	0.79 (insol.)	F. A. Gonyer

from sjögrenite to mansaseite. A similar, but less well-defined, parallel change takes place in the peak temperatures of the DTA curves of the members of the pyroaurite and sjögrenite groups. The members that have the smallest cell dimensions have the highest peak temperatures; that is, the decomposition reactions of hydrotalcite take place at a temperature higher than corresponding reactions in stichtite, and the reactions of stichtite are, in turn, higher than those of pyroaurite. Similarly, the decomposition reactions of manasseite take place at a temperature higher than the corresponding reactions in barbertonite, and the reactions of barbertonite are, in turn, higher than those of sjögrenite.

Compound Carbonates, with Sulfates, Halides

The DTA curves for the compound carbonates, with sulfates, halides are shown in Fig. 9.

Phosgenite, $PbCO_3 \cdot PbCl_2$ (84449). The specimen is from Monte Poni, Sardinia. The decomposition due to the loss of CO_2 becomes rapid at 360°, though the reaction may have begun slowly a hundred degrees earlier. The reaction reaches a peak at 435°, and ends at 445°. The second endothermic break is due to the melting of the decomposition product. Powder x-ray pictures of samples heated to 475° and 590° are identical. The pattern corresponds to neither PbO, $PbCl_2$, nor a mixture of the two.

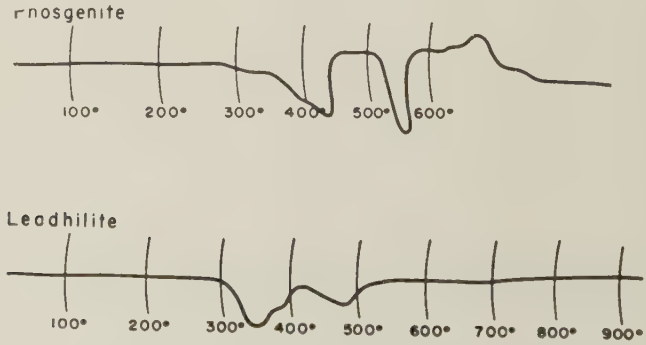

Fig. 9. Differential thermal analysis curves of phosgenite and leadhillite.

Leadhillite, $2PbCO_3 \cdot 2Pb(OH)_2 \cdot PbSO_4$. The specimen is from Eureka Mine, Utah. The decomposition of leadhillite is similar to the decomposition of hydrocerussite (Fig. 3). The loss of hydroxyl water begins at 300°, reaches a peak at 345°, and merges almost completely with the first stage in the decomposition of the $PbCO_3$ part of the structure, and ends at 400°. There is a characteristic shoulder at 375°. The total decomposition of the carbonate begins at 420°, reaches a peak at 485°, and ends at 520°. A powder x-ray picture of a sample heated to 600°

gives a pattern corresponding to neither PbO, $PbSO_4$, nor a mixture of the two.

Acknowledgment

The author wishes to acknowledge the interest and encouragement shown by Professors E. S. Larsen, Jr., C. S. Hurlburt, Jr., and Clifford Frondel of the Department of Mineralogy and Petrography, Harvard University. He is especially indebted to Dr. Michael Fleischer, U. S. Geological Survey, for helpful suggestions and critical reading of the manuscript.

References

Beck, Carl W. (1950), An amplifier for differential thermal analysis: *Am. Mineral.*, **35,** 508–524.

Berkelhamer, L. H. (1945), An apparatus for differential thermal analysis: *Bureau of Mines, R. I.* **3762,** 17 pages.

Brill, Otto (1905), Über die Dissoziation der Karbonate der Erdalkalien und des Magnesiumkarbonats: *Zeit. anorg. Chem.*, **45,** 285.

Cuthbert, F. L., and Rowland, R. A. (1947), Differential thermal analysis of some carbonate minerals: *Am. Mineral.*, **32,** 111–116.

Dana, J. D. (1892), *A System of Mineralogy:* Sixth Edition, John Wiley & Sons, Inc., New York City.

Davis, W. A. (1906), Study of basic carbonates: *J. Soc. Chem. Ind.*, **25,** 788.

Faust, George T. (1949), Differentiation of aragonite from calcite by differential thermal analysis: *Science*, **110,** no. 2859, 402–403.

Frederickson, A. F. (1948), Differential thermal curve of siderite: *Am. Mineral.*, **33,** 372.

Friedrich, K., and Smith, L. G. (1912): *Met.* vol. 9, 409. Cited in Mellor, J. W. (1927), A Comprehensive Treatise on Inorganic and Theoretical Chemistry: vol. **IV,** 353.

Frondel, Clifford (1941), Constitution and polymorphism of the pyroaurite and sjögrenite groups: *Am. Mineral.*, **26,** 295–315.

Frondel, Clifford (1943), Mineralogy of the oxides and carbonates of bismuth: *Am. Mineral.*, **28,** 521–540.

Heinrich, E. Wm. (1947), Beyerite from Colorado: *Am. Mineral.*, **32,** 660–669.

Hurlbut, C. S. Jr. (1946), Artinite from Luning, Nevada: *Am. Mineral.*, **31,** 365–369.

Jaffe, Howard W., Sherwood, Alexander M., and Peterson, Maurice J. (1948), New data on Schroeckingerite: *Am. Mineral.*, **33,** 152–157.

Larsen, E. S., and Gonyer, F. A. (1937), Dakeite, a new uranium mineral from Wyoming: *Am. Mineral.*, **22,** 561–563.

Mellor, J. W. (1927), A Comprehensive Treatise on Inorganic and Theoretical Chemistry: vols. **I–XVI,** Longmans, Green and Co., Ltd., London.

Nováček, Radim (1939), The identity of dakeite and schroeckingerite: *Am. Mineral.*, **24,** 317–323.

Pavlovitch, Stoyan (1935), The action of heat upon some natural oxides of manganese: *Compt. Rend. Acad. Sci.*, Paris, **200,** 71–73.

Schumb, W. C., and Rittner, E. S. (1943), Polymorphism of bismuth trioxide: *J. Am. Chem. Soc.*, **65,** 1055–1060.

Sillén, L. G. (1938), *X*-ray Studies on bismuth trioxide: *Arkiv., Kemi., Min., Geol.*, **12A,** No. 18.

Sillén, L. G. (1941), On the crystal structure of monoclinic α-Bi_2O_3: *Zeit. Krist.*, **103,** 274.

Šplíchal, J., Škramovský, S., and Goll, J. (1936), Thermal decomposition of carbonate minerals: *Věda přírodní*, **17,** 206–213.

SEARLESITE FROM THE GREEN RIVER FORMATION OF WYOMING*

JOSEPH J. FAHEY†

WITH *X*-RAY NOTES BY JOSEPH M. AXELROD**

ABSTRACT

The third recorded occurrence of searlesite, hydrous sodium borosilicate, is in the Green River formation of southwestern Wyoming.

It is found in flat anhedral crystals in the oil shale and in subhedral crystals as much as 7 inches long in the trona bed, 10 feet thick, at a depth of 1500 feet.

The optical properties of the searlesite from Wyoming are in close agreement with those previously published. The indices of refraction, measured with sodium light, are: $\alpha = 1.516$, $\beta = 1.531$, and $\gamma = 1.535$ ($2V = 55°$, neg., calculated). *X*-ray diffraction photographs and a chemical analysis confirm the identity of the Wyoming mineral as searlesite.

INTRODUCTION

The Green River formation in southwestern Wyoming affords the third recorded occurrence of searlesite, a hydrous sodium borosilicate. This mineral was first described in 1914 by Larsen and Hicks,[1] from the old Searles deep well at Searles Lake, San Bernardino County, California, and named after Mr. John W. Searles, the pioneer who put down the well. It was found in clay at a depth of 540 feet as white spherulites about a millimeter in diameter. Great difficulty was experienced in preparing a sample for chemical analysis due to the intimate association of tiny grains of calcite, quartz, feldspar, chlorite, and hornblende. The analyzed sample contained about 40% of this extraneous material. Larsen states that the optical properties were measured with difficulty and that his results were only approximate.

The second locality of searlesite is the Silver Peak Range, Esmeralda County, Nevada, described in 1934 by Foshag.[2] The crystallographic and optical constants of searlesite from this location were published by Rogers[3] in 1924. These crystals are prismatic and seldom exceed 3 mm. in length. The sample analyzed by Foshag contained less than one per cent of impurities and his analysis was very close to the theoretical composition, $Na_2O \cdot B_2O_3 \cdot 4SiO_2 \cdot 2H_2O$.

* Published by permission of the Director, U. S. Geological Survey.

† U. S. Geological Survey, Washington, D. C.

[1] Larsen, Esper S., and Hicks, W. B., Searlesite, a new mineral: *Am. Jour. Sci.*, **38**, 437–440 (1914)

[2] Foshag, William F., Searlesite from Esmeralda County, Nevada: *Am. Mineral.*, **19**, 268–274 (1934).

[3] Rogers, Austin F., The crystallography of searlesite: *Am. Jour. Sci.*, **7**, 498–502 (1924).

Occurrence and Association

The third recorded occurrence of searlesite is at three places in the Green River formation in Sweetwater County, Wyoming. These places are the locations of the drill core of the John Hay, Jr., Well No. 1, approximately 18 miles west of the town of Green River; the drill core of the Union Pacific Well No. 4 that was put down $2\frac{3}{4}$ miles west of the John Hay, Jr., Well No. 1; and the shaft, and trona bed reached by this shaft of the Westvaco Chemical Corporation, formerly the Westvaco Chlorine Products Company. This shaft is approximately $3\frac{1}{2}$ miles north of the John Hay, Jr., Well No. 1 and $4\frac{1}{4}$ miles northeast of the Union Pacific Well No. 4. The exact location of the shaft is 1650 feet south and 1010 feet west of the north and east boundaries of Sec. 15, T.19 N., R. 110 W., 6 P.M. Wyoming. Drilling was started August 16, 1946, and completed to a total depth of 1552 feet on September 22, 1947.

Searlesite occurs at depths of 1480 feet and 1706 feet respectively, in the John Hay, Jr., Well No. 1 and the Union Pacific Well No. 4. This indicates a dip of the shale to the west of 216 feet in $2\frac{3}{4}$ miles, the elevations at the surface of the wells being 6355 feet and 6365 feet in the order named. In the shaft of the Westvaco Chemical Corporation searlesite was found at a depth of 1300 feet. The elevation at the top of the shaft is 6227 feet. These figures point to a dip of the strata to the north of 52 feet in the $3\frac{1}{2}$ miles between the John Hay, Jr., Well No. 1, and the shaft.

In the two drill cores and in the shaft searlesite is found in oil shale with shortite and tiny crystals of pyrite. At the bottom of the shaft at a depth of 1500 feet searlesite is found in association with trona.

The saline mineral assemblage of the Green River formation is unique. Two species, shortite and bradleyite, heretofore reported in no other location, are found associated with trona, pirssonite, gaylussite, and the rare mineral northupite. Shortite is ubiquitous through a vertical distance of more than 600 feet. Trona and northupite, though restricted to definite horizons, are found in great abundance.

Chemical Composition and Physical Properties

A crystal from the trona bed (depth 1500 ft.) of the Westvaco Mine was carefully crushed so that a minimum of fines was formed, then sieved, and the portion passing 80 and retained on 100 mesh was allowed to remain in distilled water, changed daily, for $1\frac{1}{2}$ months. This was done in order to remove the small percentage of sodium carbonate known to be present. Searlesite is not affected by such treatment; a sample so treated for 6 months showed no change of the indices of refraction.

The usual methods of chemical analysis were employed; B_2O_3 was titrated on a sample that had been decomposed by HCl, using mannitol

and methyl red and phenolphthalein indicators. Na_2O was determined by the J. Lawrence Smith procedure, and the H_2O determined as the loss in weight on heating the sample to 800° C. for one hour. No B_2O_3 is lost at this temperature. The results of the analysis are recorded in Table 1.

Table 1. Chemical Analysis of Searlesite from the Green River Formation, Sweetwater Co., Wyoming

J. J. Fahey, *Analyst*

Composition		Ratios
SiO_2	58.88%	3.992
B_2O_3	16.95	0.991
Na_2O	15.31	1.005
K_2O	none	
H_2O −110° C.	none	
H_2O +110° C.	8.90	2.013
Al_2O_3	0.04	
Fe_2O_3	0.04	
CaO	none	
MgO	0.03	
Total	100.15	

G. = 2.460

Formula: $Na_2O \cdot B_2O_3 \cdot 4SiO_2 \cdot 2H_2O$

When treated with (1+2) HCl, either cold or hot, searlesite behaves similarly to biotite mica under these circumstances. Silica remains quantitatively as a skeleton that retains the shape of the original grain, and can be filtered off without difficulty. The index of refraction of this siliceous skeleton is between 1.455 and 1.460.

The specific gravity of searlesite is 2.460 determined with an Adams-Johnston pycnometer of 5 cm. capacity, made of fused silica. This is in good agreement with the determination by Rogers[4] (2.45) obtained by suspension in a solution of methylene iodide and benzol.

Searlesite fuses readily to a glass that has an index of refraction of 1.515.

Crystallography

In both the core of the John Hay, Jr., Well No. 1 and that of the Union Pacific Well No. 4, the searlesite is found as segments about 3 mm. thick of flat anhedral crystals that lie parallel to the bedding of the oil shale. These crystals are so oriented that the perfect cleavage parallel

[4] *Op. cit.*, p. 501.

to the front pinacoid is always parallel to the bedding of the oil shale. Also this condition obtains in the shaft of the Westvaco Chemical Corporation at the 1300-foot level. However, in the stratum of trona 10 feet thick that is reached by the shaft at a depth of 1500 feet, subhedral crystals of searlesite up to 7 inches long, 4 inches wide, and one inch thick are not uncommon. The largest crystals heretofore reported (Esmeralda County, Nevada) are approximately 3 mm. long. Due to the presence of minute quantities of organic matter, they are light brown in color. These crystals are randomly oriented in the trona bed and commonly have the front pinacoid (100) and the prisms (110) and ($\bar{1}10$) developed.

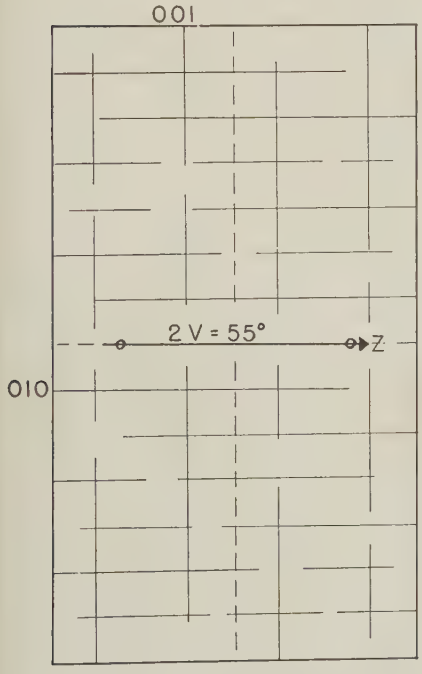

Fig. 1. Orthopinacoidal section showing traces of the (010) and ($\bar{1}02$) cleavages and the emergence of the optic axes.

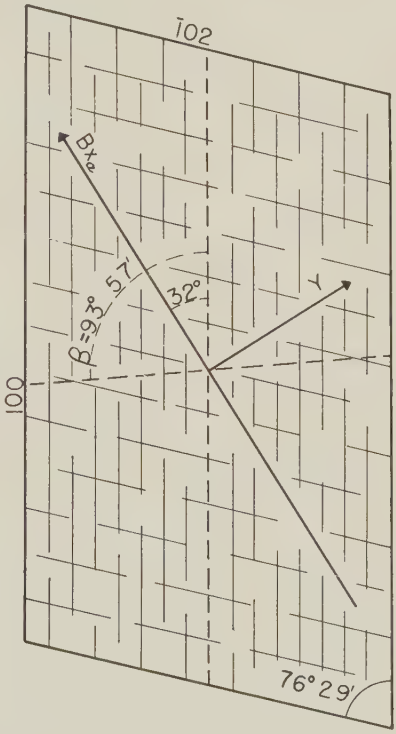

Fig. 2. Clinopinacoidal section showing traces of the perfect cleavage (100) and the poor cleavage ($\bar{1}02$). The optic axial plane is normal to the section.

Two cleavages heretofore unreported are found as traces on the perfect cleavage (100), parallel to the front pinacoid shown in Fig. 1. These are the ($\bar{1}02$) cleavage and the clinopinacoidal cleavage (010). Both are

imperfect but unmistakably present. A thin section cut parallel to the clinopinacoid (Fig. 2) shows the traces of the perfect cleavage parallel to the front pinacoid and the imperfect ($\bar{1}02$) cleavage, parallel to the rear dome that Rogers and Foshag, not having x-ray data, mistook for the base. The inclination of the optic axial plane to the c axis is 32° and β is equal to 93° 57′, the latter figure determined by the x-ray study, the form (001) not being present.

The indices of refraction measured with sodium light are: $\alpha = 1.516$, $\beta = 1.531$, and $\gamma = 1.535$. These values check well with those of Rogers[5] and Foshag.[6]

TABLE 2. *X*-RAY POWDER DIFFRACTION DATA FOR SEARLESITE FROM WYOMING
(Fe/Mn radiation, $\lambda = 1.9373$ Å)

d(obs.)	*I*	*hkl*	*d*	*I*	*d*	*I*
8.01	10	100	1.825	2	1.131	½
5.32	1	110	1.765	2	1.110	2
4.31	3	10$\bar{1}$	1.746	1	1.079	½
4.06	5	101	1.690	½		
3.98	2	200	1.647	½		
3.70	1	11$\bar{1}$	1.632	½		
3.54	3	111	1.616	½		
3.48	4	210	1.605	½		
3.24	4	120	1.592	½		
3.21	3	20$\bar{1}$	1.554	2		
2.99	2	201	1.473	½		
2.92	3	21$\bar{1}$	1.451	½		
2.76	2	211	1.431	½		
2.66	3	121	1.406	½		
2.49	1	310	1.334	½		
2.45	2	002	1.320	1		
2.41	1	30$\bar{1}$	1.304	1		
2.39	1	10$\bar{2}$	1.292	½		
2.28	1	102	1.282	½		
2.16	½	311	1.260	½		
2.12	1	320	1.239	1		
2.06	1	13$\bar{1}$	1.224	½		
2.02	½	230, 202, 022	1.215	½		
1.992	1		1.200	½		
1.978	1		1.182	1		
1.945	½		1.161	½		
1.916	1		1.153	½		
1.896	1		1.140	½		

[5] *Op. cit.*, p. 501.
[6] *Op. cit.*, p. 272.

X-Ray Analysis

The x-ray powder pattern of the searlesite from the shaft of the Westvaco Chemical Corporation is identical with that of the searlesite from Nevada described by Rogers and Foshag. Measurements of the stronger lines of the pattern and the Miller indices, obtained from Weissenberg studies, are given in Table 2.

For the single crystal investigation, a small crystal of the searlesite from Nevada was chosen. Weissenberg photograph (with Cu/Ni radiation) taken about the b and c axes and a rotation photograph taken about the a axis combined with positive results of piezoelectric tests made by Dr. Paul Smith of the Naval Research Laboratory show the crystal to be monoclinic with the space group $P2_1$-(C_2^2). The unit cell has the following dimensions:

$a_0 = 7.972 \pm 0.010$ Å
$b_0 = 7.052 \pm 0.010$ Å
$c_0 = 4.900 \pm 0.010$ Å
$\beta = 93° 57' \pm 10'$
(The error figures are estimates)

Specific gravity:

Calculated (x-ray)	2.46_4
Foshag	2.44
Rogers	2.45
Fahey (this paper)	2.460

The axial ratio is $a:b:c = 1.130:1:0.695$ and the cell content is $2(NaBSi_2O_6 \cdot H_2O)$.

These axial ratios and the value for beta are different from those of Rogers and Foshag and are related to them through the following transformations:

$a = -1/2\ A\ -1/6\ C$	$A = -2a - c$
$b = -1/2\ B$	$B = -2b$
$c = 1/3\ C$	$C = 3c$

Lower case letters refer to the x-ray description.

Figure 3 shows, on the clinopinacoid, the relationship of the unit cell to the dome faces and to the axial directions derived by Rogers.

The axial ratios found by Rogers and Foshag from goniometric measurements were recalculated to conform to the unit cell found by using x-rays. Interfacial angles were then calculated from the x-ray data. The values derived from the x-ray measurements and from the morphological measurements are compared in Table 3. The dominance of the $(\bar{2}01)$ face caused Rogers to select a different a axis from that found by x-ray measurements, but when the data are recalculated to a common basis, the agreement is very good.

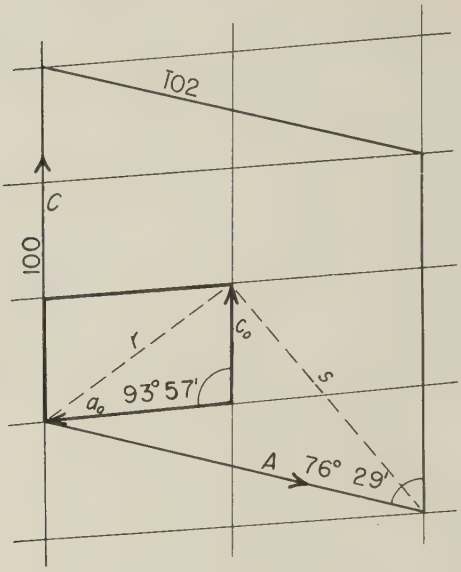

FIG. 3. Projection on the clinopinacoid of the x-ray unit cell, the crystal axes derived by Rogers, and the dome faces.

TABLE 3. COMPARISON OF CRYSTAL CONSTANTS DETERMINED FROM MORPHOLOGY AND FROM X-RAY MEASUREMENTS

	X-ray	Rogers	Foshag
$a:b:c$	1.130:1:0.695	1.119:1:0.689	1.121:1:0.691
β	93°57′	93°58′*	93°56′*
a	(100)	(100)	(100)
b	(010)	(010)	(010)
m	(110)	(110)	(110)
r	($\bar{2}$01)	(101)	(101)
s	(101)	($\bar{1}$01)	($\bar{1}$01)
$m \wedge b$	41°35′	41°50′	41°49′ (range=51′)
$r \wedge a$	40°41′	40°37′	40°35′ (range=38′)
$s \wedge a$	55°35′	55°30′	55°32′ (range=28′)

* Recalculated from Rogers' and Foshag's data to correspond to x-ray orientation.

ACKNOWLEDGMENTS

The authors wish to express their thanks to their colleagues, Marie L. Lindberg, Michael Fleischer, George T. Faust, William T. Pecora, and C. L. Christ for their helpful suggestions and critical reading of the manuscript.

STUDIES OF URANIUM MINERALS (VI): WALPURGITE*

HOWARD T. EVANS, JR.,† *Massachusetts Institute of Technology, Cambridge, Mass.*

ABSTRACT

Walpurgite, a hydrated bismuth uranium arsenate from Schneeberg, Saxony, has been studied by x-ray diffraction using the Buerger precession method. The lattice is triclinic with the following elements: $a_0=7.13$ Å, $b_0=10.44$ Å, $c_0=5.49$ Å, $\alpha=101°\ 40'$, $\beta=110°\ 49'$, $\gamma=88°\ 17'$; $a:b:c=0.683:1:0.525$. The crystals are commonly elongated parallel to [001], flattened parallel to (010) and twinned on (010). The morphological data of Weisbach and Fischer are correlated with the x-ray data through the following transformations: Weisbach to x-ray $x0\bar{1}/0x\bar{1}/001$ (x undetermined); Fischer to x-ray $0\bar{1}\bar{1}/302/001$. From the volume of the unit cell as determined by x-rays, it is concluded that available data on composition and density are unreliable because of the scarcity of pure material. The best formula is one proposed by Fischer: $2Bi_2O_3 \cdot UO_3 \cdot As_2O_5 \cdot 3H_2O$.

Walpurgite was described and named in 1871 by Weisbach (6) as a hydrated bismuth uranium arsenate from Schneeberg, Saxony. The crystals, yellow triclinic twins resembling gypsum crystals in shape, were partially described by Weisbach (7) in 1877. The crystal morphology was recently treated in detail by Fischer (4) on the basis of a study of twinned and untwinned crystals from Schneeberg and Joachimsthal. The present paper presents a complete determination of the unit cell on the basis of an x-ray study using the Buerger precession method. This information is used to redefine the results of Weisbach and Fischer and to attack the problem of composition.

X-RAY STUDY

Small twinned crystals from Schneeberg were mounted in two positions and three intersecting reciprocal lattice planes were photographed with the Buerger precession camera. The [hk0] reciprocal lattice plane is shown in Fig. 1. In this photograph the composition plane is normal to the lattice plane, and, because of the high absorption in the crystal of the x-rays, the pattern on the left is mainly generated by one individual, while that on the right is due mainly to the other. From these films, the reciprocal elements were measured directly and the elements of the direct lattice were calculated therefrom. In the direct lattice, the three shortest axes were found and the new axial angles calculated. These axes were then finally oriented with $c<a<b$ and with α and β obtuse, according to the rules of convention proposed by Donnay (2). From these

* Contribution from the Department of Mineralogy and Petrography, Harvard University, No. 321.

† Present address: Philips Laboratories, Inc., Irvington-on-Hudson, New York.

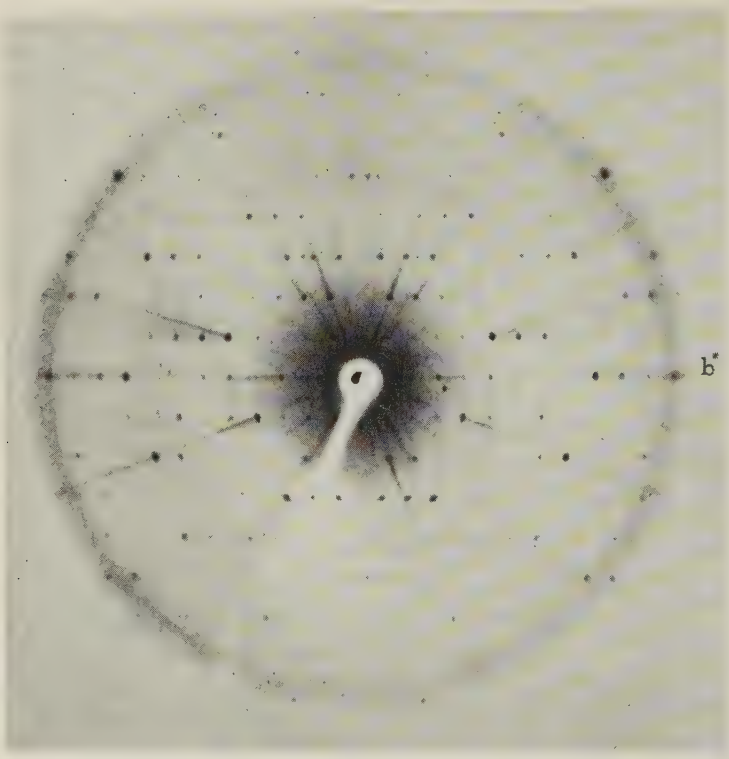

FIG. 1. Precession photograph of (*hk*0) plane, of walpurgite twin crystal (Mo Kα radiation).

final axial elements, the projection and polar elements were derived using the relations given by Evans (3). These results are given in Table 1. The twin plane is *b*(010).

MORPHOLOGY

Walpurgite crystals are almost invariably twinned, and the habit described by Weisbach is very characteristic (Fig. 2). He listed four forms, which were not sufficient to give a complete morphological unit cell. Fischer lists fourteen forms found on twinned crystals and three single crystals from Schneeberg and Joachimsthal. These forms are listed in Table 2, with symbols and letters given by Weisbach, Fischer and the *x*-ray determination. The relationship between the *x*-ray lattice and the lattices of Weisbach and Fischer was found by the identification of the twinning plane and the direction of elongation, parallel to the *c* axis in all three settings. A gnomonic projection of the *x*-ray lattice was made, and the (001) pole of each of the other two settings was identified from the polar angles given by the respective authors. Thus,

Weisbach's (001) is equivalent to the x-ray $(\bar{1}\bar{1}1)$, and Fischer's (001) is the x-ray $(\bar{1}21)$. The gnomonic projection showing all reported forms and the three unit cells is shown in Fig. 3. From this projection, the following transformation matrices are derived:

$$\text{Weisbach to } x\text{-ray} \begin{pmatrix} \bar{x} & 0 & \bar{1} \\ 0 & \bar{x} & \bar{1} \\ 0 & 0 & 1 \end{pmatrix} (x \text{ not determined})$$

$$\text{Fischer to } x\text{-ray} \begin{pmatrix} 0 & \bar{1} & \bar{1} \\ 3 & 0 & 2 \\ 0 & 0 & 1 \end{pmatrix}$$

Some of the angles reported by Weisbach and Fischer are listed in Table 3 for comparison.[1] Fischer's two single crystals are shown in Fig. 4 redrawn in the new orientation.

TABLE 1. CRYSTALLOGRAPHIC ELEMENTS OF WALPURGITE

Symmetry: Triclinic; space group prob. $P\bar{1}=C_i^1$.

Axial elements:

$a_0 = 7.13$ Å $\quad \alpha = 101°40'$

$b_0 = 10.44$ Å $\quad \beta = 110°49'$

$c_0 = 5.49$ Å $\quad \gamma = 88°17'$

$a:b:c = 0.638:1:0.525$

Polar elements:

$a^* = 0.1502 \quad \lambda = 78°10'$

$b^* = 0.0979 \quad \mu = 69°10'$

$c^* = 0.1992 \quad \nu = 87°22'$

$p_0:q_0:r_0 = 0.748:0.488:1$

Projection elements:

$x_0' = 0.380 \quad p_0' = 0.824$

$y_0' = 0.224 \quad q_0' = 0.537$

$\nu = 87°22'$

Cartesian matrices:

$v_1 = -0.0448 \quad v_2 = 0.978$

Direct:

$$M = \begin{pmatrix} 6.667 & -0.468 & 0 \\ 0 & 10.217 & 0 \\ -2.535 & -2.112 & 5.487 \end{pmatrix} \text{(in Å)}$$

Reciprocal:

$$\overline{M^{-1}} \begin{pmatrix} 0.1500 & 0 & 0.0693 \\ 0.0069 & 0.0979 & 0.0408 \\ 0 & 0 & 0.1822 \end{pmatrix} \text{(in Å}^{-1}\text{)}$$

[1] The axial elements are not compared for the following reasons: Weisbach's elements are incomplete; Fischer's axial elements cannot be reconciled with the polar angles which he observes (the latter agree well with the x-ray lattice, while no rational relationship can be found among the axial elements).

Composition

Several analyses of walpurgite have been recorded in the literature, and these are shown in Table 4.

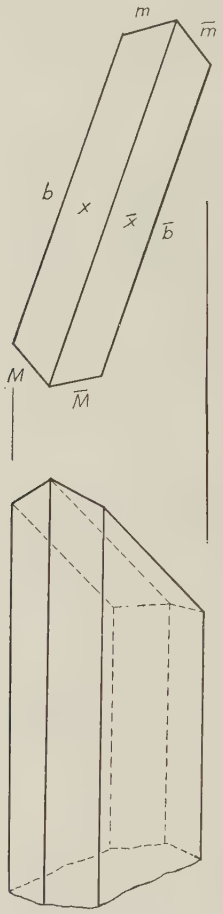

Fig. 2. Walpurgite twin, after Weisbach; Schneeberg (common habit).

Several different formulae have been proposed on the basis of these analyses, usually with a molecular weight roughly three times that corresponding to column 5 of Table 4. Because of the relatively small size of the unit cell, 373.7 Å^3, none of these can be correct. But even the relatively simple formula given by Fischer's micro-analysis on 34 mg. is not compatible with the density of 5.76 given by Weisbach (7). The formula given demands a density of 6.69. A redetermination of the

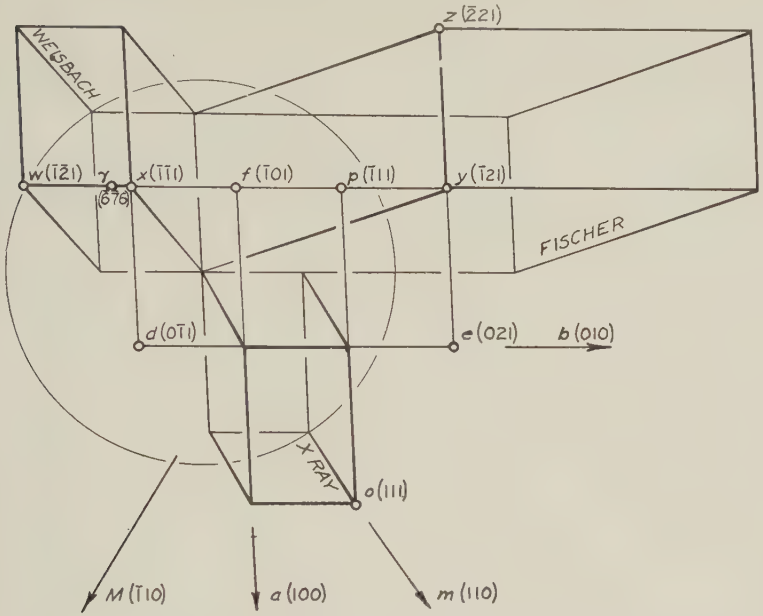

FIG. 3. Gnomonic projection for walpurgite showing unit cells of Weisbach (completed), Fischer and *x*-ray.

TABLE 2. WALPURGITE CRYSTAL FORMS

X-ray	Fischer, 1946	Weisbach, 1877
b 010	100	*b* 010
a 100	010	
m 110	1$\bar{3}$0	*m* 110
M 1$\bar{1}$0	130	*μ* 1$\bar{1}$0
e 021	0$\bar{1}$1	
g 0$\bar{1}$1	$\bar{1}\bar{1}$1	
h $\bar{1}$01	$\bar{2}\bar{0}\bar{3}$	
o 111	$\bar{1}$21	
p $\bar{1}$11	$\bar{1}$03	
z $\bar{2}$21	011	
x $\bar{1}\bar{1}$1	$\bar{1}$01	*c* 001
y $\bar{1}$21	001	
γ $\bar{6}\bar{7}\bar{6}$	$\bar{1}$9.0.18	
w $\bar{1}\bar{2}$1	$\bar{4}$03	

density by Miss Mary E. Mrose using the Berman balance gave a value of 5.95.

TABLE 3. SOME WALPURGITE ANGLES COMPARED

Angle (New setting)	X-ray (calc.)	Fischer (obs.)	Weisbach (obs.)
$(010)\wedge(1\bar{1}0)$	58°45′	58°18′±24′	59° 2′
$(010)\wedge(110)$	55 4	55 8	53 50
$(010)\wedge(\bar{1}\bar{1}1)$	72 13	72 29	70 52
$(100)\wedge(010)$	87 22	88 23±47′	86 6
$(100)\wedge(\bar{1}\bar{1}1)$	113 31		114 1
$(1\bar{1}0)\wedge(\bar{1}\bar{1}1)$	80 8		80 40
$(\bar{1}\bar{1}0)\wedge(\bar{1}\bar{1}1)$	70 36		82 59
$(010)\wedge(\bar{1}21)$	40 57	40 29 ±13′	
$(\bar{1}00)\wedge(\bar{1}21)$	76 40	76 29 ±10	
$(\bar{1}21)\wedge(\bar{1}\bar{1}1)$	66 50	66 53 ±26	
$(\bar{1}21)\wedge(\bar{2}21)$	13 52	22 56 ±23	
$(\bar{1}21)\wedge(021)$	28 29	27 59 ± 5	
$(100)\wedge(0\bar{1}1)$	70 52	72 15 ±14	

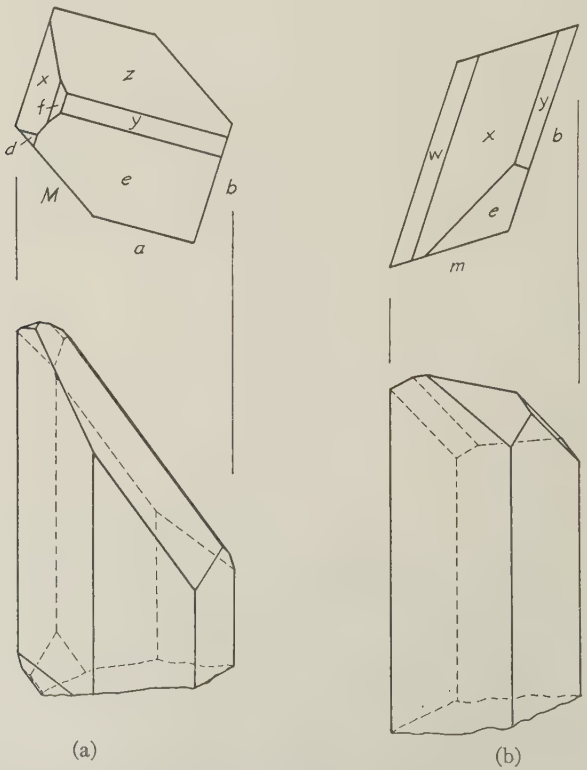

FIG. 4. Walpurgite single crystals, after Fischer: (a) Schneeberg; (b) Joachimsthal.

Walpurgite crystals are generally opaque yellow plates, sometimes with a clear zone at the termination. Fischer's analysis was made on the transparent terminations of the crystals. Gonyer's analysis and the other analyses together with the density measurements were made on samples consisting mostly of opaque material. According to Fischer the opaque parts contain disseminated basic bismuth carbonate. It appears

Table 4. Walpurgite Analyses

	1	2	3	4	5
Bi_2O_3	61.43	59.34	61.8	61.87	62.1
UO_3	20.29	20.54	18.7	16.16	19.0
P_2O_5			0.9	5.88	
As_2O_5	11.88	13.03	14.1	12.45	15.3
H_2O	4.32	4.65	3.7	3.42	3.6
Total	97.92	97.56	99.2	99.78	100.0

1, 2. Weisbach, 1873(6).
3. Fischer, 1948 (5).
4. New analysis by Gonyer (1949) on Schneeberg material.
5. $2Bi_2O_3 \cdot UO_3 \cdot As_2O_5 \cdot 3H_2O$.

likely that the opaque material contains finely disseminated impurities and air or minute open cavities, making these measurements unreliable. Because of the small quantity of clear material available, it has not been possible to improve the data on composition and density. It seems likely that Fischer's analysis gives the best information regarding composition.

Acknowledgments

The cooperation of the Department of Mineralogy at Harvard University has been invaluable for the progress of this work: thanks are due to Prof. Clifford Frondel for the loan of material, to Miss Mary E. Mrose for density measurements, and to Mr. F. A. Gonyer for a chemical analysis. The *x*-ray facilities for the crystallographic investigation were provided by the Laboratory for Insulation Research at the Massachusetts Institute of Technology.

References

1. Dana, E. S., "Dana's System of Mineralogy," 6th ed., p. 860, John Wiley & Sons, New York, 1897.
2. Donnay, J. D. H., *Am. Mineral.*, **28**, 313–328 (1943).
3. Evans, H. T., Jr., *Am. Mineral.*, **33**, 60–63 (1948).
4. Fischer, E., *Zeits. Krist.*, **106**, 25–33 (1946).
5. ———, *Jb. Min.*, Monatsh., Abt. A, 44 (**1948**).
6. Weisbach, A., *Jb. Min.*, 870 (**1871**).
7. ———, *Jb. Min.*, 1 (**1877**).

ZINCIAN ROCKBRIDGEITE*†

MARIE LOUISE LINDBERG AND CLIFFORD FRONDEL,
U. S. Geological Survey, Washington, D. C., and
Harvard University, Cambridge, Massachusetts.

ABSTRACT

Zincian rockbridgeite, $(Fe'', Mn'')(Fe'''_{4-y}, Zn_y)(PO_4)_3(OH)_{5-y} \cdot yH_2O$, is found in fibrous crusts as an alteration product of triphylite in pegmatite at Maxedo, Portugal. It is orthorhombic with cleavages (100) perfect, and (010) fair. The space group is $B2_12$ (D_2^5); $a_0=13.97$, $b_0=16.88$, and $c_0=5.19$ Å. The color is black. The streak and powder are dark green. H=4 to 4½; G=3.51. Indices of refraction and pleochroism: $\alpha=1.82$ (X=greenish blue), $\beta=1.83$ (Y=greenish to yellow brown), $\gamma=1.88$ (Z=deep blue); biaxial positive; 2V moderate with strong dispersion. Analysis: Na_2O 0.13, K_2O tr., Li_2O 0.01, CaO none, FeO 10.86, MnO 2.11, ZnO 5.20, Fe_2O_3 41.19, Mn_2O_3 none, P_2O_5 33.73, H_2O 6.75; insol. 0.30, total 100.28%.

INTRODUCTION

The mineral here described as zincian rockbridgeite was first encountered during the course of a study of dufrenite-like minerals by one of the authors and a summary notice of the mineral has already been published (Frondel, 1949). Zincian rockbridgeite has been found as a hydrothermal alteration product of triphylite in the pegmatite at Vianua do Castelo, Maxedo, Portugal. The material from Maxedo is associated with reddingite, which forms crystalline masses deposited upon crusts of zincian rockbridgeite, together with quartz and small amounts of granular sphalerite. Similar material from Hagendorf, Bavaria, is associated with phosphoferrite (the iron analogue of reddingite), eosphorite, vivianite, and wolfeite (the iron analogue of triploidite). Members of the frondelite-rockbridgeite series can be differentiated from zincian rockbridgeite on the basis of the intensities of the strongest lines in the powder photograph.

PHYSICAL AND OPTICAL PROPERTIES

Zincian rockbridgeite occurs as crusts and small botryoidal masses with a radial fibrous or thin-bladed structure. The surface of the masses is drusy and composed of subparallel aggregates of minute crystals with rounded and exfoliated terminations. No measurable crystals were found. The color is black, and the streak or fine powder is dark green. The mineral is opaque in large pieces, but crushed grains transmit

* Published by permission of the Director, U. S. Geological Survey.

† Contribution from the Department of Mineralogy and Petrography, Harvard University, No. 320.

light feebly and have a deep greenish-blue color. The luster of cleavage surfaces is vitreous and brilliant; the luster of the drusy, free surfaces is dull to satiny. The mineral appears to be fresh and unaltered and in this respect differs from dufrenite and members of the frondelite-rockbridgeite series, as ordinarily found. Hardness 4 to $4\frac{1}{2}$. Specific gravity 3.51. There are two cleavage directions parallel to the direction of the fibers; (100) is perfect and (010) fair.

Optically, zincian rockbridgeite is biaxial, positive, with strong dis-

TABLE 1. CHEMICAL ANALYSES AND RATIOS OF ZINCIAN ROCKBRIDGEITE FROM MAXEDO, PORTUGAL

	Analysis	Ratios	Oxygen Equivalent	Metal Equivalent	Atoms per cell		
P_2O_5	33.73	0.2376	1.1880	0.4752	P	12.29	12.29
FeO	10.86	0.1511	0.1511	0.1511	Fe	3.91	
MnO	2.11	0.0298	0.0298	0.0298	Mn	0.77	
CaO	none						4.81
Li_2O	0.01	0.0003	0.0003	0.0006	Li	0.02	
K_2O	trace						
Na_2O	0.13	0.0021	0.0021	0.0042	Na	0.11	
ZnO	5.20	0.0639	0.0639	0.0639	Zn	1.65	14.99
Fe_2O_3	41.19	0.2579	0.7737	0.5158	Fe	13.34	
H_2O	6.75	0.3747	0.3747	0.7494	H	19.39	19.39
Insol.	0.30						
Total	100.28	Total O = 2.584			O Atoms = 66.85		

Lindberg, *analyst.*

Molecular weight by x-ray = 2587.2 (G = 3.51).

Ideal cell contents of zincian rockbridgeite

$(Fe'', Mn'')_4(Fe'''_{16-x}Zn_x)(PO_4)_{12}(OH)_{20-x}, xH_2O$

Cell contents from analysis

$(Fe'', Mn'')_{4.81}(Fe'''_{13.34}Zn_{1.65})(PO_4)_{12.26}(OH)_{16.23}1.58H_2O$

Formula

$(Fe'', Mn'')(Fe'''_{4-y}, Zn_y)(PO_4)_3(OH)_{5-y} \cdot yH_2O$

persion, and 2V medium. The Z vibration direction is perpendicular to the best cleavage. Lath-like cleavage flakes show parallel extinction. The indices of refraction and the absorption colors of the Maxedo material are: $\alpha = 1.82$ (X = greenish blue), $\beta = 1.83$ (Y = greenish to yellow brown), $\gamma = 1.88$ (Z = deep blue). The absorption formula is $Z > X > Y$.

CHEMICAL COMPOSITION

An analysis of zincian rockbridgeite from Maxedo, Portugal, is given in Table 1. The mineral is of unusual interest because of the large content

of ZnO, 5.20%. The atoms per cell were found by multiplying by the following factors: (1) by 0.01 to convert from a percentage to a fraction scale; and (2) by 2587.2, the molecular weight determined from the x-ray cell contents and specific gravity. Because simple ratios were first obtained by grouping zinc with other divalent ions, $Fe''Fe'''_4(PO_4)_4(OH)_4 \cdot H_2O$ was at first thought to be the formula of the mineral. The formula, however, did not satisfy the space-group requirement of a minimum of four equivalent positions per unit cell, there being 6.5 atoms of divalent metals and 13.3 atoms of trivalent metals. Further, x-ray study by both single-crystal and powder methods indicates that the mineral is isostructural and equidimensional with frondelite-rockbridgeite and hence should conform to the formula of that series $(Fe'', Mn'')Fe'''_4(PO_4)_3(OH)_5$. H. Neumann (1949) in his discussion of the mineralogy and geochemistry of zinc points out that zinc minerals and ferrous iron-magnesium minerals with a corresponding formula usually have a different crystal structure and that there is a tendency for zinc to show selective replacement for atoms with tetrahedral coordination. If zinc substitutes for ferric iron rather than for ferrous iron, a formula similar to that of rockbridgeite is obtained. The substitution of divalent zinc for trivalent iron apparently is compensated electrostatically by a concomitant conversion of hydroxyl to water. The cell contents for this substitution are shown in Table 1. The formula $(Fe'', Mn'')(Fe'''_{4-y}, Zn_y)(PO_4)_3(OH)_{5-y} \cdot yH_2O$, can be derived from the cell contents by dividing by four, the number of equivalent positions in the unit cell. In this division, x/4 was set equal to y in the formula in order not to have a fraction appear as a variable.

Zincian rockbridgeite was formed by the hydrothermal alteration of triphylite containing admixed sphalerite, from which the zinc was derived. The mineral recalls the occurrence at Hagendorf of phosphophyllite, $Zn_2(Fe'', Mn)(PO_4)_2 \cdot 4H_2O$, which similarly is a secondary mineral found associated with rockbridgeite, phosphosiderite, strengite, fairfieldite, and vivianite, and was derived by the alteration of triphylite admixed with sphalerite. Phosphophyllite was not observed on the present specimens.

Zincian rockbridgeite is easily fusible to a magnetic globule. It is soluble in dilute and concentrated HCl, but insoluble in dilute and concentrated HNO_3 and H_2SO_4. It yields H_2O in a closed tube. A spectrographic analysis by H. R. Harrison, Department of Mineralogy, Harvard University, showed the following elements in amounts less than 0.0X%: Ca, Al, Si, Mg, Be, V, B.

The x-ray powder diffraction data suggested that rockbridgeite from Chanteloube, France (U.S.N.M., R5197), may have an intermediate

position in the rockbridgeite-zincian rockbridgeite series, and a partial analysis of the material was made (see Lindberg, 1949, p. 543, for optical constants):

insoluble 1.98, P_2O_5 32.80, Fe_2O_3 53.03, Mn_2O_3 none, FeO 0.13, MnO 3.53, ZnO 0.13, H_2O 7.94 (Al_2O_3, CaO, MgO, K_2O, Na_2O not determined), total 99.54%.

X-Ray Data

Single-crystal rotation and Weissenberg photographs were taken using iron radiation and a manganese filter and rotating about the *b* and *c*

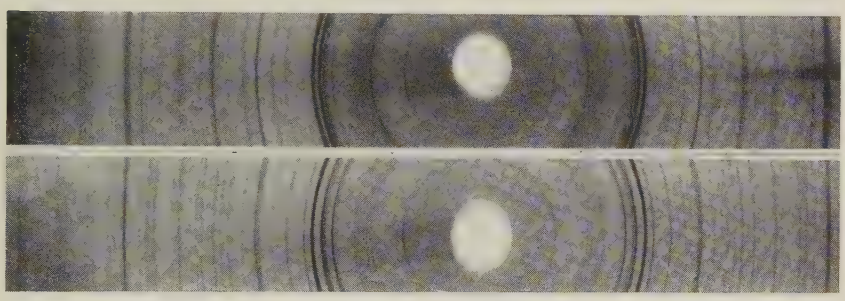

PLATE 1. Powder photographs of zincian rockbridgeite (top) and frondelite (bottom).

axes of fibers of zincian rockbridgeite. C_{2l} symmetry for the 0- and n-level Weissenberg pictures was clearly observed, and the orthorhombic character of the mineral hence confirmed. The lengths of the unit cell edges are $a_0 = 13.97$, $b_0 = 16.88$, and $c_0 = 5.19$ Å; the axial ratio is $a_0 : b_0 : c_0 = 0.8276 : 1 : 0.3075$. The volume of the unit cell is 1223.9 Å^3. The same space group extinctions noted for frondelite (Lindberg, 1949, p. 546) were observed for zincian rockbridgeite; the space group is $B_{22_12}(D_2^5)$.

In Table 2 are given the intensity and *d* values for corresponding lines of frondelite and zincian rockbridgeite, and the powder photographs are shown in Plate 1. Because of the large number of solutions possible for varying *hkl* for lines of high sin θ, lines with *d* spacings less than 1.5 Å were not solved. The intensity of certain lines, particularly those of low 2θ are quite different and a casual comparison suggests that the minerals are not related. The cell edges and space group, however, are the same as for frondelite, and the substitution of zinc for ferric iron doubtless accounts for different intensities. It is well known that two isomorphous crystals in which atoms of different diffracting powers occupy corresponding sites give diffraction patterns in which corresponding reflections have different intensities.

In the powder photograph of zincian rockbridgeite, (020) and (210) are much weaker than in frondelite. The greatest differences in intensi-

TABLE 2. COMPARISON OF *X*-RAY DIFFRACTION DATA FOR FRONDELITE AND ZINCIAN ROCKBRIDGEITE

(Iron radiation, manganese filter)
($\lambda = 1.9373$)

Frondelite				Zincian rockbridgeite		
From rotation and Weissenberg photographs		a_0 13.89 b_0 17.01 c_0 5.21		13.97 16.88 5.19		
Index	I	Observed d	Calculated d	I	Observed d	Calculated d
020	1	8.59	8.51	½	8.40	8.44
200	2	6.90	6.94	3	6.99	6.99
210	1	6.46	6.43	½	6.40	6.45
101	1	4.86	4.88	3	4.84	4.86
111	2	4.69	4.69	1	4.68	4.68
230	1	4.36	4.39	1	4.37	4.38
040	1	4.23	4.25	1	4.20	4.22
131	1	3.68	3.70	1	3.67	3.68
240	4	3.61	3.63	2	3.61	3.61
400	2	3.44	3.46	1	3.47	3.49
301						3.47
410	5	3.38	3.40	2	3.42	3.42
311		3.38	3.39	10	3.33	3.39
420	10	3.20	3.21	9	3.21	3.23
321						3.21
141						3.19
250	3	3.05	3.05	2	3.04	3.04
430	1	2.949	2.960	½	2.968	2.97
331		2.949	2.954	½	2.968	2.95
060	1	2.825	2.835	½	2.812	2.813
151	3	2.779	2.791	1	2.775	2.774
440	1	2.679	2.690	1	2.690	2.690
341	1	2.679	2.685	1	2.690	2.691
002	2	2.597	2.605	2	2.603	2.595
501	3	2.444	2.451			2.460
161			2.452			2.436
202		2.444	2.439			2.432
450			2.432			2.427
351	2	2.415	2.421	3 broad	2.429	2.418
212		2.415	2.414		2.429	2.408
222	1	2.340	2.345	1	2.322	2.338
270	2	2.292	2.294	1	2.279	2.279
610		2.292	2.294			
232	1	2.234	2.224		missing	
460				½	2.185	2.191

TABLE 2. *Continued*

Frondelite				Zincian rockbridgeite		
From rotation and Weissenberg photographs:		a_0 13.89 b_0 17.01 c_0 5.21		13.97 16.88 5.19		
Index	I	Observed d	Calculated d	I	Observed d	Calculated d
171	1	2.175	2.175	½	2.160	2.160
080	2	2.121	2.126	½	2.119	2.110
052	2	2.064	2.068	2	2.059	2.057
422	2	2.030	2.024	1	2.032	2.022
252	3	1.979	1.983	2	1.972	1.974
432	2	1.957	1.956		missing	
181			1.949	½	1.937	1.936
062	1	1.913	1.918	½	1.980	1.907
701	3	1.849	1.852	1	1.869	1.863
262			1.849	1	1.845	1.840
480	1	1.808	1.813	½	1.808	1.806
800		missing		1	1.746	1.746
571				1	1.726	1.722
272	1	1.723	1.722	½	1.714	1.713
820	2	1.694	1.700			1.710
0.10.0				½	1.687	1.688
123			1.689			
830				2	1.665	1.667
490	2	1.659	1.661	1	1.651	1.652
840				2	1.615	1.614
323	5	1.598	1.597	2	1.602	1.593
642						1.603
143			1.597			
333	2	1.562	1.563	1	1.561	1.558
153	2	1.537	1.537	1	1.543	1.530

ties occur at values of d between 3.7 and 3.2. For frondelite there are two pairs of doublets (3.68, 3.61; 3.44, 3.38) followed by the strongest line at 3.20. In zincian rockbridgeite there are two pairs of doublets (3.67, 3.61; 3.47, 3.42) followed by the two strongest lines at 3.33 and 3.21. The differences in intensity and spacings are tentatively explained thus: in frondelite the line with d-spacing 3.38 (observed) corresponds to the (410) and (311) reflections occurring at 3.40 and 3.39 Å (calculated). In zincian rockbridgeite the (410) and (311) reflections are separated and occur at 3.42 (410) (observed and calculated) and 3.33 (311) (observed), 3.39 (calculated). The intensity differences are assumed due in part to

isomorphous substitution of zinc. The Weissenberg pictures of both frondelite and zincian rockbridgeite show strong reflections for (311) and (410). There is a greater difference between observed and calculated values for the (311) reflection than was noted for other reflections; the reason for this difference is not readily apparent. It may be noted that the *d*-spacing for this line of intensity 10 is 3.33, not 3.40 as reported by Frondel (1949, p. 538 "Maxedo unknown").

Acknowledgments

The authors are indebted to H. R. Harrison of Harvard University for making the spectrographic analysis, and to Joseph J. Fahey, K. J. Murata, George T. Faust, C. L. Christ, and Michael Fleischer for helpful suggestions during the preparation of the manuscript.

References

Frondel, Clifford (1949), The dufrenite problem: *Am. Mineral.*, **34,** 513–540.

Lindberg, Marie Louise (1949), Frondelite and the frondelite-rockbridgeite series: *Am. Mineral.* **34,** 541–549.

Neumann, H. (1949), Notes on the mineralogy and geochemistry of zinc: *Mineralog. Mag.* **28,** 575–581.

THE EFFECT OF VARIOUS IMPURITIES ON THE CRYSTALLIZATION OF AMORPHOUS SILICIC ACID

L. S. Birks and J. H. Schulman, *Naval Research Laboratory, Washington 20, D. C.*

Abstract

Five added impurities were found effective in causing amorphous silicic acid to transform to quartz several hundred degrees above its stability limit. These were the carbonates of magnesium, calcium, strontium, barium, and manganese. Five other impurities, Al_2O_3, Bi_2O_3, Li_2CO_3, Na_2CO_3 and $NiCO_3$ did not cause the transformation to quartz but did accelerate the transformation to cristobalite. BeO was the only impurity added for which no crystallization was observed. The lattice constant for the quartz formed in the presence of the five effective impurities was the same as for powdered natural quartz. No explanation is offered for the specific action of the impurities in effecting the crystallization to the quartz structure.

Introduction

It was reported recently (1) that when a mixture of calcium carbonate and silicic acid was heated at 1150° C., quartz as well as cristobalite was formed. This observation has since been confirmed by Bailey (2). Because of the unusual effect of the formation of quartz some 300° C. above its transition temperature, we decided to investigate the action of other impurities besides calcium carbonate. The impurities chosen were $MgCO_3$, $CaCO_3$, $SrCO_3$, $BaCO_3$, BeO, Na_2CO_3, Li_2CO_3, Bi_2CO_3, Al_2O_3, $NiCO_3$, $MnCO_3$ and the percentage added to the silicic acid ranged from 0.25 to 10 mole per cent. The silicic acid was Mallinckrodt "Special Bulky" grade.

Method and Results

The transformations of the silicic acid were studied in the high temperature x-ray diffraction apparatus described by Birks and Friedman (3). This comprised a focusing Geiger counter spectrometer with the specimen heated in a vacuum oven. Specimen preparation was as follows: A 100 mesh platinum gauze was spot welded to a $1\frac{1}{4}\times1\frac{1}{2}$ inch piece of 5 mil platinum foil to be mounted on the heater element. A platinum-platinum 10 per cent rhodium thermocouple was spot welded to the center of the gauze to measure the specimen temperature. Finally, the powder to be examined was pressed into the gauze and scraped off flush with the surface. The actual area of the specimen irradiated by the x-rays was restricted to a spot $\frac{1}{2}$ inch square over which the temperature was uniform.

After pumping the apparatus to 10^{-4} mm. of Hg., an x-ray pattern

was made at room temperature, and then the temperature was raised at 15° C. per minute to 1200° C. Another x-ray pattern was made as soon as the temperature reached 1200° C. and again after holding at

Table 1

Impurity added	Mole per cent of impurity	Observations
$MgCO_3$	0.25–1%	Practically no crystallization.
$MgCO_3$	2.5	Weak cristobalite and quartz at 1300° C. after 30 min.
$MgCO_3$	5.0	Cristobalite and quartz at 1200° C. after 30 min.
$MgCO_3$	10.0	Quartz on reaching 1200° C.
$CaCO_3$	.25	No crystallization.
$CaCO_3$	.5	Weak cristobalite on reaching 1300° C.
$CaCO_3$	1.0	Quartz and cristobalite at 1300° C., both increasing after 30 min.
$CaCO_3$	2.5	Quartz and cristobalite at 1300° C.
$CaCO_3$	5.0	Quartz and cristobalite at 1300° C.
$CaCO_3$	10.0	Cristobalite at 1200°, quartz at 1250 to 1300° C.
$SrCO_3$	.25	No crystallization.
$SrCO_3$	.5	Weak quartz and cristobalite at 1300° C. after 30 min.
$SrCO_3$	1.0	Quartz and cristobalite at 1250° C.
$SrCO_3$	5.0	Weak quartz and very weak cristobalite, some tridymite after 30 min.
$SrCO_3$	10.0	Quartz, cristobalite and some tridymite after 30 min. at 1200° C.
$BaCO_3$	.25–.5	No crystallization.
$BaCO_3$	1.0	Strong cristobalite and weak quartz after 30 min. at 1250° C.
$BaCO_3$	5.0	Cristobalite at 1250° C.
$BaCO_3$	10.0	Cristobalite and perhaps quartz at 1200° C.
$MnCO_3$	5.0	Weak cristobalite on reaching 1250°, cristobalite and quartz after 30 min. at 1250°.
BeO	5.0	No crystallization.
Al_2O_3	5.0	Weak cristobalite after 30 min. at 1300°.
Bi_2O_3	5.0	Cristobalite at 1250° C.
Li_2CO_3	5.0	Strong cristobalite at 1200° C. or lower.
Na_2CO_3	5.0	Strong cristobalite at 1200° C. or lower.
$NiCO_3$	5.0	Weak cristobalite after 30 min. at 1300° C.
Silic acid with no impurity added	—	No crystallization after 30 min. at 1300° C.

1200° C. for a half hour. The temperature was then raised to 1250° C. and 1300° C. and the procedure repeated at each temperature.

In no case where quartz was formed, did its amount decrease with higher temperature. This indicated that once formed, it was stable at high temperature at least for periods up to two hours. The quartz and

cristobalite formed at high temperature both persisted on cooling to room temperature, substantiating the interpretation of the earlier paper that the quartz did not form by transformation from cristobalite. The results for the various specimens are tabulated in Table 1.

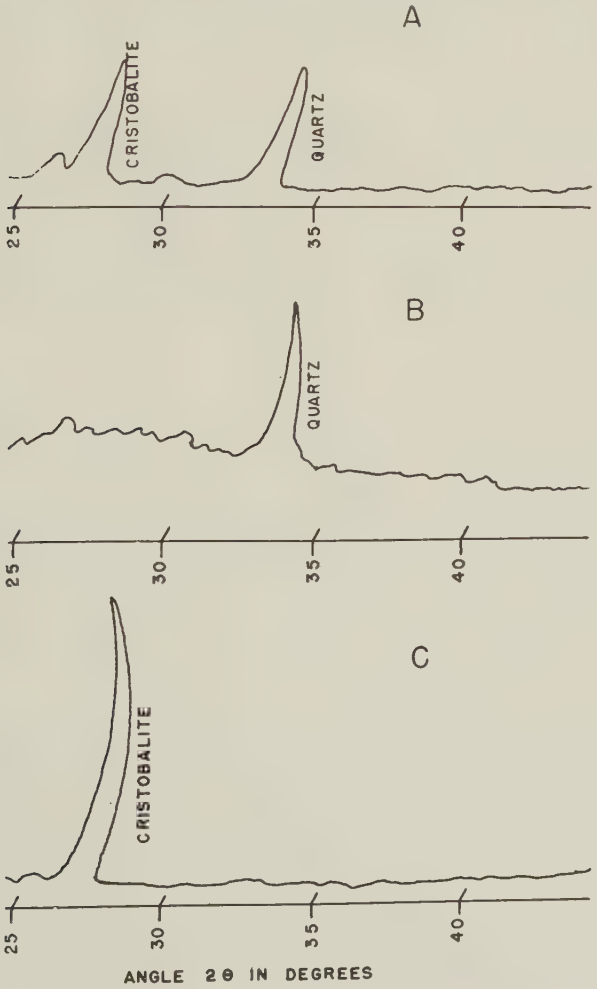

FIG. 1. Unretouched Geiger counter records of typical diffraction patterns. (A) 1% $CaCO_3$, after 30 minutes at 1300° C.; (B) 10% $MgCO_3$, after 10 minutes at 1300° C.; (C) 5% $LiCO_3$, after 30 minutes at 1250° C.

It may be seen from the table that four other impurities, in addition to the $CaCO_3$ previously found effective, caused crystallization to the quartz structure. These effective impurities were Mg, Sr, Ba, and Mn.

Bailey (2) reported that MgO did not cause quartz to be formed; however the maximum temperature he used was 1150° C. We did not observe quartz until the temperature had reached 1200° C. which could account for the apparent discrepancy.

Typical *x*-ray patterns are shown in Fig. 1. (A) shows a transformation to both quartz and cristobalite, (B) shows only quartz and (C), only cristobalite.

An attempt was made to determine whether or not quartz, formed in the presence of additives, had appreciably different cell dimensions from pure quartz. Four samples of silicic acid, containing 5 mole per cent $MgCO_3$, $CaCO_3$, $SrCO_3$ and $BaCO_3$, respectively, were heated for 8 hrs. at 1300° C. *X*-ray patterns made on a 10 cm. radius asymmetric focussing camera at room temperature showed no difference in lattice constant between any of these preparations and powdered natural quartz.

Conclusions

The crystallization of amorphous silicic acid into the quartz structure at temperatures several hundred degrees above the stability limit of quartz, has been shown to take place in the presence of four alkaline earth impurities and also in the presence of manganese. Precision lattice constant determinations gave no evidence that these impurities have entered into the quartz structure formed in their presence. In amounts of the order of one mole per cent or greater, most of the impurities studied very noticeably accelerated the crystallization of the silicic acid into the cristobalite structure, whether or not they were effective in producing quartz.

We can offer no explanation of the specific action of the five impurities found effective for quartz formation. The suggestion of Bailey that a liquid silicate is responsible for the conversions does not seem to be borne out by literature data (4), which show no liquidus in the alkaline earth oxide-SiO_2 systems in the temperature range investigated by him or by us.

Acknowledgment

We wish to thank Mr. R. T. Seal for his help in preparing the *x*-ray diffraction patterns and Mrs. Esther W. Claffy for preparing the samples.

References

1. Schulman, J. H., Claffy, E. W., and Ginther, R. J., *Am. Mineral.*, **34,** 68 (1949).
2. Bailey, D. A., *Am. Mineral.*, **34,** 601 (1949).
3. Birks, L. S., and Friedman, H., *R.S.I.*, **18,** 576 (1947).
4. Hall, F. P., and Insley, H., *J. Am. Ceramic Soc.*, **30** (1947).

SIGNIFICANCE OF THE ORTHOCLASE-ALBITE-ANORTHITE, AND THE $NaAlSiO_4$-$KAlSiO_4$-SiO_2 EQUILIBRIUM DIAGRAMS IN IGNEOUS PETROGENY

Riad A. Higazy, *Farouk I University, Alexandria, Egypt.**

Abstract

High temperature studies of silicate systems indicate that rocks which form at the latest stages of the differentiation of a basaltic magma should have salic normative proportions which lie in the low temperature region of the $NaAlSiO_4$-$KAlSiO_4$-SiO_2 equilibrium diagram. Their normative feldspar content should lie approximately on the cotectic curve of the Or-Ab-An equilibrium diagram. The chemical compositions of some potash- and soda-rich acidic rocks do not harmonize with these requirements. It is suggested, therefore, that such rocks are sometimes enriched in potash or soda through metasomatic processes, in other cases they are derived from the crystallization of potash-rich granitic or soda-rich spilitic magmas respectively, which form by differential remelting of the crust.

Introduction

The potash-rich rocks have normative feldspar contents corresponding to points in the orthoclase field of the Or-Ab-An equilibrium diagram (Bowen, 1928, p. 231). The salic normative constituents other than anorthite of most of these rocks exceed 80 per cent. The plot of the proportions of the salic normative constituents exclusive of anorthite of such potash-rich acidic rocks lies outside the region of low temperature representing the residual magma in the system $NaAlSiO_4$-$KAlSiO_4$-SiO_2 (Schairer & Bowen, 1935; and Bowen, 1937, p. 12). High temperature studies, on the other hand, indicate that rocks formed as products of the latest stages of primary crystallization of a basaltic magma should not have normative feldspar contents which lie in the orthoclase field, and they should have salic normative constituents placing them in the low temperature "valley" in the system $NaAlSiO_4$-$KAlSiO_4$-SiO_2 equilibrium diagram.

The discrepancy between the results of the above-mentioned equilibrium diagrams and the composition of the potash-rich acidic rocks with regard to their magmatic mode of origin needs discussion.

Some Examples of Potash-Rich Rocks

Noble (1948) gave chemical analyses of some potash-rich rhyolites from the Homestake Mine, Lead, South Dakota. He classified these rhyolites into two divisions; namely, high potash and low potash types. Soda and potash of the high potash type ranges from 0.23 to 0.59 per

* On a study leave at Stanford University.

cent and 9.17 to 13.16 per cent, respectively. The potash: soda ratio in these rocks ranges from 15.5:1 to 48.8:1. He mentions that Washington (1917, p. 107) has listed ten other rocks which have chemical compositions similar to those of Lead, South Dakota. They are rhyolites,

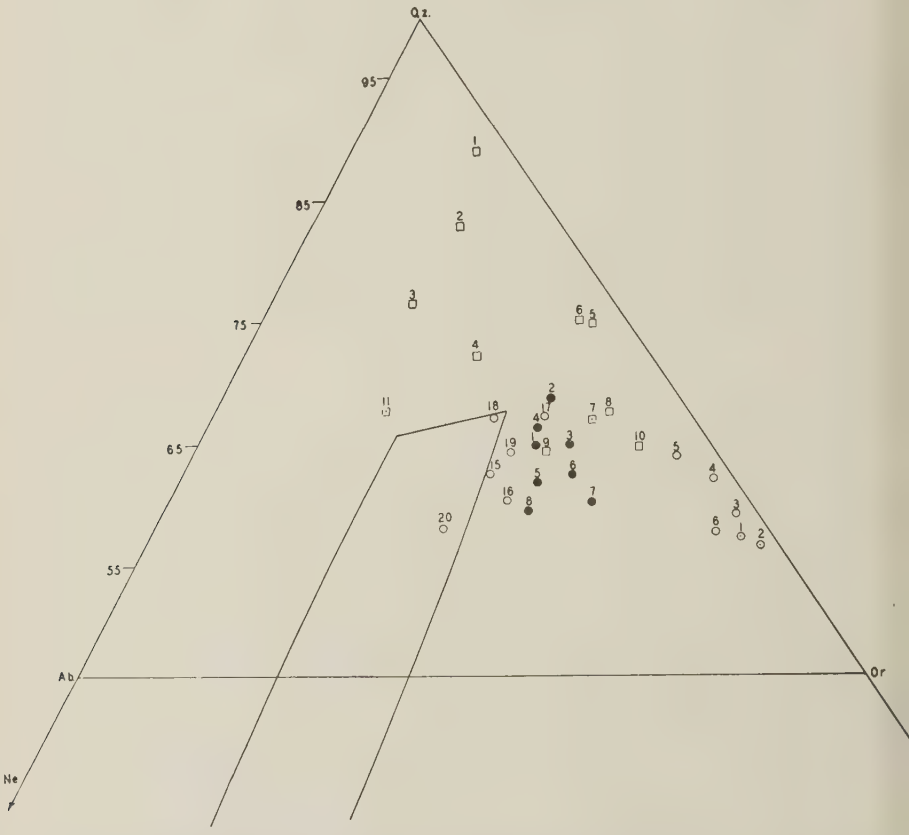

FIG. 1. Squares 1 to 11 = 1 to 11 (Terzaghi, 1948, p. 21). Circles 1 to 6 = 1 to 6 (Noble, 1948, p. 932, high-potash type). Circles 15 to 20 = 15 to 20 (Noble, 1948, p. 932, low-potash type). Solid circles 1 to 8 = averages of rhyolite, rhyolite family 116, sodaclase rhyolite, leuco-rhyolite, all aplites, alkali aplite, runite, and sodaclase granite respectively (Johannsen, 1931, pp. 509–513).

granites, and quartz prophyries. The normative feldspar contents of the rocks studied by Noble (1948, p. 933) as well as those given by the author (Higazy, 1949, Fig. 4) lie in the orthoclase field of the Or-Ab-An equilibrium diagram. In addition to these rocks, there are two rocks (Washington, 1917, p. 79), namely, a porphyry and a pitchstone which have identical chemical character to the high-potash rhyolites studied

by Noble. The porphyry has a potash:soda ratio of 28.5:1 and the pitchstone has a higher ratio since it possesses 6.75 per cent of K_2O and traces of Na_2O.

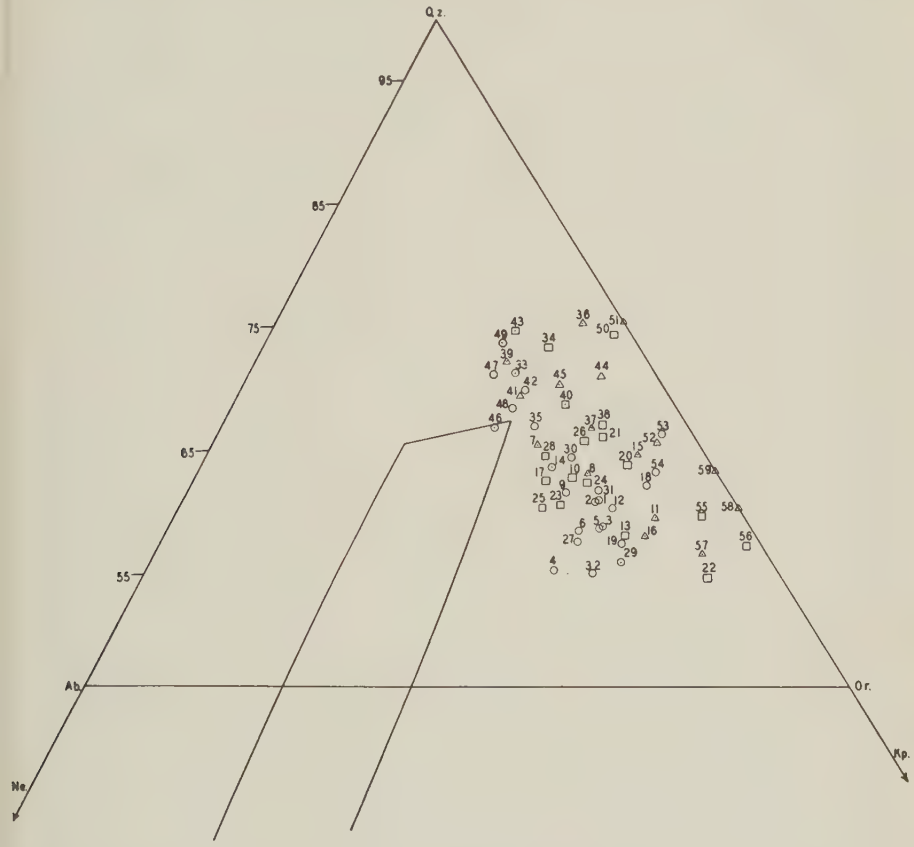

FIG. 2. Circle = deep-seated rocks, triangle = volcanic rocks, square = hypabyssal rocks. 1 to 5 and 6 to 32 = 1 to 5 and 7 to 33. Order quardofelic britannare. Subrang dopotassic omeose (Washington, 1917, p. 109), 33 to 45 = 1, 2, 3, 11, 12, 13, 15, 18, 22, 25, 27, 30, and 31. Order quarfelic columbare. Subrang dopotassic magdeburgose (Washington, 1917, p. 57), 46 to 49 = 10, 31, 32, and 60. Order quarfelic columbare. Subrang sodipotassic alaskose (Washington, 1917, p. 61), 50 and 51 = 1 and 2. Order quarfelic columbare. Subrang perpotassic (Washington, 1917, p. 79), 52 to 59 = 4, 5, 7, 8, 9, 10, 11, and 12. Order quardofelic britannare. Subrang perpotassic lebachose (Washington, 1917, p. 107).

The low-potash rhyolites of the Homestake Mine have soda and potash ranging from 1.84 to 4.48 per cent and 5.11 to 7.50 per cent, respectively. The potash:soda ratio in this type varies from 1.2:1 to 3.3:1. Examples of such rocks given by the author (Higazy, 1949, Fig. 4) are more abun-

dant than those of the high-potash type. They are granites, aplites, and pegmatites; quartz and granite porphyries; rhyolites, pitchstones, obsidians, and comendites—that is, rocks which are supposed to crystallize at the latest stages of the differentiation of the basaltic magma. The normative feldspar contents of the low-potash rhyolites of Lead, South Dakota (Noble, 1948, Fig. 1B), as well as those of the above mentioned examples (Higazy, 1949, Fig. 4), also lie in the orthoclase field. The salic normative proportions, excluding anorthite, of all the cited rocks lie outside the low temperature region of the $NaAlSiO_4$-$KAlSiO_4$-SiO_2 equilibrium diagram, close to its Or point as illustrated in Figs. 1 and 2.

Terzaghi (1948) gave chemical analyses of some potash-rich rhyolites from the Esterel region, France. In these rocks soda and potash ranges from 0.54 to 3.95 per cent and 2.45 to 8.71 per cent, respectively. The potash:soda ratio ranges from 0.8:1 to 11.6:1. It is 0.8:1 in a vitric rhyolite and 0.9:1 in a spherulitic rhyolite. Both of these rocks have normative feldspar content lying outside the orthoclase field of the Or-Ab-An diagram (Terzaghi, 1948, Fig. 1). The potash:soda ratio in the other nine rhyolites studied by Terzaghi ranges from 1.9:1 to 11.6:1. In four rocks the ratio lies within the range of the low-potash type of Noble. The plot of the salic normative constituents excluding anorthite of the Esterel region rocks falls outside the low temperature "valley" of the $NaAlSiO_4$-$KAlSiO_4$-SiO_2 equilibrium diagram, closer to its Q (SiO_2) point as shown in Fig. 1.

Johannsen (1931) gave average chemical compositions of rhyolites, sodaclase rhyolites, leuco-rhyolites, all aplites, alkali aplites, runite, and sodaclase granites. The normative salic constituents of these averages excluding anorthite form more than 80 per cent of the rock composition. The proportions of these constituents are plotted on the $NaAlSiO_4$-$KAlSiO_4$-SiO_2 equilibrium diagram (Fig. 1). They lie outside the "valley" of the residual liquids.

Origin of the Potash-Rich Rocks

The potash-rich rocks may be explained as originating in two ways; namely, (a) crystallization differentiation and (b) metasomatic alterations.

Crystallization differentiation

The formation of a potash-rich liquor at the latest stages of magmatic crystallization has first been shown to be possible by Bowen (1928, p. 231). He postulated a reaction relation between anorthite and orthoclase enabling liquids to cross the cotectic curve of the Or-Ab-An system during the end of the magmatic crystallization history. This supposition

was considered by Noble (1948) to be true and accordingly he favored the differentiation theory to account for the genesis of the rhyolites he studied. However, the reaction relation has recently been found by Schairer and Bowen (1947) to be non-existent so that this hypothesis can no longer hold. Terzaghi (1935) thought that the presence of the normative feldspar content of the potash-rich rocks in the orthoclase field might be due to pressure. However, pressure should have but a negligible effect in the case of the rhyolites since they are extrusive types. Moreover, the author (Higazy, 1949) has shown that pressure does not seen to be responsible for the presence in the orthoclase field of the normative feldspar content of the deep-seated potash-rich rocks of granitic compositions derived from the differential crystallization of a purely basaltic magma. It might be argued that the volatiles affect the course of the crystallization, but the presence of other rocks supposed to form at the latest stages of crystallization whose normative feldspar contents do not lie in the orthoclase field and whose salic normative constituents lie in the low temperature region of the $NaAlSiO_4$-$KAlSiO_4$-SiO_2 diagram leads to the belief that the influence of the fugitive components cannot be the reason that compositions of the potash-rich rocks fail to conform to the crystallization differentiation theory as expressed by the feldspar and the $NaAlSiO_4$-$KAlSiO_4$-SiO_2 equilibrium diagrams. Nockolds (1946) studied some granitic rocks and found that their normative feldspar contents lie approximately on the cotectic curve of the Or-Ab-An equilibrium diagram. These rocks studied by Nockolds could be the result of the latest stages of crystallization of the basaltic magma. This, of course, would only be true in the case that the cotectic curve of the Or-Ab-An diagram is accepted to represent compositions which form at the latest stages of magmatic differentiation.

It may be true that the potash-rich rhyolites of the Lead region (Noble, 1948) are of a truly magmatic origin and have been derived from the differential crystallization of a basaltic magma, but neither the Or-Ab-An nor the $NaAlSiO_4$-$KAlSiO_4$-SiO_2 equilibrium diagram can satisfactorily account for their compositions. If such were the case, it would not be reasonable for petrologists to use the presence of the normative compositions of the different rocks types in certain portions of the equilibrium diagrams as proof or disproof of their derivation from the differentiation of a basaltic magma. If, however, we assume these diagrams to be valid in every case we must seek some other explanation for the origin of these rocks that do not conform to them.

One possible mode of origin of the potash-rich rhyolites is their formation from a primordial rhyolitic magma. Fenner (1948) believes in the presence of two immiscible liquids at high temperature, a rhyolitic one

and a basaltic one; these two liquids re-unite to form a single liquid before crystallization starts unless the two liquids have become separated from each others influence. The potash-rich rhyolites might on this assumption be the result of the crystallization of a rhyolitic magma originally rich in potash. The rhyolites of the Gardiner River area in Yellowstone Park impregnating the basalts of an earlier flow have been shown by Fenner (1948) to support his view. If this were true, one would not expect to find that the compositions of the rhyolites formed in this way follow the rules expressed by both the feldspar and the $NaAlSiO_4$-$KAlSiO_4$-SiO_2 equilibrium diagrams since these apply only in the case of crystallization differentiation of a purely basaltic magma. Under this assumption we can have two types of rhyolites. One type forms as the latest product of the differentiation of a purely basaltic magma, or a re-united mixture of both basaltic and rhyolitic magmas, the rhyolite magma being subordinate in amount. The other type is the product of the crystallization of a purely rhyolitic magma or a re-united mixture of both rhyolitic and basaltic magmas, the basaltic magma being subordinate in amount. The former category of rhyolites would have normative compositions which are in harmony with the phase equilibrium diagrams; examples of these rocks may be those selected by Bowen from the Eastern African lavas (Bowen, 1937). The rhyolites of the latter category would not necessarily have normative compositions which conform to the demands of the differentiation theory because they form substantially from an originally rhyolitic magma.

There are also soda-rich rhyolites. The normative salic constituents of this type also lie outside the field of the low temperature in the $NaAlSiO_4$-$KAlSiO_4$-SiO_2 equilibrium diagram close to its Ab point. Examples of this type are some aplites, microgranite, albite pegmatite, granite porphyry, granophyre, felsite, quartz keratophyre, and soda rhyolites (Washington, 1917, p. 77). Potash in these rocks varies from 0.00 to 0.99 per cent, while soda ranges from 4.53 to 6.89 per cent; the normative orthoclase and albite range from 0.00 to 6.12 and 37.73 to 58.16 per cent, respectively. Hatch (1889, p. 72) gives the chemical composition of a soda felsite from Brittas Bridge, Co. Wicklow, Ireland, which has 0.16 per cent potash and 7.60 per cent of soda. Thomas (1911), in his study of the Skomer volcanic rocks (Pembrokeshire) among which a soda rhyolite possessing 0.38 per cent of potash and 6.40 per cent of soda and whose orthoclase and albite normative percentages are 2.22 and 53.97 respectively, considered the chief mineralogical and chemical peculiarities of the Skomer rocks to be primary and he regarded the series in part as being rich in original soda and as having pantellerian affinities (Thomas, 1911, p. 210). Bowen (1945) in his studies of the

equilibrium relations in portions of the quaternary system, Na_2O-CaO-Al_2O_3-SiO_2, shows that fractional crystallization in these compositions could give rise to differentiates analogous to tephrites, phonolites, and alkali rhyolites (soda-rich). The system studied by Bowen (1945) does not contain any potash. It seems probable that if K_2O were added to this system instead of Na_2O, similar differentiates could develop; namely, leucitites, leucite basalts, leucite bearing phonolites, and alkali rhyolites (potash-rich). There are no studies concerning the presence of both Na_2O and K_2O in a system containing CaO, Al_2O_3, and SiO_2 and the prediction of the actual situation in such a quintuple system would indeed be difficult. The studies of the system $NaAlSiO_4$-$KAlSiO_4$-SiO_2 where potash and soda are equally represented indicate, however, that the latest products of differentiation will be restricted to those which have normative salic constituents which lie in the low temperature region of that system. Compositions which are relatively rich in either potash or soda cannot be explained. It seems, therefore, on the basis of what we know from the dry equilibrium phase diagrams, that the soda-rich and the potash-rich rhyolites could develop as the latest differentiates of two separate magmas, a soda-rich and a potash-rich liquor, respectively. This assumption cannot hold if we consider a primordial basaltic magma as the original material since there is no evident way at present of separating potassium- and sodium- alumino silicates in the differential crystallization of a basaltic magma.

In the pegmatite phase, we may get replacing solutions composed essentially of albitic materials with negligible amounts of potash. In other cases, however, the replacing hydrothermal solutions may be composed substantially of microclinic materials with no or negligible amounts of soda. The question now is; are the albitic or soda-rich material and the microclinic or potash-rich material derived from the same original source? If they came from one source, then it can be assumed that there had been immiscibility between the sodium and the potassium alumino silicates in the hydrothermal stages and this immiscibility might have been assisted by the enrichment in water in the hydrothermal stage. If immiscibility between the sodium and the potassium alumino silicates is effective in the hydrothermal stage, has it also any influence at higher temperatures at which the rhyolites form? Experiments supporting the immiscibility between the alkali alumino silicates at relatively high temperatures are not available. In the absence of such experiments, it is doubtful that this process occurs; it is more reasonable to assume that the albitic soda-rich and the microclinic potash-rich materials have been derived from two different sources.

Wahl (1949) states that during geosynclinal orogenies at least four

different kinds of parental magmas are formed by differential remelting of the crust; (1) spilitic and picrospilitic magmas, (2) granodioritic and dacitic-andesitic magmas, (3) basaltic magma, and (4) granitic magma. Furthermore, under cratogenic conditions other magmas are obtained. One of these magmas is a granitic one which differentiates into potash granite and gabbro-norite-anorthosite. The occurrence of such a granitic magma which is analogous in composition to rhyolitic compositions would solve the problem of the potash-rich acidic rocks. The soda-rich rocks, however, seem to be related to the spilitic and picrospilitic magmas, whereas the normal subalkalic rocks are apparently the differentiates of either a dacitic-andesitic magma or a basaltic magma or both.

Metasomatic alterations

Potash enrichment has been ascribed by some authors to secondary processes. Fenner (1936) has shown that thermal waters containing alkali halides and bicarbonates are still in the process of altering the rhyolite of the Yellowstone Park region. Terzaghi (1948) attributed the enrichment in potash of the rhyolites of the Esterel region, France, to alteration processes. Terzaghi arrived at that conclusion after some field evidences and the investigation of the textures of the studied rhyolites. The presence of the normative feldspar proportions of these rocks in the orthoclase field of the Or-Ab-An equilibrium diagram and the existence of the salic proportions outside the region of low temperature in the $NaAlSiO_4$-$KAlSiO_4$-SiO_2 equilibrium diagram is believed due to the secondary enrichment in potash. The vitric rhyolite studied by Terzaghi possesses a normative feldspar content which lies outside the orthoclase field and close to the cotectic curve of the feldspar equilibrium diagram. This might indicate that the rhyolite before devitrification and alteration was formed as an end stage of the differentiation of a basaltic magma. The formation of some potash-rich pegmatites of the Black Hills, South Dakota, has been shown by the author (Higazy, 1949) to be due to metasomatic processes. This conclusion has been drawn from the study of the chemical compositions and the textural features of the investigated rocks. Examples of secondary soda enrichment are numerous in the literature and need not be cited here. It may then be true that the other potash- and soda-rich rocks are altered by metasomatic processes but this conclusion cannot be arrived at except from field evidences and through investigation of the textural features of every individual occurrence of these rocks. Until we have such studies and more information about every individual case of the potash- and soda-rich rocks it should be stated that it is possible for these rocks to form directly by magmatic crystallization with no alteration. However, the possibility of these rocks

forming from the differentiation of a basaltic magma is very remote, if not altogether non-existent, unless the equilibrium systems which are discussed in this paper are changed in one way or the other in order to harmonize with the extreme compositions which we get in the case of the potash- and soda-rich rocks. The complications and the changes in these systems which are supposed to be due to pressure, water, volatile components, or even the combination of all these factors do not seem to affect the principal results derived from these equilibrium systems. It might possibly be proved that by means of some mechanism or relationship between the different components unknown at the present, that these factors have a significant influence in modifying the principles of crystallization in the studied equilibrium diagrams. Available data and experiments, on the other hand, do not point in that direction. The assumption of the presence of potash- and soda-rich magmas seems to solve the problem of the magmatic derivation of the potash- and soda-rich rocks respectively. Metasomatic processes by flowing pore solutions or diffusion of individual particles (Ramberg, 1944) may also be significant.

Conclusions

The Or-Ab-An and the $NaAlSiO_4$-$KAlSiO_4$-SiO_2 equilibrium diagrams fail at present to account for the derivation of the potash- and the soda-rich rocks from the differentiation of a basaltic magma. Until a reasonable mechanism for their formation from such a magma is known it is assumed that they are in some cases the differentiates of potash-rich rhyolitic and soda-rich spilitic magmas respectively. In other cases, they are probably metasomatic rocks formed from the alteration of other subalkalic rocks. The field and textural features for every individual occurrence must be known to establish their metasomatic derivation.

Acknowledgment

I wish to express my grateful thanks to Dr. J. R. Goldsmith of the University of Chicago for reading the manuscript, to Dr. N. L. Bowen and Dr. J. F. Schairer for their criticism and their valuable suggestions.

References

Bowen, N. L. (1928), The evolution of the igneous rocks, Princeton.

——— (1937), Recent high-temperature research on silicates and its significance in igneous geology: *Am. Jour. Sci.*, **33**, 1–21.

——— (1945), Phase equilibria bearing on the origin and differentiation of alkaline rocks: *Am. Jour. Sci.*, **243-A**, 75–89.

Fenner, C. (1936), Yellowstone Park borehole investigations: *Jour. Geol.*, **44**, 226–315.

——— (1948), Immiscibility of igneous magmas: *Am. Jour. Sci.*, **246**, 465–502.

HATCH, F. H. (1889), On the occurrence of soda-felsites (keratophyres) in Co. Wicklow, Ireland: *Geological Mag.*, **6,** 70–83.

HIGAZY, R. A. (1949), Petrogenesis of perthite pegmatites in the Black Hills, South Dakota: *Jour. Geol.*, **57,** 555–581.

JOHANNSEN, A. (1931), The average chemical compositions of various rock-types: Sonder Abdruck aus dem neuen *Jahrbuch f. Mineralogie, etc., Beilage-Band* **64,** Abt. A., (Brauns Festband), 505–516.

NOBLE, J. A. (1948), High potash dikes in the Homestake Mine, Lead, South Dakota: *Bull. Geological Soc. Am.*, **59,** 927–940.

NOCKOLDS, S. R. (1946), The order of crystallization of the minerals in some Caledonian plutonic and hypabyssal rocks: *Geological Mag.*, **83,** 215.

RAMBERG, H. (1944), The thermodynamics of the earth's crust I. Preliminary survey of the principal forces and reactions in the solid crust: *Norsk. Geologisk Tidskrift*, **24,** 104.

SCHAIRER, J. F., AND BOWEN, N. L. (1935), Preliminary report on equilibrium-relations between feldspathoids, alkali-feldspars, and silica: *Trans. Am. Geophys. Union*, 16th Ann. Meeting, 325–328.

——— AND ——— (1947), The system anorthite-leucite-silica: *Bull. de la Comm. Geologique de Finlande*, **140,** 67–87.

TERZAGHI, R. (1935), The origin of the potash-rich rocks: *Am. Jour. Sci.*, **30,** 141–142.

——— (1948), Potash-rich rocks from the Esterel, France: *Am. Mineral.*, **33,** 18–30.

THOMAS, H. H. (1911), The Skomer volcanic series (Pembrokeshire): *Quart. Jour. Geological Soc. London*, **67,** 210.

WAHL, W. (1949), Isostacy and origin of sial and sima and of parental rock magmas: *Am. Jour. Sci.*, **247,** 145–167.

WASHINGTON, H. S. (1917), Chemical analyses of igneous rocks: *U. S. Geological Surv., Prof. Paper* **99.**

CRESTMORE SKY BLUE MARBLE, ITS LINEAR THERMAL EXPANSION AND COLOR

Joseph L. Rosenholtz and Dudley T. Smith,
Rensselaer Polytechnic Institute, Troy, New York.

Abstract

Thermal studies were made of the Sky Blue marble from Crestmore, California. The coefficients of linear thermal expansion were determined from 20° to 700° C. for specimens cut with N-S, E-W and vertical geographic orientations. First cycle values are very high and indicate a condition of high strain which is largely relieved by heat treatment. The computed optic axis concentration shows a marked E-W preferred orientation which may be correlated with the geological structure. The sky-blue color is attributed to residual strain.

Introduction

Thermal studies of oriented specimens of Yule marble (1) have indicated the possibility of correlating linear thermal expansion with the stresses involved in deformational processes. Dr. Eleanora B. Knopf, in discussing this question with Professor A. O. Woodford of Pomona College, suggested that such an investigation of the Sky Blue marble found at Crestmore might present interesting results.

Through the kindness of Professor Woodford, several large samples were collected in the field, some of which were oriented as to dip and strike. The grain size is so varied that there was hope of obtaining a few sufficiently large grains to withstand the rigors of cutting oriented specimens and thereby permit single crystal studies to be made. Unfortunately, none could be obtained large enough for this purpose and, through Professor Woodford's efforts, suitable specimens were selected having a 2–3 mm. grain size. Test sepcimens were cut from a single field sample taken from the Commercial Quarry, Crestmore, California, at about 900′ elevation, 2700′ East and 1500′ North, Riverside Cement Company coordinates. The field sample surface dipped 27° E. and the strike was N 10° E. Test specimens having N-S, E-W., and vertical orientations were cut from this sample.

Procedure

The method used for measurement of the coefficient of linear thermal expansion, α, has been fully described (1). In order to determine the effect of heat treatment upon the relief of permanent strain, the two cycle heating-cooling technique was followed. Experience with Yule marble indicated the possibility of introducing what appear to be thermal strains in the vicinity of 350°. In an attempt to eliminate this possibility,

a series of oriented specimens were first studied cyclically to 400° C. The length recovery after the second heating cycle was much greater than it should have been had the deformational strains been removed. It was therefore decided to proceed exactly as in the case of the Yule marble and to use two heating-cooling cycles to 700° C.

The values of the coefficients of thermal expansion are given in Table 1 for each geographic orientation and for both heating-cooling cycles.

TABLE 1. COEFFICIENTS OF LINEAR THERMAL EXPANSION OF CRESTMORE SKY BLUE MARBLE

First Heating-Cooling Cycle

20° C. to	N-S×10⁶	E-W×10⁶	Vertical×10⁶	Volume coefficient ×10⁶ calc.
100°	6.44	21.62	3.75	31.81
200°	10.11	26.83	7.67	44.61
300°	13.11	31.11	10.21	54.43
400°	15.00	34.08	12.08	61.16
500°	17.02	36.35	13.64	67.01
600°	18.95	37.73	14.83	71.50
700°	20.78	39.19	16.20	76.17
Length recovery after cooling	0.54%	0.85%	0.56%	

Second Heating-Cooling Cycle

20° C. to	N-S×10⁶	E-W×10⁶	Vertical×10⁶	Volume coefficient ×10⁶ calc.
100°	2.19	12.62	−0.25	14.56
200°	4.38	14.67	0.66	19.71
300°	6.39	17.57	2.50	26.46
400°	8.55	20.08	4.13	32.76
500°	10.81	22.52	5.87	39.20
600°	13.28	25.09	8.32	46.69
700°	15.96	27.86	10.79	54.61
Length recovery after cooling	0.11%	0.21%	0.13%	

The curves shown in Fig. 1 indicate that the rate of increase of α is more regular after the strains are relieved during the first heating-cooling cycle. For comparison with a calcite single crystal, the calculated volume

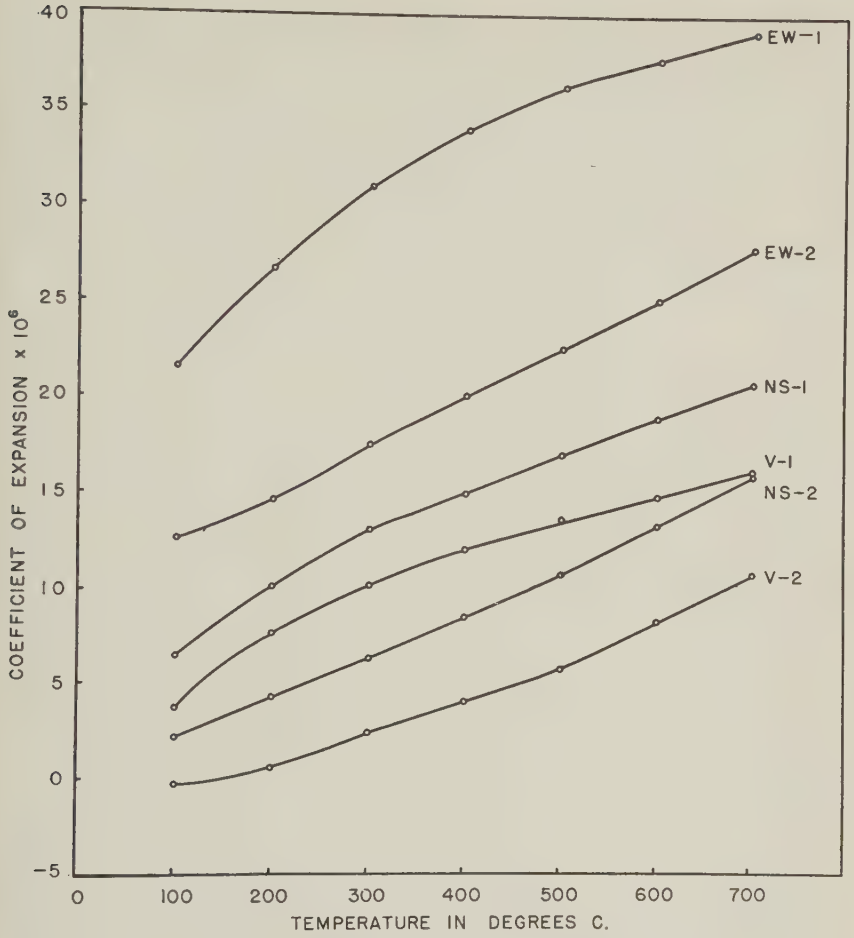

FIG. 1. The coefficients of linear thermal expansion from 20° C. for two heating-cooling cycles of Crestmore Sky Blue marble.

expansion coefficients are shown in Fig. 2. The correspondence at 100° is very good between calcite and second cycle marble. This is an indication that structural strains have been largely removed. As the temperature is increased, however, the volume change in the marble diverges appreciably. This may well be due to the introduction of strains induced by heating because of the marked anisotropy of thermal expansion of calcite.

ORIENTATION OF THE MARBLE

Woodford (2) has found that, while the structure at Crestmore is quite uncertain, there are some observable suggestions of bedding having an

easterly dip. He indicates* that, for the area from which the field specimen was obtained, any expansive force related to the intrusion of the quartz monzonite porphyry would probably have been directed approximately in the same direction as the normal to the problematical bedding planes in the marble. This indicates a maximum stress in the E-W direction whether thermal or deformational stresses or both are involved.

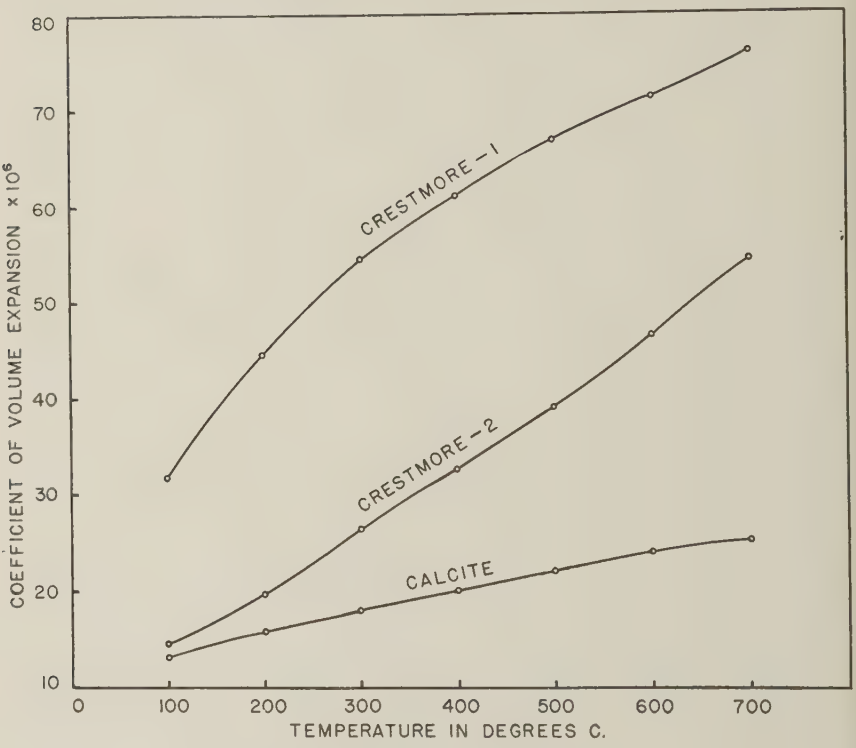

FIG. 2. Calculated coefficients of volume thermal expansion from 20° C. of Crestmore Sky Blue marble and a calcite single crystal.

The authors have recently made studies of linear thermal expansion of compressed cylinders of magnesium and medium soft steel (3). They found that α increases in a stress range beginning at the yield point and continuing until extensive plastic deformation occurs, after which it begins to decrease. It is inferred, therefore, that a high value of α may be correlated with a large stress history and, since α for Sky Blue marble is a maximum in the E-W orientation, it is logical to assume that this was the direction of maximum stress. Although the structural details

* Personal communication.

are not clear, this assumption corresponds with the available field facts and may be used to point the way in the evaluation of obscure field information.

As for preferred grain orientation, calculations based upon the coefficients obtained from the second heating-cooling cycle at 20°-100° C. indicate that 59 per cent of the grains have their optic axes concentrated in the E-W direction, with 25 per cent N-S and 16 per cent vertical. Although these calculated concentrations are based upon the assumption that only *c* or *a* orientations exist in each geographic direction, the results show the decided preference in the E-W direction.

The Color of Sky Blue Marble

The name of this recrystallized limestone is most descriptive of its color. Of particular interest is the fact that the blue marble makes an irregular envelope 100 to 150 feet thick, about an intrusion of quartz monzonite porphyry; it is, in turn, enveloped by white marble. The blue marble, which appears quite uniform to the unaided eye, shows microscopic black segregations scattered throughout. Segregations which have been weathered slightly are surrounded by ferric oxide stains.

Small pieces of the blue marble were heated to various temperatures, beginning at 100° C. and increasing by 25° intervals. The samples were held at each temperature for 30 minutes. The first observable fading was produced by heating at 225° C; it was more pronounced at 250° and was complete at 275°, resulting in a light cream-white color. If the heating rate is not sufficiently slow, the blue marble samples shatter explosively into white cleavage fragments in the vicinity of 275° C.

It seemed advisable to ascertain whether the color changes noted might be due to chemical effects. Professor Arthur A. Burr of Rensselaer Polytechnic Institute kindly agreed to make spectrographic and powder *x*-ray examinations of the blue marble as well as specimens which were heated to 275° and 700° C., in order to seek out possible coloring constituents. The spectrographic examination showed a small amount of iron and no other coloring elements; furthermore, the concentration of iron was the same in all three specimens. No irregularities of any kind were revealed by the *x*-ray examination. While structural strain is readily shown by *x*-ray, in this case the strain was doubtless relieved by the pulverization.

It is obvious that the color change induced by heat treatment under 300° C. was not due to chemical changes. The only apparent reason for the blue color appears to be residual strain which is relieved by heating. It is perfectly reasonable to assume that structural changes due to thermal or deformational stresses may produce pronounced color effects.

This condition may be brought about in some alloys by cold working processes and it may well be that particular stress conditions can produce color changes in calcite.

This raises the large question as to why most marbles are not blue. Disregarding definite coloring constituents, stress conditions are so variable, both as to character and intensity, that the answer cannot be known until the specific conditions which are color inducing are discovered.

Acknowledgments

This research was made possible by assistance from the Rensselaer Polytechnic Institute Research Fund. The authors are especially grateful to Professor Woodford for collecting the specimens and for information he has supplied relative to field observations. They also are indebted to Professor Burr for his spectrographic and x-ray examinations of the marble specimens.

References

1. Rosenholtz, J. L., and Smith, D. T.: *Am. Mineral.*, **34**, 846–854 (1949)
2. Woodford, A. O.: *Calif. Jour. Mines and Geology*, Report **XXXIX**, State Mineralogist, July 1943, 333–365.
3. Rosenholtz, J. L., and Smith, D. T.: *J. Appl. Phys.*, **21**, 396–399 (1950).

NEW DATA ON LOSSENITE, LOUDERBACKITE, ZEPHAROVICHITE, PEGANITE, AND SPHAERITE

Richard M. Pearl,*
Colorado College, Colorado Springs, Colorado.

Abstract

Lossenite of Milch (1894) from Laurium, Greece, is shown to be a mixture of scorodite and beudantite. Louderbackite of Lausen (1928) from the fire zone of the United Verde mine at Jerome, Arizona, is identical with roemerite. Zepharovichite of Bořický (1869) from Třenice, Bohemia, is very probably identical with wavellite. Peganite of Breithaupt (1830) from Langenstriegis, Saxony, is identical with variscite as earlier stated by Larsen and Schaller (1925). Sphaerite of Zepharovich (1867) from Zaječow, Bohemia, is probably identical with variscite.

Lossenite

Lossenite was described by Milch (12) in 1894 as a new orthorhombic mineral resembling scorodite in habit. It was found with scorodite and calcite at Laurium, Greece, in druses in a ferruginous quartzose rock. It occurred in acute pyramids, one-half to three millimeters in length, brownish red in color and often altered on the surface. Lacroix (5) in 1915 found beudantite associated with scorodite at this locality and expressed his belief that the original determination of lossenite had been made on a mechanical mixture of beudantite and scorodite. The chemical analysis of the original lossenite and the calculated percentage compositions of beudantite ($PbFe_3(AsO_4)(SO_4)(OH)_{16}$) and of scorodite ($FeAsO_4 \cdot 2H_2O$) are tabulated below for comparison.

	PbO	Fe_2O_3	As_2O_5	SO_3	H_2O	$CaCO_3$	SiO_2	Total
"Lossenite"	10.63	34.53	33.44	3.74	15.55	1.46	1.13	100.48
Beudantite	31.35	33.68	16.14	11.24	7.59			100.00
Scorodite		34.60	49.79		15.61			100.00

A re-examination of type material from Laurium in the Harvard collection (No. 89508) shows the "lossenite" to be partly covered with rhombohedrons of beudantite. This identification of beudantite was suggested by the appearance of the pseudo-cubic crystals and proved by their optical properties and the *x*-ray powder pattern. If the sample upon which the original analysis was made was actually scorodite containing particles of this beudantite, there would be an adequate explanation for the presence of the lead and the sulfate in addition to the constituents due to the scorodite. This is presumed to have been the case,

* Contribution from the Department of Mineralogy and Petrography, Harvard University, No. 323.

especially since Milch described some of the lossenite crystals as being covered with an olive-green alteration layer, whereas the larger crystals had a coating of iron hydroxide. These are obviously two different minerals on the specimen examined here; it is the beudantite crystals that show the alteration layer, which has a greenish yellow color and a bright luster, and is exceedingly thin.

The x-ray powder pattern of the lossenite, carefully selected for its freedom from beudantite, is the same as that of scorodite from Utah. The interplanar spacing is somewhat greater in the lossenite than in this particular scorodite, indicating a very slightly larger unit cell, but this increase is within the range of scorodite, in which there may be a substitution of aluminum for iron (toward mansfieldite) and of phosphorus for arsenic (toward strengite).

Lossenite and scorodite are optically similar. The indices of refraction of lossenite ($n\mathrm{X}=1.783$, $n\mathrm{Y}=1.788$, $n\mathrm{Z}=1.818$) are within the ordinary range of published values for scorodite and are relatively close to the values $n\mathrm{X}=1.771$, $n\mathrm{Y}=1.805$, $n\mathrm{Z}=1.820$ found for the scorodite from the Kiura mine, Bungo, Japan. Both lossenite and scorodite are optically positive, with $\mathrm{X}=a$, $\mathrm{Y}=c$, $\mathrm{Z}=b$, and $r>v$. The other physical properties and the crystallography of lossenite are similar to those of scorodite. For the unit pyramid of lossenite, $\phi=50°\ 12'$, $\rho=55°\ 53'$ (calculated from Milch's original inadequate data); and of scorodite, $\phi=49°\ 02'$, $\rho=55°\ 42'$.

Louderbackite

Louderbackite was described by Lausen (11) in 1928 as a new mineral formed under fumarolic conditions, together with eight other hydrous sulfates (four of which were also regarded as new species), as a result of a fire in the United Verde copper mine at Jerome, Arizona. It occurs as a translucent to transparent thin crystalline crust of pale chestnut-brown color.

The absence of certain critical data in the original description of louderbackite, together with apparent similarities between louderbackite and roemerite, suggested the advisability of re-examining this mineral. The study was made on a type specimen of louderbackite from Jerome (H. 90534). The reported chemical analysis of louderbackite is given below in comparison with the calculated percentage composition of roemerite.

	Na_2O	FeO	Fe_2O_3	Al_2O_3	SO_3	H_2O	Total
Louderbackite	0.88	7.01	20.84	2.55	39.34	31.33	101.95
Roemerite		8.94	19.86		39.83	31.37	100.00

The x-ray powder pattern of louderbackite is identical with that of

roemerite. Any changes in structural dimensions due to difference in chemical composition between the two specimens is imperceptible. The indices of refraction of louderbackite as newly determined diverge somewhat from those of roemerite as shown in the following tabulation:

	Louderbackite Lausen (11)	Louderbackite (New data)	Roemerite Rammelsberg (New data)	Roemerite California (10)
nX	1.544	1.543	1.525	1.526
nY	1.558	1.560	1.571	1.571
nZ	1.581	1.582	1.582	1.583

A difference in composition must be responsible for this divergence. The different indices also account for the fact that louderbackite is optically positive, whereas roemerite is negative. 2V is about 40° or 45° for both minerals. Louderbackite is non-pleochroic, whereas roemerite is pleochroic in colorless and lemon yellow. The very strong disperison ($r>v$), not previously recorded for louderbackite, is characteristic of both minerals, as may be expected from the chemical composition. The other physical properties of both minerals are closely alike. It is improbable that louderbackite is orthorhombic as stated; in sodium light, used to eliminate the anomalous interference colors, the extinction is found to be inclined rather than parallel. The triclinic crystallization of roemerite is well known. Attention should be called to the chemical analysis of louderbackite. Depending upon the selection of material and the adequacy of the analysis, louderbackite may be regarded as an aluminian variety of roemerite, explaining thereby the optical differences between them.

Zepharovichite

Zepharovichite was described as a new mineral from Třenice near Cerhovic, Bohemia, in 1869 by Bořický (1). The chemical analyses were based upon admittedly impure material, and Dana (3) long ago expressed doubt that the species was valid because of its resemblance in composition to callainite, which he regarded as a distinct mineral. Callainite has since been shown by Lacroix (4) to be in all probability identical with variscite. Two of the original analyses of zepharovichite are given below in comparison with the calculated composition of wavellite.

	CaO	Fe_2O_3	Al_2O_3	P_2O_5	H_2O	SiO_2	Total
Zepharovichite	0.54		28.44	37.46	26.57	6.05	99.06
Zepharovichite	1.38	0.86	29.60	37.80	28.98	0.46	99.08
Wavellite			37.11	34.47	28.42		100.00

No optical data were given in the original description. A later observation by Slavik (14) put the mean index of refraction at 1.55, the fibers

having positive elongation. Larsen (6) recorded a similar index, with a birefringence about 0.01 to 0.02, on material from the original locality, and stated that the mineral may be impure wavellite. A specimen labelled zepharovichite (H. 101399) from Cerhovic, Bohemia, occurring as a white fibrous crust with the same optical properties, gave an x-ray powder pattern like that of authentic wavellite from Montgomery County, Arkansas. In view of these facts, zepharovichite appears to be identical with wavellite. Some uncertainty still remains, however, since the specimen examined is not of the type material.

Peganite

Peganite was described in 1830 by Breithaupt (2) as a new mineral, occurring in a thin crystalline crust on a siliceous rock at Langenstriegis, east of Frankenberg, Saxony. The general appearance of the material, its chemical composition, and its association with wavellite have since suggested a possible identify with variscite. Moschetti (13) in 1918 re-analyzed a specimen from the original locality and found the formula to be the same as that of variscite. Larsen and Schaller (7) further suggested the identity of peganite and variscite from optical data—the indices of refraction, sign, 2V, elongation, and extinction being similar. They recommended that the name peganite, which, though older, had been proposed for a mineral that was improperly analyzed, be discarded.

Peganite from the type locality (H. 101400) has been re-examined by both optical and x-ray methods. The material answers to the original description, consisting of dark- and bright-green radiating fibers in botryoidal crusts and has indices of refraction ($n\mathrm{X}=1.562$, $n\mathrm{Y}=1.582$, $n\mathrm{Z}=1.588$) that check with those obtained by Larsen and Schaller. This authenticated peganite gave an x-ray powder pattern exactly like that of authentic specimens of the green variscite from Fairfield, Utah, described by Larsen and Shannon (8) and by Larsen (9). The name peganite should by now be fully discredited.

Sphaerite

Sphaerite was described in 1867 by Zepharovich (15) as a new mineral occurring in small globules at Zaječow, north of St. Benigna, Bohemia. Larsen (6) published some optical data on a specimen from Cerhovic, Bohemia. The optical properties of a specimen of sphaerite labelled as from Cerhovic, Bohemia, in the Harvard collection (H. 98201) are within the range of microcrystalline variscite. The mineral occurs as greasy, bluish gray spherulitic shells and appears coarsely fibrous to platy under the microscope. It is associated with wavellite, which is in characteristic radiating globules. The indices of refraction are $nX=1.564$, $nY=1.577$,

$nZ = 1.590$. The optic sign is negative, but the elongation is positive. $2V$ is large, about 70°.

Another specimen of sphaerite labelled as from Třenice, Bohemia, (H. 98149) gives closely similar indices of refraction and other optical properties, and both specimens check with the data given by Larsen for so-called sphaerite from these localities. The x-ray powder patterns of the sphaerite from Cerhovic and Třenice are identical with that of variscite from Fairfield, Utah.

The original analysis of sphaerite from Zaječow is given below in comparison with the calculated percentage composition of variscite.

	CaO	MgO	Al_2O_3	P_2O_5	H_2O	Total
Sphaerite	1.55	3.04	42.56	27.90	24.06	99.11
Variscite			32.26	44.94	22.80	100.00

It is impossible to reconcile the analyses of the two minerals. Significant amounts of CaO and MgO have been reported in analyses of variscite, but the greater amount of aluminum and the lesser amount of phosphorus in sphaerite as compared to variscite is not easily explained as due other than to gross admixture. No evidence of such admixture was found in the present optical and x-ray study, and it appears that sphaerite is wholly identical with variscite. A re-examination of type material would be desirable.

Acknowledgment

Grateful acknowledgment is made to Dr. Clifford Frondel for his supervision and generous help throughout.

References

1. Bořický, E.: *Sitzber. Ak. Wien*, **59**, 593 (1869).
2. Breithaupt, A.: *J. Chemie u. Phys.*, **60**, 308 (1830).
3. Dana, E. S.: System of Mineralogy, 6th ed., 825 (**1892**).
4. Lacroix, A.: *Min. de la France*, **4**, 480 (1910).
5. ——— *Bull. soc. min.*, **38**, 35 (1915).
6. Larsen, E. S., Jr.: *U. S. Geol. Surv., Bull.* **679**, 135, 158 (1921).
7. ——— and Schaller, W. T.: *Am. Mineral.*, **10**, 23 (1925).
8. ——— and Shannon, E. V.: *Am. Mineral.*, **15**, 307 (1930).
9. Larsen, E. S., III: *Am. Mineral.*, **27**, 281 (1942).
10. Landon, R. E.: *Am. Mineral.*, **12**, 279 (1927).
11. Lausen, C.: *Am. Mineral.*, **13**, 220 (1928).
12. Milch, L.: *Zeit. Krist.*, **24**, 100 (1894).
13. Moschetti, L.: *Atti Accad. Sci. Torino*, **53**, 1062 (1918).
14. Slavik, F.: *Rozpravy České Ak.*, **26**, Cl. 2, no. 60 (1917).
15. Zepharovich, V. R.: *Sitzber. Ak. Wien*, **56**, 24 (1867).

NONTRONITE AT BINGHAM, UTAH

Bronson Stringham and Allen Taylor,
University of Utah, Salt Lake City, Utah.

Abstract

Nontronite has been found in abundance on the upper southwest levels of the Kennecott Copper Mine at Bingham, Utah. The rocks in this area were originally arkosic quartzites with dolomitic and/or argillaceous impurities. Contact action in these rocks has developed interstitial diopside, tremolite and pyrophyllite. Nontronite is present in localized areas as a weathering product of these minerals, where pyrite was present to supply sufficient iron for its development. Chemical analysis shows the mineral to have the formula:

$$(Al_{.77}Fe_{1.02}Mg_{.31})\ (Al_{.33}Si_{3.67})O_{10}(OH)_{2\times.36}.$$

Field evidences point to the conclusion that this nontronite formed in slightly acid solutions.

Introduction

During the progress of mapping the geology and hydrothermal alteration areas in the Bingham Copper Mine, nontronite was discovered in abundance in arkosic quartzite areas. The geological conditions at Bingham, Utah, are fairly well known through the writings of Boutwell (1905), Keith (1905), Butler (1920), Beeson (1917) and others. In brief, however, the geology may be stated as follows: a series of folded Pennsylvanian quartzites interbedded with several limestone lenses have been intruded by a comparatively small complex igneous mass called the Bingham stock. Contact action and hydrothermal alteration has materially changed the original character of all types of rock in the immediate area of the mine.

Occurrence of the Nontronite

The greenish nontronite is found in the altered quartzites generally at some distance from the intrusion, in areas where excavation in mining operations has not proceeded to great depth. These areas include the highest 10 levels in the south-west section of the mine, where the best specimens are obtained, and the upper 7 or 8 levels on the east side of Bingham Canyon. The nontronite seems to be present in two ways: (1) in patches associated with limonite chiefly in the vicinity of the uppermost levels, and (2) along cracks and joints, not particularly associated with limonite, in a somewhat larger area lower down in the quartzite, where it appears to have been transported as a dispersed phase in ground waters.

The original clastic sediments of the Bingham area were arkosic sandstones with orthoclase as the principal feldspar. Dolomitic and clay material apparently were the chief impurities. Since deposition the

quartz and feldspar sand grains have been completely recrystallized, and contact action accompanying the intrusion has changed the interstitial material to tremolite (see Fig. 1*A*), pyrophyllite (see Fig. 1*B*) and diop-

FIG. 1. Arkose, Bingham, Utah (×72). showing recrystallized quartz (Q) and orthoclase (Or) with nontronite (N) altering from interstitial tremolite (T) in *A*, and interstitial pyrophyllite (P) in *B*. In *C* nontronite is present in square patches presumably pseudomorphous after pyrite; while transported nontronite is seen in a veinlet cutting quartz and orthoclase and terminating against a bleb of limonite (Lm).

side all of which are generally present in an interstitial position and are rarely observed to occur together. Thin sections of the nontronite-bearing rocks show that fine aggregates of nontronite are present along the edges and sometimes completely within these interstitial "contact" minerals (see Fig. 1*A* and 1*B*). Figure 1*C* shows a comparatively pure arkose

which contains nontronite in square or oblong patches and also in a veinlet which traverses quartz and orthoclase grains alike. The square patches are believed to represent former pyrite crystals thus furnishing evidence that nontronite may be pseudomorphous after pyrite. The veinlet is an example of the type of nontronite which has been transported.

In all instances where patches of nontronite are found, a limonite vein or veins are present in the immediate vicinity. Figure 2 shows an actual

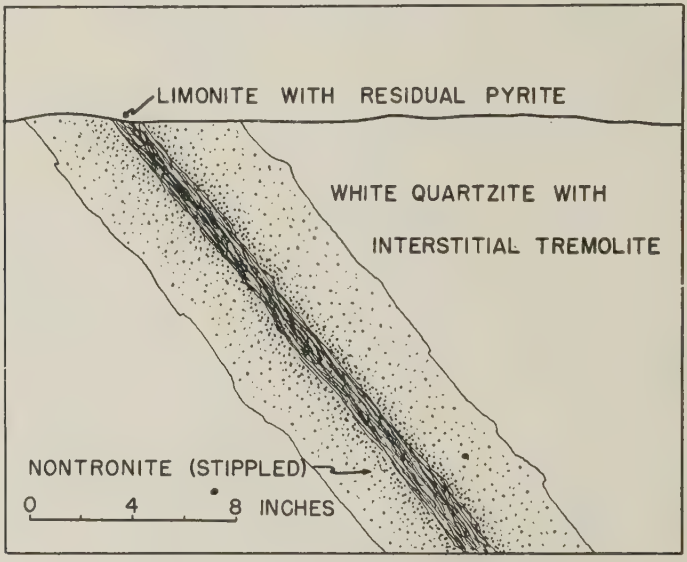

FIG. 2. Shows a section of a limonite vein in quartzite with nontronite equally developed on both sides.

condition which is representative of this relationship. Here a 2 to 3 inch limonite vein containing a few remnant pyrite crystals, traverses white quartzite where tremolite is the interstitial mineral. The white quartzite is colored greenish by nontronite for a distance of 4 to 5 inches on either side of the limonite vein. Thin sections of the greenish rock show the condition described above (Fig. 1*A*), that nontronite is altering from the tremolite.

MINERALOGY

Allen and Scheid (1946), and Ross and Hendricks (1945), have covered the literature on nontronite rather thoroughly and information relating to previous work need not be repeated here except simply to state that nontronite is now considered to be the high iron member of the montmorillonite-beidellite mineral group.

Chemical Analysis.—Special care was necessary in selecting specimens of nontronite for analysis. Some material was obtained from a particularly rich area near the top southwest part of the mine which contained only a very little quartz and orthoclase as an impurity. This material was quite wet when first collected but dried immediately when it was exposed to the air at room temperature. This dried sample was ground to 200 mesh and then centrifuged to obtain as pure a sample as possible. The chemical analyses given in Table 1 were made by Mr. Harold R. Bradford at the University of Utah. With these figures a formula was calculated, according to the Ross and Hendricks method as $(Al_{.77}Fe_{1.02}Mg_{.31})\ (Al_{.33}Si_{3.67})\ O_{10}\ (OH)_2\ (NaK(Ca/2))_{.36}$. This formula

Table 1. Chemical Analysis and Formula of Nontronite from Bingham, Utah

H. E. Bradford, *Analyst*

SiO_2	48.56
Al_2O_3	12.46
Fe_2O_3	17.91
MgO	2.77
CaO	2.15
K_2O	.15
Na_2O	.06
H_2O (−)	8.83
H_2O (+)	5.66
	98.55

Formula calculated according to the method of Ross and Hendricks.

$(Al_{.77}Fe_{1.02}Mg_{.31})(Al_{.33}Si_{3.67})O_{10}(OH)_{2\times.36}$

proves to be similar to the type nontronite of Ross and Hendricks in that $Al_{.33}$ substitutes in the tetrahedral coordination, but differs in that Fe^{+++} is lower. It is probable that some K was present in the analyzed sample as orthoclase, and thus perhaps should not be used in calculating the base exchange factor. Omitting K the value of the base exchange factor, (Na(Ca/2)), is .35.

X-Ray—A powder *x*-ray pattern was taken of the Bingham material and compared with a check pattern made from authentic nontronite from Colfax, Washington, and the two patterns were found to be practically identical.

Optics—The index of refraction of the Bingham nontronite was found to be $\alpha = 1.560$ and $\gamma = 1.593$ with $\gamma - \alpha = 0.033$. These measurements were not made on especially prepared samples and hence do not correspond to

Ross and Hendricks (1945, p. 55) measurements on nontronite of similar composition from Spokane, Washington.

Differential thermal analysis—Curves were obtained on Bingham nontronite using conventional apparatus. A check was made with Colfax, Washington nontronite, considered to be authentic, to make sure that our apparatus was giving standard results and this curve compared favorably with those published by Kerr, Hamilton, and Kulp (1949).

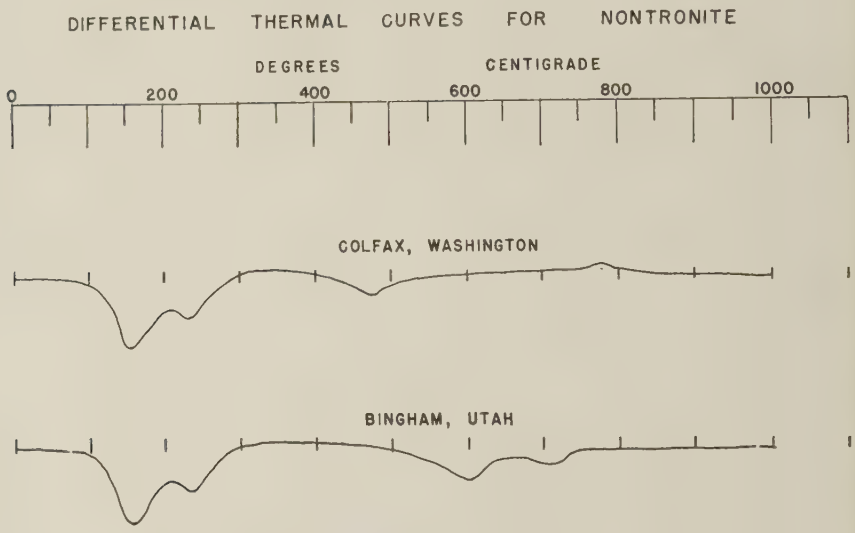

Fig. 3. Thermal curves of nontronite.

Several samples were run on the Bingham material and in each case the results were the same. The curves from the two different localities are compared in Fig. 3. The first endothermic peak at 160° to 170° C. shows the initial expulsion of interlayer water and the second endothermic peak at 230° to 240° C. is the result of the breakdown of the hydrated, interlayer calcium hydroxide molecules. For the Bingham material the next endothermic peak at 600° C. represents the breakdown of the hydroxyl groups in the lattice. This peak takes place at a higher temperature than the Colfax material due to the fact that it contains less iron and more aluminum. The hydroxyl ions are presumed to be bonded more strongly to the aluminum ions and it therefore requires a higher temperature to effect this break. Following at 700° to 720° C. is a small but broad endothermic peak the cause of which is not known. The endothermic peak at 720° C. on the Bingham material appears to mask the expected exo-

thermic peak at 780° C. seen on the Colfax material where it is thought that the rearrangement of the nontronite lattice to form a new lattice of spinel type occurs (Grim and Bradley, 1940). The 720° C. peak is broad and flat with greatest slope on the high temperature side which indicates that perhaps exothermic effects are becoming predominant over endothermic effects as the temperature increases.

Origin of the Nontronite

In considering the origin of the nontronite at Bingham it is found that events apparently began with formation of ferrous and sulfate ions from pyrite by percolating ground waters containing dissolved oxygen. The solutions were then acid and they began to migrate and mingle with fresh accessions of ground water as well as the constituents of the country rock. During this mingling the pH of the solutions increased by dilution, some ferrous iron was oxidized to ferric iron by additional oxygen, and the solubility product of ferric hydroxide was continuously approached but not exceeded. At this time nontronite was formed by reaction of these solutions with tremolite, pyrophyllite, diopside, and orthoclase (Fig. 1*A* and 1*B*). Complete pseudomorphous replacement of pyrite by nontronite also apparently took place at this time as is shown in Fig. 1*C*.

Subsequently, with increasing pH of the solutions by dilution, the solubility product of ferric hyroxide was exceeded and ferric hydroxide gel was precipitated and subsequently converted to limonite. This sequence of events is thought to be correct since limonite is observed to cut both transported nontronite and nontronite in situ in field and microscopic examples. See Figs. 1*C* and 2.

Since nontronite is found forming from minerals which were developed by hydrothermal alteration, and further, since nontronite is associated with zones and veins of limonite resulting from the destruction of pyrite by weathering processes, it is concluded that nontronite is exclusively a product of weathering at Bingham, and further this nontronite was formed in a slightly acid environment.

This view is different from the one proposed by Allen and Scheid (1946) for the formation of the nontronites of the Columbia River region. They concluded that those nontronites were formed in alkaline solutions in areas of poor drainage.

The writers wish to express their appreciation to the officials of the Kennecott Copper Corporation for their encouragement during the progress of this study and to the University of Utah Research Committee for supplying the thermal analysis equipment, also to the Geological Society of America who supplied the funds for the field study.

References

1. Allen, V. T., and Scheid, V. E. (1946), Nontronite in the Columbia River region: *Am. Mineral.*, **31,** 294–312.
2. Beeson, J. J. (1947), The disseminated copper ores at Bingham, Utah: *AIME trans.*, **54,** 356–401.
3. Boutwell, J. M., and Keith, Arthur (1905), Economic geology of the Bingham mining district, Utah: *USGS, Prof. paper* **38**.
4. Butler, B. S. (1920), Ore deposits of Utah: *USGS, Prof. paper* **111**.
5. Grim, R. E., and Bradley, W. F. (1940), Investigation of the effect of heat on the clay minerals illite and montmorillonite: *Jour. Am. Ceramics Soc.*, **23,** 247.
6. Kerr, P. F., Kulp, J. Lawrence, and Hamilton, P. K., Differential thermal analysis of reference clay mineral specimens. *American Petroleum Institute Project* **1949**. Preliminary report No. 3. May, 1949.
7. Ross, C. S., and Hendricks, S. B. (1945). Minerals of the montmorillonite group: *USGS, Prof. paper* **205-B**.

CORRELATION OF PHYSICAL PROPERTIES AND CHEMICAL COMPOSITION IN THE PLAGIOCLASE, OLIVINE, AND ORTHOPYROXENE SERIES

Arie Poldervaart*

Abstract

Physical properties of the plagioclase, olivine, and orthopyroxene series are plotted against chemical composition in a series of diagrams. The limitations of the various methods used to determine compositions of rock-forming minerals by optical means are discussed in detail, and lines of further work on the three mineral series are noted. A plea is made for the use of molecular percentages and for standard nomenclature in these, and other mineral groups.

Introduction

For some years the author has collected data on common rock-forming minerals published in the literature. The present paper presents this information in several diagrams pertaining to the three best-known solid solution series; albite-anorthite, forsterite-fayalite, and enstatite-orthoferrosilite.

The assessment of the chemical composition of a mineral by the determination of a set of optical properties is one of the chief aims of the petrographer. Frequently he also requires further information; concerning the temperature of crystallization of the mineral, its composition in terms of oxides as well as of mineral molecules, and other physical properties in addition to those already measured, but which cannot be determined in a single rock slice. This information is scattered throughout the literature, and is often not presented in a uniform manner, necessitating cumbersome calculations. The present diagrams bring together all information required in routine petrographic procedure. They have been checked against modern analytical data, but to avoid overcrowding, the analyses have not been plotted on the curves.

The nomenclature of the plagioclase series on a decimal, *molecular* percentage basis (Calkins, 1917) is now accepted by most petrologists, but the same cannot be said of other mineral series. There is still much confusion in mineral nomenclature, enhanced by the fact that compositions are indiscriminately expressed as weight or as molecular percentages.

In an attempt to apply Calkins' decimal, molecular percentage nomenclature also to other mineral series, Deer and Wager (1939) proposed a similar classification for the olivine series, while the author (1947) sub-

* Geological Survey, Lobatsi, Bechuanaland Protectorate.

sequently extended this system of nomenclature to the orthopyroxene series. The writer repeats his plea (1947, 1949, also *vide* Benson, 1944) for standard nomenclature and the use of molecular percentages in expressing mineral compositions. A scale has been included in the present diagrams, whereby molecular percentages are converted to weight percentages, for use in modal calculations.

Mineral compositions in the plagioclase, olivine, and orthopyroxene series are normally determined optically with an accuracy of ± 2 per cent, but this can be increased by measuring several crystals and taking mean values. Much depends on the purity of the mineral in question, and on the methods employed in assessing its optical constants. It is always best to use two unrelated methods; for instance, to determine for olivines and orthopyroxenes both the optic axial angle and one of the refractive indices. If such measurements are repeated several times on different crystals, and the results are found to agree closely, both with one another and with the values given by the corresponding curves, the derived composition can be accepted with confidence. Anomalous values may be due to incorrect measurements, presence of impurities, strain, zoning, and other causes, and should be studied in greater detail, by the determination of other physical constants, and by close observation of the natural habitat of the mineral. If possible this should be followed by its isolation and chemical analysis.

Plagioclase Series

Probably no other mineral series has been studied in such detail as the plagioclase series. Yet there remains ample scope for further work, in particular in defining the influence of admixtures and of temperature on the optical properties of the series. The plagioclase feldspars really belong to a ternary system with components albite, anorthite, and orthoclase, but it has become customary to consider them as a simple binary system. Yet correlations of optical properties and chemical composition in a triangular diagram would be of great value (Alling, 1936), while the coexistence of plagioclase feldspars and potash-soda feldspars (Niggli, 1941) is another field of study requiring further work. Yet another problem is the association of plagioclase and quartz in myrmekitic and other intergrowths (Drescher-Kaden, 1948; Poldervaart and von Backström, 1949). The thermal relations of the albite-anorthite series have been studied by Bowen (1913), and his classic thermal diagram is probably the best known in petrology.

A large number of methods have been devised to correlate physical properties with chemical composition. Since plagioclase occurs in nearly every igneous rock and in many metamorphic and sedimentary rocks,

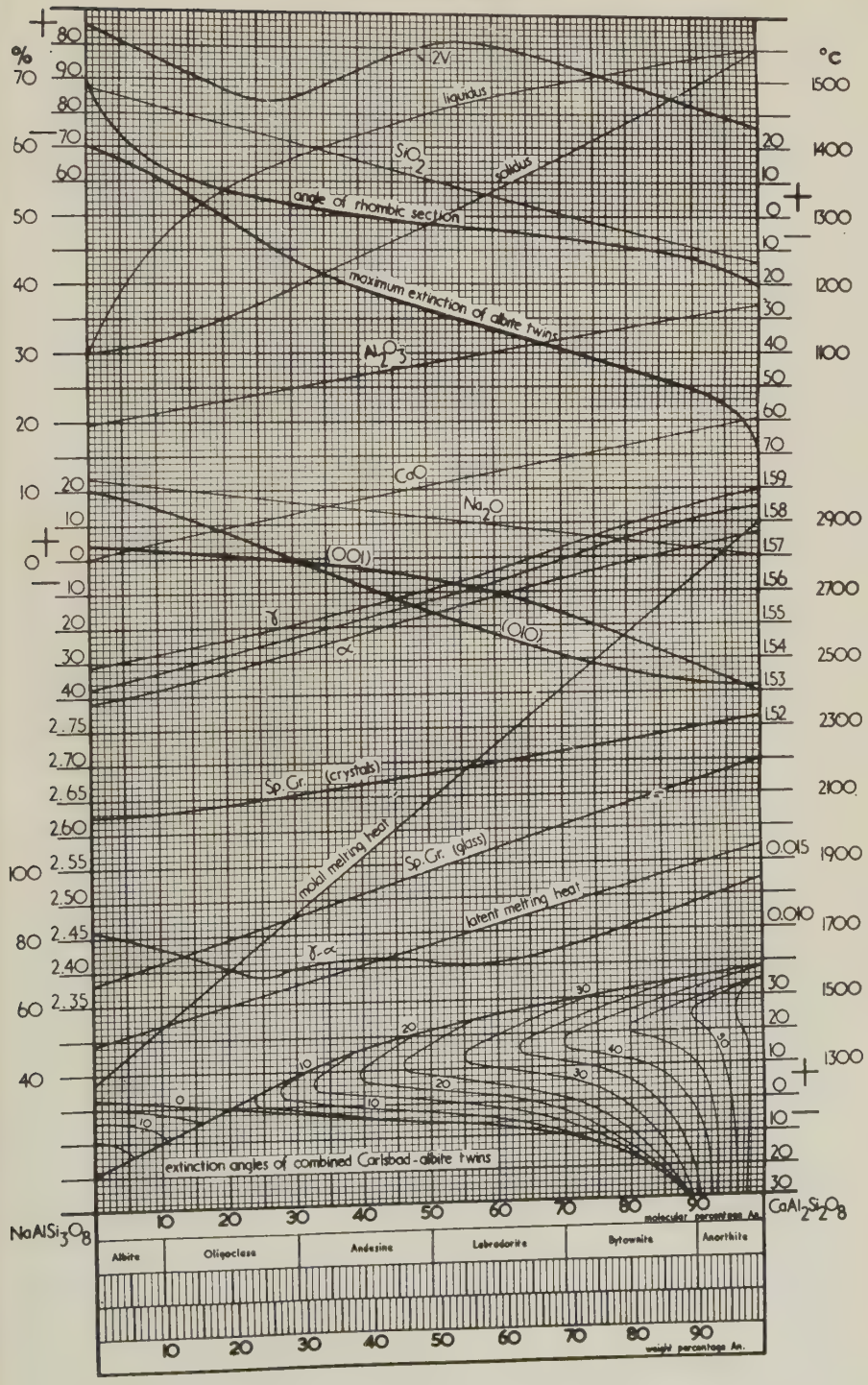
PLAGIOCLASE SERIES.
%
°C
ZV
liquidus
solidus
SiO_2
angle of rhombic section
maximum extinction of albite twins
Al_2O_3
CaO
Na_2O
(001)
(010)
γ
α
Sp. Gr. (crystals)
molal melting heat
Sp. Gr. (glass)
latent melting heat
γ-α
extinction angles of combined Carlsbad-albite twins
$NaAlSi_3O_8$
$CaAl_2Si_2O_8$
molecular percentage An.
Albite
Oligoclase
Andesine
Labradorite
Bytownite
Anorthite
weight percentage An.

FIG. 1

the determination of the An content of the feldspar is one of the most essential and common parts of petrological procedure. Yet many problems remain in determining compositions of members of the series by optical means. It is seldom realized how difficult is the correct determination of the average plagioclase composition in a rock in which the feldspar is strongly zoned (Wenk, 1945). Merely taking the mean of extreme values determined in one or more crystals rarely provides the correct result, unless a large number of crystals is examined. Determination of the mean index of refraction by comparison of a large number of grains orientated at random is less time-robbing, but likewise not very accurate. Probably the best procedure in this case is to ascertain the mean specific gravity by floating the crush in a liquid, of which the density is next determined.

The influence of admixtures on the optical properties of plagioclase feldspars is largely unknown. The most common of these are K_2O, Fe_2O_3, BaO, and SrO. An Or content up to 10 per cent apparently does not affect the physical constants of the plagioclase, but with more than 10 per cent Or the indicatrix is changed (Chudoba and Engeld, 1937). Fe_2O_3 also occurs in plagioclase to a limited extent (Faust, 1936; Ramberg, 1949), apparently replacing Al_2O_3, but its influence on the optical properties is unknown. BaO and SrO also enter the molecule, but their influence is equally uncertain. Excessive Al_2O_3 apparently distorts the ionic structure and results in anomalous optical properties (Perrier, 1930; Beljankin, 1931). Temperature also appears to affect the indicatrix, and different curves have been drawn for plagioclase of effusive and deep-seated rocks (Barber, 1936; Köhler, 1942; Scholler, 1942), though presumably there are feldspars which fit neither curves, having crystallized at intermediate temperatures and pressures.

Methods used to ascertain sets of optical properties, which in turn are correlated with composition, may be divided into two classes; universal stage methods and refractive index methods. Some workers prefer the former to the latter, but Wenk (1945) has shown that there is no valid reason for such preference. Each case should be considered on its own merits, and a method employed which is of the required accuracy, the most easily applied, and the least time consuming. Slightly altered or clouded crystals are best determined by universal stage methods. In zoned crystals refractive index methods tend to emphasize lower An values, since the edges of cleavage fragments are employed, while universal stage methods emphasize higher An values, as crystal cores are most conveniently used (Wenk, 1945). Some methods are more cumbersome and require more time than others. Since in one section there are

generally scores of plagioclase crystals, it is usually more profitable to select suitably orientated crystals, and to apply the easier and speedier method. Again, some methods are more accurate than others. It is good policy to aim at maximum accuracy, but there are often natural limitations, when less accurate methods may be employed successfully.

Refractive index methods may be divided into: (1) the ordinary immersion method using sodium light, (2) the single variation method, and (3) the double variation method; the three methods being of increasing accuracy in the order stated. The double variation method, perfected by Emmons (1929), is undoubtedly the most accurate, but it requires elaborate and expensive apparatus and consumes more time than the other two methods. Hence its application will remain limited to the better equipped laboratories, and to instances where such high accuracy is required. The single variation method, as applied by Tsuboi (1923, 1934) to the plagioclase series, is for most purposes the most accurate and convenient method. Yet the ordinary immersion method is the most commonly used. With practice it is more rapid than either the single- or the double variation method, while its accuracy is sufficient for normal purposes. In using either method, it is well to note that Tsuboi's curve for the lower index of (001) cleavage fragments does not differ appreciably from that of (010) cleavage fragments, nor from the α index curve. Thus it is normally sufficiently accurate to determine the lower index of either (001) or (010) cleavage fragments, and to plot this value on the α curve, in order to ascertain the composition of the plagioclase. The paucity of data on plagioclase An_{60-80} should be noted. More data in this composition range are required to check the present curves.

Universal stage methods may be divided into: (1) the Rittmann zone method (1929), and (2) the Fedorow method. Both methods have been discussed in an admirable manner by Emmons (1943). The Rittmann zone method, more rapid and convenient than the Fedorow method, is best applied to plagioclase with less than 60 per cent An, while the Fedorow method gives the best results for plagioclase with more than 60 per cent An. The two methods are complementary.

Maximum extinction angles on albite twin lamellae in oriented sections provide an accurate and convenient means of determining compositions of plagioclase with less than 50 per cent An. Extinction angles on combined Carlsbad-albite twins are also very accurate, but normally such twins are somewhat rare. Extinction angles on (001) and on (010), and the "angle of the rhombic section" appear to be less accurate. The optic axial angle of plagioclase with more than 60 per cent An also varies consistently enough to form a means of determining its composition.

The specific gravity, hardness (Holquist, 1914), and width of albite twin lamellae (Donnay, 1940), have also been correlated with the composition of the plagioclase feldspars.

The present diagram includes the following curves:

1. Liquidus-solidus.
2. Specific gravity of crystals and corresponding glass.
3. Molal and latent heat of melting.
4. Weight percentages of Na_2O, CaO, Al_2O_3, and SiO_2.
5. Optic axial angle.
6. Refractive indices and birefringence.
7. Extinction angles on (001) and on (010).
8. "Angle of the rhombic section."
9. Maximum extinction angle of albite twin lamellae.
10. Extinction angles of combined Carlsbad-albite twins.

For other curves and stereograms, applied in universal stage methods, reference is made to Emmons (1943), or Winchell (1946).

Olivine Series

The composition of most naturally occurring olivines may be expressed in terms of Mg_2SiO_4 (forsterite) and Fe_2SiO_4 (fayalite). This solid solution series has been studied thoroughly, and variations of physical properties with composition are known with accuracy. Deer and Wager (1939) have shown that the results obtained by Bowen and Schairer (1935) in their study of the system MgO-FeO-SiO_2 are faithfully reproduced in natural olivines.

Generally it is most convenient to find the composition of olivine in a rock from the determination of one or more of the refractive indices. Yet it is advisable to determine the optic axial angle as well. This second determination forms a good check on the first, while zoned olivines (Tomkeieff, 1939) are more easily identified and measured by this means. Frequently olivines from the same rock show a range in composition, though individual crystals are unzoned. Both this tendency and zoning are most pronounced in olivines of intermediate composition. In the range between Fa_{40} and Fa_{80}, a gap in the crystallization sequence of the series may be encountered, especially in strongly differentiated intrusions. This is in accord with Bowen and Schairer's results, but it does not imply the existence of a gap in the miscibility curve of the series.

The chief admixtures of natural olivines are Fe_2O_3, NiO, Cr_2O_3, MnO, and CaO. The first three oxides tend to be associated with magnesian olivines, while the last two are often more prominent in the iron-rich members of the series. For the purpose of calculating compositions of olivines belonging to the forsterite-fayalite series, MnO is generally added to FeO, while other admixtures are neglected.

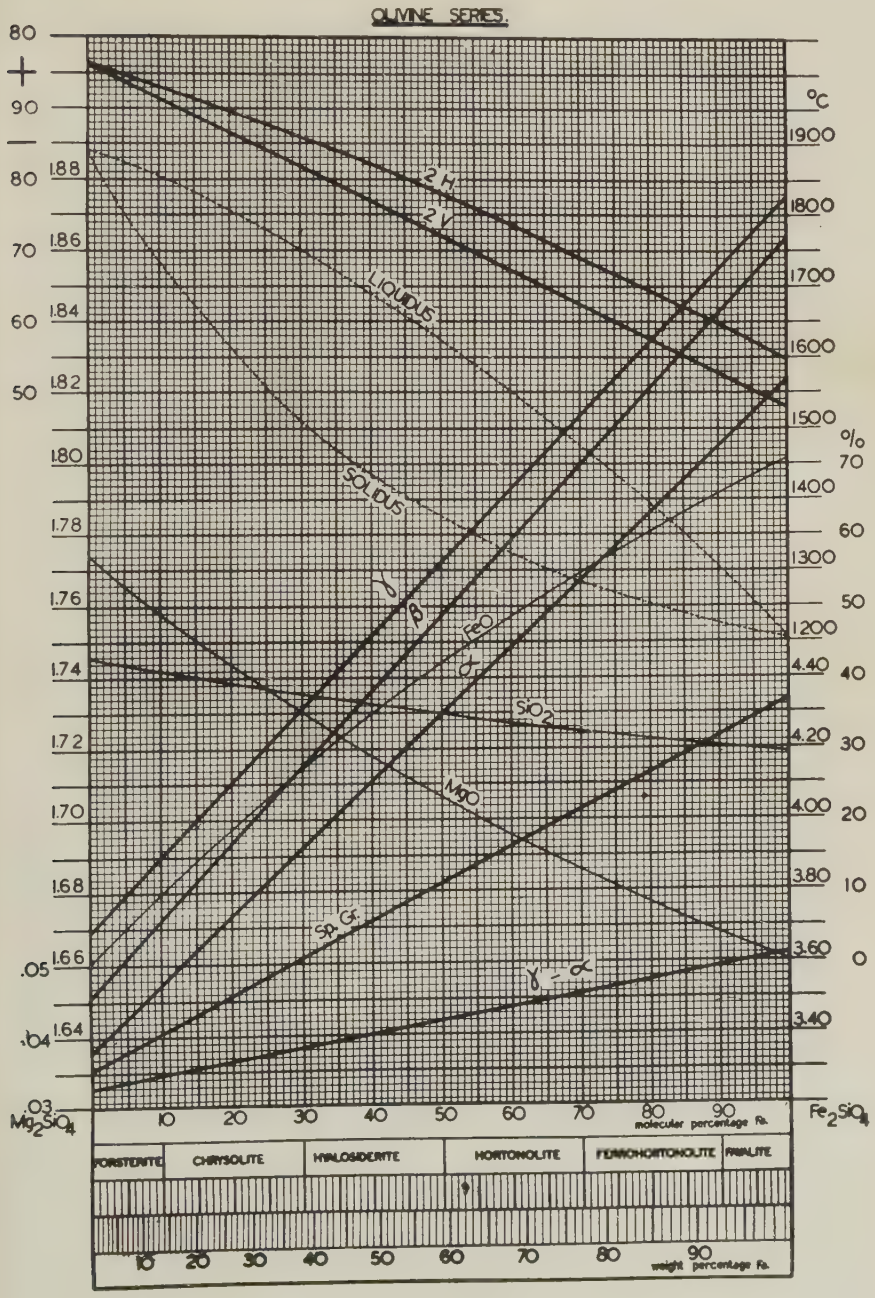
OLIVINE SERIES.
80
+
90
—
80
70
60
50
1.88
1.86
1.84
1.82
1.80
1.78
1.76
1.74
1.72
1.70
1.68
1.66
1.64
.05
.04
.03
2 H
2 V
LIQUIDUS
SOLIDUS
X
Z
FeO
Y
SiO2
MgO
Sp. G.
γ − α
°C
1900
1800
1700
1600
1500
1400
1300
1200
%
70
60
50
40
30
20
10
0
4.40
4.20
4.00
3.80
3.60
3.40
10 20 30 40 50 60 70 80 90
molecular percentage Fa.
Mg2SiO4
Fe2SiO4
FORSTERITE
CHRYSOLITE
HYALOSIDERITE
HORTONOLITE
FERROHORTONOLITE
FAYALITE
10 20 30 40 50 60 70 80 90
weight percentage Fa.

FIG. 2

Part of the Fe_2O_3, NiO, and Cr_2O_3 shown in analyses is probably present as small inclusions of chrome-magnetite or picotite, in the form of minute octahedra, dendrites, or thin plates and wedges parallel to (001) or (100) of the olivine host. Part is undoubtedly dissolved in the molecule, and Bowen and Schairer (1935) have found that small amounts of Fe_2O_3 remained in their melts in equilibrium with metallic iron, being incapable of further reduction.

The amounts of MnO and CaO found in natural olivines are generally small. Yet both forsterite and fayalite form solid solution series with tephroite, Mn_2SiO_4, the intermediate members being known respectively as picrotephroite and knebelite. Solid solution series probably also exist between forsterite and monticellite, $MgCaSiO_4$ (Ferguson and Merwin, 1919), fayalite and the double salt $FeCaSiO_4$ (Bowen, Schairer, and Posnjak, 1933), and tephroite and glaucochroite, $MnCaSiO_4$. Apparently monticellite, $FeCaSiO_4$, and glaucochroite are miscible in all proportions. Selected data of these rare olivines are given in Table 1.

Table 1. Data for Manganese and Calcium Olivines

Index	1	2	3	4	5	6	7
SiO_2	31.39	32.95	29.94	31.48	37.36	36.67	34.80
FeO	—	—	46.88	—	1.40	7.57	4.11
MnO	65.34	46.99	18.83	38.00	.04	.17	13.39
MgO	3.15	18.11	3.01	—	24.90	21.11	17.65
CaO	—	.71	—	28.95	33.08	32.56	27.38
rest	—	1.05	1.14	1.74	1.28	1.64	2.54
total	99.88	99.81	99.80	100.17	98.06	99.72	99.87
α	1.759	1.711	1.805	1.686	1.641	1.654	1.663
β	1.786	1.727	1.838	1.722	1.649	1.664	1.674
γ	1.797	1.740	1.847	1.735	1.655	1.674	1.680
2V (−)	65°	85°	54°	61°	—	82°	75°

1. Tephroite (Magnusson, 1918).
2. Picrotephroite (Magnusson, 1918).
3. Ironknebelite (Magnusson, 1918).
4. Glaucochroite (Gümbel, 1894).
5. Monticellite (Schaller, 1935).
6. Monticellite (Larsen, Hurlbut, Griggs, Buie, and Burgess, 1941).
7. Monticellite (Hallimond, 1921).

The present diagram includes the following curves:

1. Liquidus-solidus.
2. Specific gravity of crystals.
3. Weight percentages of MgO, FeO, and SiO_2.
4. True and apparent optic axial angle.
5. Refractive indices and birefringence.

At present the data are still too scarce to allow for accurate correlations of optical properties with chemical composition.

Orthopyroxene Series

Studies of correlations of physical properties and chemical composition in the orthopyroxene series have been published by Walls (1935), Henry (1935), Hess and Phillips (1940), Burri (1941), Kuno (1941), and the present writer (1947). The curves do not differ materially, hence the determination of the composition of orthopyroxenes by optical means appears to be reasonably accurate. Yet there remains scope for further studies on this mineral series.

Since most orthopyroxene cleavage fragments in a crush lie on a (110) face, the γ index can generally be determined with the greatest ease and accuracy. The optic axial angle may show anomalous variations. Hess and Phillips (1940) have found that in deformed (but not recrystallized) anorthosites and gabbros many orthopyroxenes have abnormally large optic axial angles. Intermediate orthopyroxenes of some metamorphic or igneous rocks may have optic angles as low as 45°, although 51° is generally accepted as the minimum optic axial angle of orthopyroxenes of this composition. These anomalous values may be the result of strain, or of the presence of impurities, notably Al_2O_3.

Kuno (1941) has found that the dispersion about X changes twice in the series; at about Of_{13} from $r<v$ to $r>v$, and at about Of_{47} back again to $r<v$. Again the presence of impurities may well change the type of dispersion.

The phenomenon of pleochroism in orthopyroxenes is also not clearly understood. Yet it is known that pleochroism is unrelated to the Of content of the mineral.

One of the most intriguing fields of study concerns the co-existence of the orthorhombic and monoclinic pyroxenes; including those of low optic axial angle (pigeonites). Without doubt this problem is as important in petrogenesis as that of the co-existence of plagioclase and alkali feldspars. Bowen and Schairer's results (1935) show that enstatite-orthoferrosilite form a typical isodimorphous series with clinoenstatite-ferrosilite, the monoclinic series consisting of the high temperature modifications. Pigeonites are the natural representatives of the clinoenstatite-ferrosilite series, magmatic conditions apparently favoring the inclusion of small amounts of CaO in the molecule. Crystallization frequently starts with the formation of pigeonite, which on slow cooling inverts to orthopyroxene, the excess lime being expelled just before inversion in the form of a curious exsolution intergrowth. The intergrowth may be called *lamellar* when the optic plane of the clinopyroxene is parallel

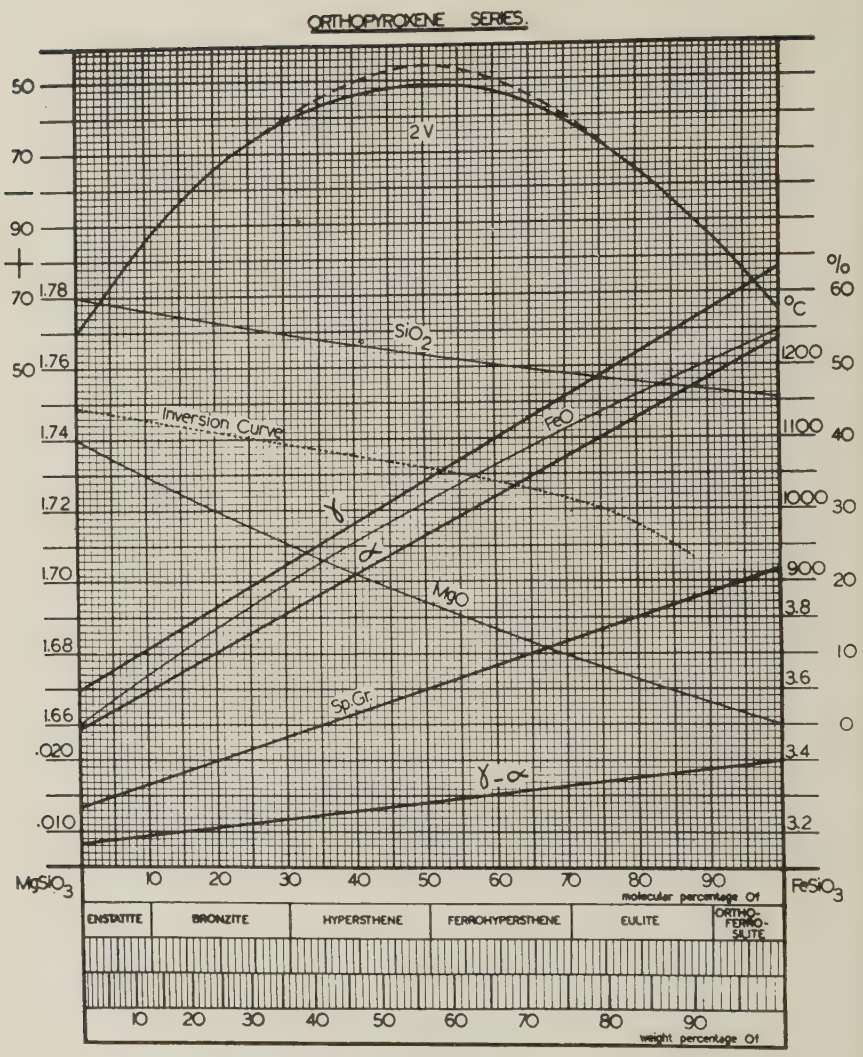

FIG. 3

to (100) of the orthopyroxene host, and *graphic* when it lacks orientation with respect to the host mineral. Many natural orthopyroxenes contain about 1.5 per cent CaO.* The relationship of orthopyroxene to pigeonite is discussed in detail by Hess and Phillips (1938, 1940), Hess (1941), and the present writer (1947). Hess considers that in magmas two pyroxene phases are normally present between MgO: FeO ratios of approxi-

* Hess believes that *all* natural orthopyroxenes contain about 1.5 per cent CaO.

mately 75:25 and 35:65, although laboratory investigations prove the existence of complete series of solid solutions between enstatite-diopside, enstatite-orthoferrosilite, and orthoferrosilite-hedenbergite, at the higher temperatures of the anhydrous melts. Guimarães (1946, 1948), on the other hand, collates the resorption of olivine, enstenitization of clinopyroxene, and rhythmic zoning of plagioclase, with assimilation of quartz rich sedimentary material. The present writer disagrees with this theory.

The chief admixtures of natural orthopyroxenes are TiO_2, Al_2O_3, Fe_2O_3, MnO, and CaO, while NiO and Cr_2O_3 may also be present in magnesian orthopyroxenes. Little is known of the influence of these admixtures on the optical properties. In calculating compositions of orthopyroxenes, MnO is generally added to FeO, while other admixtures are neglected. However, calculations in terms of En, Wo, and Fs are to be preferred when comparing orthorhombic and monoclinic pyroxenes.

Analyses with high percentages of Al_2O_3 are regarded by the writer with suspicion, as re-examination often proves the mineral to be orthorhombic amphibole. Thus "bidalotite" (Rao and Rao, 1937) has been shown by Rabbitt (1948) to be anthophyllite. Other modern analyses with unusually high Al_2O_3 are given by Lokka (1943) and Rajagopalan (1946).

The present diagram includes the following curves:

1. Inversion curve.
2. Specific gravity of crystals.
3. Weight percentages of MgO, FeO, and SiO_2.
4. Optic axial angle.
5. Refractive indices and birefringence.

Acknowledgments

The writer wishes to express his appreciation of the interest shown in his work by Professor F. Walker, of the University of Cape Town, and Mr. E. J. Wayland, Director of the Bechuanaland Protectorate Geological Survey. He is especially indebted to Professor H. H. Hess, of Princeton University, New Jersey, U. S. A., for criticism and reading of the manuscript.

References

Alling, H. L. (1936), Interpretative petrology of the igneous rocks, New York.

Barber, C. T. (1936), The effects of heat on the optical orientation of plagioclase felspars: *Min. Mag.*, **26**, 343–352.

Beljankin, D. (1931), Über chemische Anomalien in Feldspaten: *Zentralbl. Min.*, Abt. A., 356–364.

Benson, W. N. (1944), The basic igneous rocks of eastern Otago and their tectonic environment: *Roy. Soc. New Zealand, Trans.*, **74**, 71–123.

Bowen, N. L. (1913), The melting phenomena of the plagioclase feldspars: *Am. Jour. Sci.* 4th. ser., **35,** 577–599.

———, and Schairer, J. F. (1935), The system MgO-FeO-SiO_2: *Am. Jour. Sci.*, 5th. ser., **29,** 151–217.

——— ———, and Posnjak, E. (1933), The system Ca_2SiO_4-Fe_2SiO_4: *Am. Jour. Sci.*, 5th. ser., **25,** 273–297.

Burri, C. (1941), Zur optischen Bestimmung der orthorhombischen Pyroxene: *Schweiz. Min. Petr. Mitt.*, **21,** 177–182.

Calkins, F. C. (1917), A decimal grouping of the plagioclases: *Jour. Geol.*, **25,** 157–159.

Chudoba, K., and Engels, A. (1937), Der Einfluss der Kalifeldspatkomponente auf die Optik der Plagioclase: *Zentralbl. Min.*, Abt. A., **103–116, 129–149.**

Deer, W. A., and Wager, L. R. (1939), Olivines from the Skaergaard intrusion, Kangerdluqssuak, East Greenland: *Am. Mineral.*, **24,** 18–25.

Donnay, J. D. H. (1940), Width of albite twinning lamellae: *Am. Mineral.*, **25,** 578–586.

Drescher-Kaden, F. K. (1948), Die Feldspat-Quarz-Reaktionsgefüge der Granite und Gneise: *Min. Petr. Einzeldarst.*, **1,** 259 pp.

Emmons, R. C. (1929), The double variation method of refractive index determination: *Am. Mineral.*, **14,** 414–426.

——— (1943), The universal stage: *Geol. Soc. Am., Mem.* **8.**

Faust, G. T. (1936), The fusion relations of iron-orthoclase: *Am. Mineral.*, **21,** 735–763.

Ferguson, J. B., and Merwin, H. E. (1919), The ternary system CaO-MgO-SiO_2: *Am. Jour. Sci.*, 4th. ser., **38,** 81–123.

Guimarães, D. (1946), Enstenitização e o zoneamento dos plagioclásios: *Est. Min. Ger., Inst. Tecnol. Ind.*, Bol. **2.**

——— (1948), La genèse des orthopyroxènes: *Soc. Géol. Grance, Bull.*, 5e. sér., **18,** 645–661.

Gümbel, C. W. (1894), Bei dem Bleihüttenprocess in Freyhung erzeugte Monticellitartige Krystalle: *Zeitschr. Kryst. Min.*, **22,** 269–270.

Hallimond, A. F. (1921), On monticellite from a steel works mixer slag: *Min. Mag.*, **19,** 193–195.

Henry, N. F. M. (1935), Some data on the iron-rich hypersthenes: *Min. Mag.*, **24,** 221–226.

Hess, H. H. (1941), Pyroxenes of common mafic magmas: *Am. Mineral.*, **26,** 515–535, 573–594.

———, and Phillips, A. H. (1938), Orthopyroxenes of the Bushveld type: *Am. Mineral.*, **23,** 450–456.

——— and ——— (1940), Optical properties and chemical composition of magnesian, orthopyroxenes: *Am. Mineral.*, **25,** 271–285.

Holmquist, P. J. (1914), Die Schleifhärte der Feldspäte: *Geol. För. Förh.*, **36,** 401–431.

Köhler, A. (1942), Drehtischmessungen an Plagioklaszwillingen von Tief- und Hochtemperaturoptik: *Min. Petr. Mitt.*, **53,** 159–179.

Kuno, H. (1941), Dispersion of optic axes in the orthorhombic pyroxene series: *Imp. Acad. Tokyo, Proc.*, **17,** 204–209.

Larsen, E. S., Hurlbut, C. S. Jr., Griggs, D., Buie, B. F., and Burgess, C. H. (1941), Igneous rocks of the Highwood Mountains, Montana: *Geol. Soc. Am., Bull.*, **52,** 1733–1868.

Lokka, L. (1943), Beiträge zur Kenntnis des Chemismus der finnischen Minerale: *Comm. Géol. Finlande, Bull.*, **129,** 1–72.

Magnusson, N. H. (1918), Beitrag zur Kenntnis der optischen Eigenschaften der Olivingruppe: *Geol. För. Förh.*, **40,** 601–626.

Niggli, P. (1941), Gesteinschemismus und Mineralchemismus. 1. Das Problem der

Koexistenz der Feldspäte in den Eruptivgesteinen: *Schweiz. Min. Petr. Mitt.*, **21,** 183–193.

PERRIER, C. (1930), Sul plagioclasio di una plumasite di Val Sabbiola e sulla teoria della deformazioni ioniche: *R. Uff. Geol. Ital., Boll.*, **55,** 1–88.

POLDERVAART, A. (1947), The relationship of orthopyroxene to pigeonite: *Min. Mag.*, **28,** 164–172.

———, AND VON BACKSTRÖM, J. W. (1949), A study of an area at Kakamas (Cape Province): *Geol. Soc. S. Africa, Trans.*, **52,** 433–495.

RABBITT, J. C. (1948), A new study of the anthophyllite series: *Am. Mineral.*, **33,** 263–323.

RAJAGOPALAN, C. (1946), Studies in charnockites from St. Thomas Mount, Madras: *Proc. Indian Acad. Sci.*, **24,** 315–331.

RAMBERG, H. (1949), The facies classi cation of rocks: A clue to the origin of quartzofeldspathic massifs and veins: *Jour. Geol.*, **57,** 18–54.

RAO, B. R., AND RAO, L. R. (1937), On "bidalotite," a new orthorhomibc pyroxene derived from cordierite: *Proc. Indian Acad. Sci.*, **5,** 290–296.

RITTMANN, A. (1929), Die Zonenmethode. Ein Beitrag zur Methodik der Plagioklasbestimmung mit Hilfe des Theodolithtisches: *Schweiz. Min. Petr. Mitt.*, **9,** 1–46.

SCHALLER, W. T. (1935), Monticellite from San Bernardino County, California, and the monticellite series: *Am. Mineral.*, **20,** 815–828.

SCHOLLER, H. (1942), Versuche zur Temperaturabhängigkeit der Plagioklasoptik: *Min. Petr. Mitt.*, **53,** 180–221.

TOMKEIEFF, S. J. (1939), Zoned olivines and their petrogenetic significance: *Min. Mag.*, **25,** 229–251.

TSUBOI, S. (1923), A dispersion method for determining plagioclases in cleavage flakes: *Min. Mag.*, **20,** 108–122.

——— (1934), A straight-line diagram for determining plagioclases by the dispersion method: *Jap. Jour. Geol. Geogr.*, **11,** 325–326.

WALKER, F., AND POLDERVAART, A. (1949), Karroo dolerites of the Union of South Africa: *Geol. Soc. Am., Bull.*, **60,** 591–706.

WALLS, R. (1935), A critical review of the data for a revision of the enstatite-hypersthene series: *Min. Mag.*, **24,** 165–172.

WENK, E. (1945), Kritischer Vergleich von simultan nach der Drehtisch- und der Immersions-Methode ausgeführten Anorthitbestimmungen an Plagioklasen. Diskussion der beiden Methoden: *Schweiz. Min. Petr. Mitt.*, **25,** 349–382.

WINCHELL, A. N. (1946), Elements of optical mineralogy. Part 2, 3rd. ed., New York.

MINERALOGICAL SOCIETY (LONDON)

A meeting of the Society was held on Thursday, June 8, 1950, in the apartments of the Geological Society of London, Burlington House, Piccadilly, W 1 (by kind permission).

The following papers were read:

(1) The Petrology of the Evaporites of the Eskdale No. 2 Boring, East Yorkshire. Part II. The Middle Evaporite Bed.

By Dr. F. H. Stewart

The middle of the three Permian evaporite beds is 286 feet thick, and is underlain by dolomite and overlain by salt clay. It has been divided into five main zones:—Upper halite zone (8 feet thick); Halite-sylvine zone (46 feet); Halite zone (142 feet); Halite-anhydrite zone (49 feet); Anhydrite zone (41 feet).

Petrographic descriptions of the rocks are given. Halite and anhydrite occur in all zones. Dolomite is restricted to the lower part of the succession; magnesite, sylvine, carnallite, quartz and haematite to the upper part. Small quantities of boracite, pyrite and magnetite have been found. Layers containing halite-anhydrite pseudomorphs after early gypsum occur in the upper part of the halite-anhydrite zone.

There is much evidence of replacement and recrystallisation, and some of these changes were probably due to the action of percolating brines during the formation of the evaporites, while others were effected later.

(2) A Serpentine Mineral from Kennack Cove, Lizard.

By Dr. H. G. Midgley

Chemical, thermal, x-ray and optical examinations have been made on a white mineral from the Lizard occurring as small flakes which are uniaxial negative with N_e 1.545, N_0 1.555. The mineral has a formula approximating to $Mg_6Si_4O_{10}(OH)_8$; a preliminary x-ray structure analysis of single crystal rotation photographs suggests that the mineral has a layered kaolinite structure with all the octahedral positions filled with Mg ions. It is monoclinic with probable space group Cm.

(3) A Gabbro-Limestone Contact near Camphouse, Ardnamurchan.

By Dr. S. O. Agrell

The so-called augite-diorite E.S.E. of Camphouse (Ardnamurchan Memoir pp. 153–155) is shown to be a contaminated rock formed by the interaction of a gabbroic intrusion and Liassic limestones.

The contaminated series consists of pyroxene-rich gabbros, pyroxenites, pegmatitic ferrowollastonite pyroxenites and theralitic types. Secondary minerals: analcite, thompsonite, prehnite, xonotolite and hydrogarnets are abundant in most types.

The limestones have suffered extreme metamorphism with the extensive development of calcite, spurrite, rankinite, larnite, bredigite and gehlenite.

(4) Note on Garnet Crystals from Cairnie, Aberdeenshire.

By Dr. F. H. Stewart

Exceptionally large crystals of garnet (110) (211) have been found in coarsely banded garnet-biotite-sillimanite-gneisses. Analysis shows the composition: almandine 76.47, pyrope 18.58, spessartine 3.42, grossular 1.35, andradite 0.18. Well-marked partings cut the planes of schistosity and gneissic banding at low angles.

The following papers were taken as read:

(1) On a Cupriferous Lewisian Para-Gneiss.

By Mr. W. T. Harry

A Lewisian meta-sediment bears 0.24% copper in minute disseminated cryptocrystalline malachite grains. Exposures of the rock are small and appear highly localised. No vein mineralisation is apparent.

(2) The Pseudomorphs of Pyrrhotine after Pyrite in the Ballachulish Slates.

By Dr. H. Neumann

(3) Thermal Study of some Manganese Oxide Minerals.

By Mr. J. Laurence Kulp and Mr. Jose N. Perfetti.

(*Titles and abstracts kindly submitted by G. F. Claringbull, General Secretary.*)

BOOK REVIEWS

STRUCTURAL PETROLOGY OF DEFORMED ROCKS BY HAROLD WILLIAMS FAIRBAIRN, with supplementary chapters on Statistical Analysis, by Felix Chayes; ix+344 pages; Addison-Wesley Press, Inc., Cambridge, Mass., 1949. Price, $12.50.

This is nominally a second edition, although it is the first one to be printed and bound in book form. The first edition to be published by the Addison-Wesley Press was an amplification of the earlier mimeographed editions published by Queens University in 1935 and 1937; it was reproduced by an offset process in the same size as the previous mimeographed editions ($8\frac{1}{2}\times11$ in.) and had paper backs and plastic ring binder.

The current edition is cloth bound and is nicely printed on medium grade paper adequate for the line drawings, which constitute the great bulk of the illustrations. Some of the photographs are not as sharp and clear as they would have been on a better grade paper.

The format is a great improvement over that of the first edition; the text and illustrations are also considerably improved. The volume has still not developed to the stage where it could be considered a textbook; indeed the subject of petrofabrics has hardly developed to the stage where a textbook could be written. It is, however, the most complete and up-to-date single-volume reference work on the subjects of structural petrology and petrofabric analysis available in any language.

From the high price of the book one judges that the edition is extremely limited and that the publishers do not expect to sell many copies. This is unfortunate because it puts the book beyond the reach of most graduate students and probably will restrict considerably its distribution to libraries.

The book is divided into three parts. Fairbairn makes sure that Petrofabric and Experimental Facts, Part I, is sharply separated and cannot be confused with Interpretation and Application, Part II. Part III deals with Methods and Analytic Procedures. Part I summarizes the orientation rules (patterns) for the various minerals that have been studied, points out observed relations of orientation to *s*-surfaces and to folds, and outlines the available information on experimental deformation, including annealing, recrystallization and related phenomena. Comparatively little work has been done on the deformation of rock forming minerals, so many of the data are necessarily from work on metals. Part II develops hypotheses as to how the observed orientations described in Part I came about, how preferred orientation may be developed in various minerals, how *s*-surfaces can be produced, the mechanism of recrystallization in tectonites, kinds of folds and how they are formed, possible processes of rock flowage and tectonic transport, processes that could give rise to lineation, etc. Part III outlines field and laboratory techniques, including collection of oriented specimens, preparation of oriented thin and polished sections, study under the microscope both with and without the aid of the universal stage, preparation of fabric diagrams, and other techniques for presenting data. Chayes' two chapters on statistical analysis of two and three dimensional fabric diagrams are also included in Part III.

This clear separation of data from the interpretation thereof is a splendid idea. In a great many of the papers in structural petrology it is quite difficult to be sure what is ascertained fact and what is inference, i.e., the interpretation of those facts. This separate treatment has one unfortunate consequence, however; most of the grain orientation diagrams, tables, graphs, etc., are given in Part I, and when interpretation of the examples is reached in Part II the reader finds himself obliged to turn back and forth again and again and again in order to refer to the illustrations and tables so that he can follow the discussion adequately. One wonders whether a much smoother result might not have been achieved by summarizing very briefly in Part I the data for the illustrative examples used in Part II and then placing the diagrams, etc., with the detailed interpretative discussions in Part II.

The description of methods and techniques in Part III is well written and illustrated. The chapters on statistical analysis by Chayes are an innovation in this edition. He stresses the importance of using a systematic sampling plan, based on statistical methods, in the study of fabrics. In the chapter on Statistical Analysis of Two-dimensional Fabric Diagrams the application of the chi-square test of equal frequency to determine whether there is a significant degree of preferred orientation (anisotropy of fabric) is described. The familiar 0.05 and 0.01 "significance levels" are recommended in general for evaluating orientation data, but the suggestion is made that for some situations such as exploratory studies the 0.10 or even 0.20 level be used as a criterion of whether further work is justified. A scheme is offered in this chapter for the quantitative description of fabric.

In the chapter on Statistical Analysis of Three-dimensional Fabric Diagrams the chi-square test of equal frequency is examined again; the conclusion is reached that it is too sensitive for use with this type of diagram. The Winchell general test is considered and it appears to be not sensitive enough. A third test is then introduced (a correlation test developed by Chayes), "the results of which seem to be in closer accord with conclusions reached by conventional, nonstatistical methods."

It would appear when the values of significance levels must be changed for certain types of interpretations and a statistical test that accords better with nonstatistical interpretations needs to be developed that perhaps petrofabric data are not quantitative enough for precise mathematical treatment. There is considerable doubt, therefore, whether, *with our present state of knowledge*, it is worth the time and trouble required to make a statistical interpretation of petrofabric data. Chayes' choices may give the impression of juggling to make results fit hypotheses, but what he is really trying to do is to find a scheme that will be of practical use, yet not needlessly refined.

Chayes frankly discusses the limitations and restrictions of the usual statistical tests of hypotheses, but expresses the hope that the more modern developments may eventually be applied successfully to petrofabrics.

In a new edition with changed format, extensive revision and addition of much new material, errors are to be expected. Most of these are minor typographical errors which will no doubt be corrected in the next printing. There are several, however, to which attention should be called because they are likely to cause confusion. On page 12, paragraph 4, last line, "*ac*" should read "*ab*" and on page 25, paragraph 4, line 2, "parallel to *b*" should read "parallel to *a*." On page 42, line 14, "from a lamellae maximum to an axes minimum" should read "from a lamellae maximum to an axes maximum." Figure 5-2 on page 72 should be rotated 90° so that the positions of the *s*-planes will coincide with those of the corresponding *s*-planes in Figures 5-3 to 5-7. On page 79, paragraph 1, the statement is made that "The shortening is inversely proportional to the time—" What is meant is that the *rate of shortening*, or the *shortening per additional unit of time* is inversely proportional to the time. The total amount of shortening is directly proportional to the time. On page 92, paragraph 2, line 11, "at 45° to Figure 7-6" should read "at 45° to *ab* in Figure 7-6." Many commonly used metals do not even begin to anneal at 100° C., so that figure as given on page 98 is no doubt a misprint for 1000°C. It is difficult to follow the discussion of Figure 19-8 on pages 247–9 because the six letters referred to throughout the discussion have been omitted from the figure.

There are a few statements that should be rewritten in the interest of clarity. For example, if one follows the directions in footnote (1), Table 2-1, page 9, he determines a point on the *c* axis instead of the center of the plane, the point in which he is interested. The statement should be re-written to indicate that the pencil is moved *parallel to* each axis in turn rather than to an intercept on each axis. The discussion of Figure 4-10, page 63, paragraph 2 appears confused and perhaps could be recast with advantage.

In matters of interpretation of petrofabric diagrams and data there is commonly room for considerable difference of opinion. Perhaps, therefore, it is useless to mention matters of interpretation in a review, but the reviewer feels that a few examples may prove profitable to the reader. In the discussion of symmetry on page 7 most of the examples appear to be ill-chosen. Figure 2-16 is not orthorhombic, but monoclinic, with respect to the fabric axes shown. ("Figure 2-23" here is obviously a misprint for "Figure 2-32", which is all right as an example of orthorhombic symmetry.) Figure 2-35 would have been a better third example of orthorhombic symmetry than the one mentioned, Figure 2-37. Figure 2-11 is, strictly speaking, monoclinic, as stated, but it is actually more nearly orthorhombic than some of the ones cited as orthorhombic. Figure 2-14 is a much better example of monoclinic symmetry than Figure 2-15, which is really triclinic. Figure 2-43, also cited as monoclinic, is as nearly an ideal orthorhombic diagram as any shown in the entire book. Figure 2-27, cited as an example of triclinic symmetry, is almost perfectly orthorhombic. In Figure 2-66 not all of the fabric directions are shown, but the *s*-plane indicated is a symmetry plane, so the diagram is at least monoclinic. Figure 2-67 is much more obviously and completely triclinic.

On page 96, paragraph 4, the following appears, "The higher the symmetry of a crystal possessing glide planes, the more translation systems it possesses. . . . " This would appear to be inaccurate; the higher the symmetry the more glide planes a crystal *can* possess; so "possesses" should read "may possess."

On page 257, paragraph 4, Fairbairn states that another advantage of the interference figure method is the possibility of investigating the orientation of grains too small for study with the U-stage. The reviewer has found the oppositie to obtain,—that grains too small for getting an interference figure can be measured on the U-stage.

In general the literature coverage of this book is excellent, which makes the few important omissions all the more noticeable. On page 149 and in Table 2-1 (p. 9) one gets the impression that no work has been done with feldspar, but Larsson[1] made a very exhaustive and interesting study of the orientation of plagioclase during the different phases of a complex intrusion. No discussion of regional arcuation (page 229, par. 2) is complete without mention of Sahama's monumental work in Finland.[2] This paper is listed (No. 215) in the bibliography, but is not mentioned in the discussion of arcuation. In the discussion of universal stage procedures (pages 257–270) Berek's[3] book, which is one of the most lucid and useable of all descriptions of universal stage technique, is not mentioned, nor is it listed in the bibliography.

The bibliography is one of the most complete lists of articles in structural petrology and related subjects ever assembled and it should prove most useful to other workers in the field. In addition to the omissions mentioned above, however, many early papers cited on page 235 and the following pages are left out because the references are given in Sander's "Gefügekunde der Gesteine." This is unfortunate, because many people working in structural petrology do not have access to Sander's book. Moreover, the bibliography is not consistent throughout; in many references workers' first names or initials are omitted as in Nos. 27, 36, 62, 102, 143, etc. The year is given for most of the papers but in some, such as Nos. 105, 106, 125, 126, 130, 152, etc., it is omitted. For many of the papers complete titles are given, but many others are abbreviated, which is not a pleasing effect.

[1] Larsson, Walter, Der Nygård Pluton: *Bull. Geol. Inst. Upsala*, **25,** 13–134 (1935).

[2] Sahama, Th. G., Die Regelung von Quarz und Glimmer in den Gesteinen der Finnisch-Lappländischen Granulitformation: *Bull. Geol. Comm. Finlande*, No. **113,** 119 pp. (1936).

[3] Berek, M., Mikroskopische Mineralbestimmung mit Hilfe der Universaldrehtischmethoden, Gebrüder Borntraeger, Berlin (1924).

Most of the shortcomings mentioned above can easily be remedied when the book is reprinted and even if they are not they will detract but little from the most complete and up-to-date compilation of this subject extant, which is exceeded in authoritativeness only by the writings of the men who are in large part responsible for the development of this field, Walter Schmidt and Bruno Sander.

EARL INGERSON
U. S. Geological Survey

EINFÜHRUNG IN DIE GEFÜGEKUNDE DER GEOLOGISCHEN KÖRPER BY BRUNO SANDER. Springer, 1948, 215 pages.

1. TEIL: ALLGEMEINE GEFÜGEKUNDE UND ARBEITEN IM BEREICH HANDSTÜCK BIS PROFIL.

Gefügekunde is the science of fabrics, biological fabrics, metallurgical fabrics, soil fabrics, and others. Sander's viewpoint elevates fabric-science to a field equal to Petrology or Sedimentology. A fabric results from movements of particles in a field of force, as for instance, sedimentation under the influence of gravity, the rearrangement of minerals during folding, or the growth of minerals under hydrostatic conditions. Study of fabric is historical analysis of a succession of conditions. In its broadest sense fabric includes structural elements and not only microscopic dimensions. There is no reason why megascopic features should furnish more important information than microscopic ones and vice versa, and there is no relation between size and significance.

Stress plans result in corresponding strain plans and fabric analysis is merely the determination of movement plans resulting from force distribution. Fabric studies are the only accurate approach to the determination of the field of forces.

Symmetry of fabric is the unerring mirror of the symmetry of movement and its rhythm which produced it. Determination of the latter is essential for accurate definition of the former.

Sander's book is only the first part of what may be generally called Gefügekunde and comprises essentially non-microscopic elements. The second part is in press. The first part of this book defines Gefügekunde, and takes up the following topics: time and fabric, symmetry and rhythm of morphological and functional fabrics, affine and non-affine deformations, movement and symmetry in tectonic formation, symmetry of anisotropical fabric in superposition and homogeneous penetrations, mechanical stress and formation in homogeneous areas as functional fabrics, tectonic competence and fabric, fractures, planar and linear schistosities, tectonic streaming and flowage, movement and symmetry of deposition.

The second part deals with tectonic analysis of typical fabrics of non-microscopic order of magnitude. Important topics are a general review of linear and planar structures and their orientations, representation in spherical projection, B and β axes, time relationships of superimposed B axes, determination of relative movement directions perpendicular to B, types of homogeneous and inhomogeneous tectonic movement pictures with planar and linear structures, reconstruction of tectonic fabrics.

The third part supplies examples and application of fabric analysis especially to igneous, highly mobile intrusions, salt intrusions, surface flows, and a brief comparison with biological fabrics.

Literature references are not given in this volume, but promised for the second volume.

One of Sander's chief contributions is precision of observation and rigidity of analysis. He points to the many applications of measuring techniques in a field which is all too readily the object of rather vague descriptions and loose terminology.

The mystery which surrounds the subject of petrofabrics stems from the fact that the

literature is predominantly in German and that the technical language has become involved and cumbersome for those who are not thoroughly familiar with it.

This new book is to be an introduction, but really demands thorough acquaintance with the terminology. It contains a wealth of material in a minimum of space. A glossary of terms—preferably with English translation—would add to the usability, and more illustrations would help to gain friends or converts to the method. I know of few books which demand greater concentration for understanding and still fewer from whose perusal I have received more benefit.

ERNST CLOOS
The Johns Hopkins University

THE OPTICAL PRINCIPLES OF THE DIFFRACTION OF *X*-RAYS BY R. W. JAMES, Professor of Physics in the University of Cape Town. (THE CRYSTALLINE STATE—vol. II. Editor: Sir Lawrence Bragg.) xv+623 pp., $5\frac{1}{2}$ by $8\frac{1}{2}$ inches, 217+vii figs., including 19 figs. on 16 half-tone plates. London, G. Bell and Sons, Ltd. 1948. Cloth. Price, 80s.

The main value of this long awaited book lies in the thoroughness with which it covers the whole field of *x*-ray diffraction. It is a book of principles, giving a connected account of the theoretical foundation, but leaving out the experimental techniques and the results, of crystal-structure analysis. The author had already written one of the first textbooks on "*X*-Ray Crystallography," a Methuen Monograph, justly famous for its simplicity. Crystallography has gone a long way since that time, and the new volume is many times the size of its predecessor, but Professor James' lucidity of exposition has remained the same in spite of the increased complexity of the subject. This compendium—one more reason why would-be mineralogists should take integral calculus in college—is destined to become the "livre de chevet" of structural crystallographers of all feathers; its appearance has already been welcomed by a mineralogist (F. A. Bannister, *Min. Abs.*, **10**, 447, 1949), a physicist (P. P. Ewald, *Science Progress*, **37**, 572, 1949) and a metallurgist (C. S. Barrett, *J. Am. Chem. Soc.*, **71**, 3859, 1949).

It is hard to do justice to such a monumental work in the limited space of a review—the table of contents alone fills nine printed pages. The treatment begins with the diffractions of *x*-rays by identical scattering points at the nodes of a lattice according to Laue's original method; it goes on immediately to the reciprocal lattice, Ewald's construction, and Laue's interference function. Then clusters of (not necessarily identical) scattering points are considered as repeated by the lattice, and diffraction by the crystal is studied, first neglecting dynamical interaction of the scattered waves and the crystal structure, then considering it in the light of Ewald's theory. As prerequisites to a comparison of this theory with that of Laue and Bragg insofar as accounting for experimental intensities is concerned, the following topics are taken up: atomic scattering factor, treated both by the classical method and by wave mechanics, dispersion, and influence of thermal motion (diffuse scattering). The intensity formulae can now be subjected to experimental test, in the cases of mosaic crystals, perfect crystals, and powders.

The author turns next to crystal analysis and gives an excellent summary of the use of Fourier series (electron density function and Patterson function), in which he stresses the relation of the diffraction of *x*-rays to that of light and to the formation of optical images. (Fourier integrals are introduced to determine the electron distribution in atoms.) The dynamical theory is then reexamined and fitted to the continuous crystal expressed by the Fourier series. The reciprocity theorem is applied to the study of diffraction phenomena for radiation excited within the crystal (Kossel lines, and Kikuchi lines).

The last topic is the scattering of *x*-rays by non-crystalline material (gaseous, liquid,

and solid) and the related diffraction by finely powdered crystals. The effect of crystal size and that of crystal distortion on the spectra is discussed, and diffraction by fibers is briefly presented.

Four appendixes deal with the vector algebra used in the book; the definition, properties, and use of the reciprocal lattice; corrections of the scattering factor (Hönl); and the derivation of the Fourier integral. A detailed index of subjects and one of authors occupy 13 two-column pages of fine print. A list of selected references is given at the end of each of the ten chapters.

In a book of this scope and size, it is difficult to avoid all the little blemishes in the first printing—the text is not free from typographical errors, some of the references are partly wrong, there are inconsistencies in the use of the sign of the exponent in the expressions of the structure factor and the electron density (pointed out already by Miss Megaw and Mrs. Lonsdale). Well printed on good paper, with excellent drawings and plates, the volume leaves nothing to be desired as to craftsmanship; it does, alas, as far as price is concerned! Even so, a copy of this book is a sound investment; in our family, we own two.

DONNAY AND DONNAY

ON THE SYSTEMS FORMED BY POINTS REGULARLY DISTRIBUTED ON A PLANE OR IN SPACE BY M. A. BRAVAIS. Translated by A. J. Shaler, from the original in *Journal de l'Ecole Polytechnic*, Cahier 33, Tome XIX, 1–128, Paris, 1850. Crystallographic Society of America, Memoir No. 1.

Every x-ray crystallographer is probably as familiar with the 14 Bravais lattices as he is with the alphabet. But the great majority of them have never, until now, had available the opportunity to follow through the original derivation of these lattices. Professor Shaler and the Crystallographic Society are to be commended for making an English translation of this classic available. Many teachers, who have developed more or less adequate derivations of their own, will be especially interested in this presentation by Bravais. By means of a series of theorems, the argument is built up, step by step, from symmetrical nets on through the various symmetrical lattices, until the 14 lattices are rigorously deduced. It is also worthy of note that Bravais included the idea of a polar lattice, the forerunner of the reciprocal lattice, which has been developed into a most useful tool in the graphical interpretation of x-ray diffraction data.

L. S. RAMSDELL
University of Michigan

AN INTRODUCTION TO LUMINESCENCE OF SOLIDS BY HUMBOLDT W. LEVERENZ, 569 pp. and 143 figures. Published by John Wiley and Sons, Inc. Price $12.00.

Although this book deals principally with artificial phosphors, the attention of mineralogists and crystallographers, as well as that of physicists, may well be directed to this monographic pandect in an allied field of interest. During recent years the use of luminescent materials, stimulated by revolutionary wartime developments, has expanded along increasingly varied lines. Luminescent compounds were intensively employed in the tubes of radar sets and "night-seeing" devices, for marking dials of airplane instruments, charts, and maps, and for identifying objects during blackout restrictions. A few of the important commercial uses are in "fluorescent" lamps, television, fluoroscopic screens, oscilloscopes, photographic emulsions, and dyes.

The study of phosphors is a mushrooming subfield of science, for the phosphors known today are constantly and rapidly being improved not only in the techniques of their preparation but also in their applications and uses. Their development is one of the many

facets of the research effort toward a more efficient national defense that is undergoing polishing.

A negative definition of luminescence states that it is "any emission of light not due to incandescence." Many minerals and many more artificial compounds possess the property of absorbing electromagnetic vibrations of a certain wave length range and "rebroadcasting" the energy in another range. X-rays, gamma rays, alpha particles, cathode rays, long- and short-wave ultraviolet, as well as visible light, may be used for excitation, and the emitted vibrations also may fall outside of the visible region. Most luminescent minerals and other phosphors require the presence of an activator (a phosphorogen or luminogen), a minor or trace constituent which defines both the color and brilliance of the luminescence produced. According to Leverenz, phosphors may be separated into two main groups with respect to activators: (1) those made by adding a small proportion of an impurity to a pure host crystal upon heating and (2) those made by heating alone and thought to be "self-activated" due to a stoichiometric excess or structural displacement of one or more of the essential ingredient elements.

Chapters one and two deal with concepts of the structure of matter and of crystals. In the third chapter are described the syntheses of phosphors; the constitution and structure of phosphors follow in the next chapter. In long chapter five luminescence of phosphors is discussed under such sub-topics as excitation, storage, emission, decay, stimulation. quenching, and efficiency. Chapter six includes a correlation of host crystal and phosphor properties, and in chapter seven the uses of phosphors are summarized.

Five appendices, a glossary, a list of references (750 entries!), and three indexes (formula, i.e., by compound, name, and subject) close the book. A useful periodic table of the elements, encyclopedic in its scope of listed properties, is folded inside the back cover. Certainly the study of luminescence has progressed prodigiously from that natal evening at the Franklin plant of the New Jersey Zinc Company when a spark formed by pulling a knife-type switch for extinguishing the lights produced a fluorescent glow in willemite specimens lying nearby in the darkened room!

Although a considerable part of the volume is couched in the formulae and phraseology of a physics on a level somewhat above that with which the average geologist or mineralogist is conversant, nevertheless these readers too, when subjected to the excitation of certain selected "lengths," will absorb and store information on several energy levels for useful future emission.

E. Wm. Heinrich
University of Michigan

NOTES AND NEWS

Cordierite in Pegmatites—an Addendum

E. Wm. Heinrich, *University of Michigan.*

Since the publication of the article on cordierite in pegmatites (*Am. Mineral.*, **35**, 173–184, 1950), some other pertinent cordierite-pinite occurrences were reported to the writer. These include several in Bavaria: Harlachberg, Blötz by Bodenmais, Niederndorf by Kötzting, and Weiding by Altfalter (H. Laubmann, Die Minerallagerstätten von Bayern r. d. Rh., Munich, 1924). Laubmann believes the cordierite is formed by " . . . Resorption von Bestandteilen aus dem Nebengestein . . . " (p. 46). Specimens received through the generosity of Louis Moyd of Bancroft, Ontario, were collected from a locality near Fishtail Lake, Haliburton County, Ontario. Here veinlets of quartz and cordierite occur in anthophyllite-garnet-cordierite rock. This occurrence has been recorded by N. N. Evans and J. A. Bancroft (*Am. Jour. Sci.*, **175**, 509–512, 1908). G. E. Moore (*Geol. Soc. Am., Bull.* **60**, 1613–1670, 1949) records massive dark blue cordierite along edge of a quartz vein in altered amphibolite, 1.7 miles S. 40°W of Richmond, New Hampshire, and states (p. 1663), "The cordierite in this locality appears to be hydrothermal, formed as a replacement of the country rock along the quartz vein."

In October, 1950, Dr. L. J. Spencer completed 50 years as Editor of the *Mineralogica Magazine*. The December, 1950, number of the *Mineralogical Magazine* will be a special number in honor of Dr. Spencer. Also a dinner in honor of the Editor was held after the Anniversary meeting on November 2, 1950, and a presentation of a personal nature was made to Dr. Spencer at the dinner.

At Columbia University the Department of Geology, continuing its policy of rotating administrative duties, has elected Professor Walter H. Bucher to serve as Executive Officer for a period of three years. He succeeds Professor Paul F. Kerr whose term expired on June 30, 1950, and who held office during the difficult period of post-war reconstruction. Professor Marshall Kay has been elected Educational Coordinator and Professor Kerr Research Coordinator. These three will constitute an Executive Committee for the Department.

CORRECTION

Wiring Diagram of An Amplifier for Differential Thermal Analysis

Carl W. Beck, *University of New Mexico, Albuquerque, New Mexico.*

Attention has been called to two drafting errors in Figure 2, p. 509, *Am. Mineral.*, Vol. **35.** (1) The wire coming from S_4 should not connect to the 250V line—if the S_4 were turned down to the ground end it would short out the power supply. (2) The grid on tube V_5 is grounded—this is corrected by adding a 510K grid leak. Both of these errors have been corrected on the wiring diagram below.

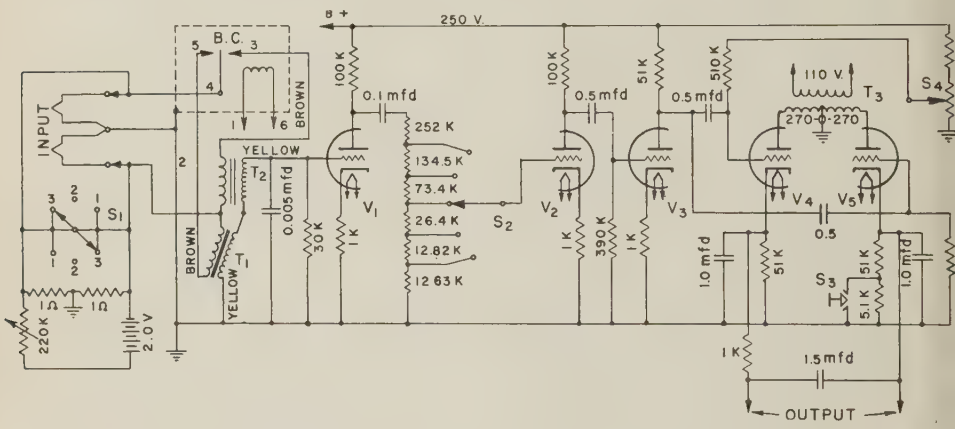

B. C. = Brown Converter
S_1 = Calibration Switch
S_2 = Sensitivity Switch
S_3 = Temperature Indicator Switch
S_2 = Centering Switch
V_1, V_2 = 6SL7
V_3 = ½ 6SN7
V_4, V_5 = 6SN7
T_1, T_2 = Thordarson T-72A59 Transceiver Transformer
T_3 = Acme B-4 Transformer, 110 V to 270–0–270

Fig. 2. Schematic diagram of amplifier.

Attention is called to an omission in the *Am. Mineral.*, **35,** 579–589, (1950), "*X*-Ray Diffraction Patterns of Asbestos." To the bottom of page 587 should be added: "Analysis of the *d* values and intensities of this latter group of minerals indicates that these patterns are actually characteristic of the amphiboles rather than chrysotile." This includes the samples from Corsica, Easton, Pa., Labrador, and Chester, Pa.

I am indebted to Mr. Donald Bailey of the Saranac Laboratory of the Trudeau Foundation for bringing this to my attention.

Suzanne van Dÿke Beatty

NEW MINERAL NAMES

Bowleyite

H. P. Rowledge and J. D. Hayton. Two new beryllium minerals from Londonderry: *J. Royal Soc. Western Australia*, **33**, 45–52 (1946–47) (Published 1948).

Chemical Properties: Two analyses were made, the first on material containing quartz, the second on a purified sample. These gave:

	1	2	3
SiO_2	32.22	33.37	31.95
Al_2O_3	35.58	36.24	41.75
BeO	8.05	7.30	2.27
FeO	none	0.17	—
MnO	none	trace	—
MgO	none	0.04	0.13
CaO	15.35	14.42	14.30
Na_2O	0.55	0.29	0.40
K_2O	0.09	0.04	0.16
Li_2O	2.61	2.39	2.73
Ignition loss	5.80	5.72	6.50
	100.25	99.98	100.19

P_2O_5, Cl, F, CO_2, and TiO_2 were tested for and found to be absent. Analysis 1 gives values calculated after deduction of 34.27% quartz, 0.13% cassiterite, and 0.20% moisture. The quartz was determined by decomposing the mineral with fuming sulfuric acid and treating the residue with warm Lunge's solution to remove the separated silica. Analysis 2 is on the moisture-free mineral.

The formula of the mineral is calculated to be $3(Be,Ca)O.2Al_2O_3 \cdot 3SiO_2 \cdot 2H_2O + n(Li, Na)_2O$.

The mineral, when finely ground, is decomposed by fuming sulfuric acid with the separation of gelatinous silica. The mineral is infusible in the Bunsen flame.

Physical and Optical Properties: Colorless to brownish-white, in flat compact waxy looking layers and in wedge-shaped micaceous aggregates. Biaxial, negative, with 2E small. The micaceous plates are normal to Bx_a or nearly so. "The maximum and minimum refractive indices of the plates on the flat lie between 1.65 and 1.66 with very weak birefringence. On edge the maximum refractive index was greater than, but near to 1.66, the birefringence being about that of quartz." Sp. gr. 3.02, 3.03.

Occurrence: Found in the Londonderry feldspar quarry, 13 miles from Coolgardie, Western Australia, in a columbite-cassiterite band of mineralization. It was closely associated with cassiterite, also at the contact of milky beryl and quartz, in fractures in the beryl, and associated with albite and duplexite (see below). Petalite and microcline also occur in the quarry.

Name: For H. Bowley, Director of Chemical Laboratories and Government Mineralogist of Western Australia.

Discussion: Further study of bowleyite in several laboratories has shown that it is identical with bityite. Analysis 3 above is that of bityite from Madagascar by Pisani (*Bull. soc. franc. mineral.*, **31**, 241 (1908). Spectrographic analysis by K. J. Murata, U. S. Geol. Survey, has shown that Pisani's BeO determination was erroneous and much too low. Details, including *x*-ray determinations by George Switzer, U. S. National Museum, and by K. Norrish, Waite Institute, South Australia, will be published elsewhere.

Duplexite

H. P. Rowledge and J. D. Hayton., *loc. cit.*

Chemical Properties: Two analyses by J. D. Hayton are given.

	1	2
SiO_2	58.92	59.13
Al_2O_3	6.88	7.00
Fe_2O_3	0.07	none
BeO	7.72	7.14
CaO	23.26	23.90
MnO	0.01	0.01
MgO	0.13	0.05
Na_2O	0.44	0.10
K_2O	0.04	none
Li_2O	trace	none
H_2O^+	2.41	2.46[a]
H_2O^-	0.06	0.06
	99.94	100.01[b]

(a) Ignition loss minus 0.11 C, 0.02 Cl, 0.03 CO_2, and 0.06% H_2O.
(b) Also contains Cl 0.02, CO_2 0.03, C 0.11%.

These analyses lead to the formula $Al_2O_3 \cdot 4BeO \cdot 6CaO \cdot 14SiO_2 \cdot 2H_2O$. The mineral is readily fusible in the bunsen flame. The powder is insoluble in strong HCl or fuming H_2SO_4.

Physical and Optical Properties: "Duplexite occurs as fan shaped crystalline aggregates up to $\frac{1}{2}$ inch in radius, sometimes forming almost complete rosettes. It is pearly white and lustrous, extremely brittle, with pronounced cleavage in two directions. When crushed, it breaks into long and short rectangular fragments. Some of these fragments show very weak birefringence, sometimes appearing isotropic, while the majority show moderate to weak birefringence and have a small extinction angle (2–5°)." Optically biaxial, positive, *n*s (Na) alpha = 1.582, beta = 1.584, gamma = 1.593, 2V approx. 22°, elongation negative. Sp. gr. = 2.71.

Occurrence: With bowleyite and associated with quartz, albite, and beryl. Cassiterite, altered milky beryl, and pucherite are present on some specimens. "The manner of occurrence suggests that the mineral was one of the last to crystallize from the mineralizing solution penetrating the pegmatite and that it has crystallized at the same time as or later than the idiomorphic quartz crystals, but before bowleyite.

Name: For Mr. S. Duplex, manager of the quarry, who first drew attention to this mineral.

Discussion: Rowledge and Hayton point out the near identity in optical characteristics with bavenite, whose composition is similar, but which contains less than 3% BeO (usually). *X*-ray study shows that duplexite and bavenite give nearly identical powder patterns (George Switzer, personal communication; report of K. Norrish sent by H. P. Rowledge, February 10, 1950.)

Further discussion will be published elsewhere.

Michael Fleischer

Lomonosovite

V. I. Gerasimovsky. Lomonosovite, a new mineral: *Doklady Akad. Nauk S.S.S.R.*, **70**, 83–86 (1950).

CHEMICAL PROPERTIES: A sodium titanium silicate-phosphate $Na_2Ti_2Si_2O_9 \cdot Na_3PO_4$, which form a complete series of solid solutions with murmanite, $Na_2Ti_2Si_2O_9 \cdot H_2O$. (Note—The three available analyses of murmanite show wide variations.) The following analyses are given:

	1	*2*	*3*	*4*	*5*	*6*	*7*
P_2O_5	12.84	11.95	8.20	5.94	4.36	0.60	—
Cb_2O_5, Ta_2O_5	3.00	1.72	5.66	6.82	3.96	5.74	7.71, 0.50
TiO_2	24.43	25.53	26.79	25.32	29.77	29.44	29.51
SiO_2	24.07	24.20	26.17	30.85	29.88	32.11	30.93
ZrO_2	2.10	2.50	0.91	1.31	1.98	2.31	1.40
Al_2O_3	—	0.38	—	—	—	0.10	—
Fe_2O_3	2.39	2.40	2.27	2.78	2.88	2.85	3.34
Mn_2O_3	—	—	0.31	0.35	—	0.91	—
MnO	3.17	3.80	1.20	1.00	1.70	1.45	2.42
MgO	0.58	0.65	0.60	0.60	0.60	0.35	0.27
CaO	0.80	1.08	1.60	1.94	1.69	2.80	2.74
K_2O	—	—	—	tr.	tr.	0.83	0.56
Na_2O	26.09	23.78	20.31	15.72	15.25	10.28	7.44
H_2O^-	0.26	—	2.24	2.52	2.53	4.17	6.46
H_2O^+	—	2.20	3.96	5.28	5.68	6.03	6.06
F	—	—	—	—	—	—	0.19
Cl	tr.	0.10	—	—	—	—	—
S	—	0.16	—	—	—	—	—
Sum	99.73	100.45	100.22	100.43	100.28	"99.96"	"99.53"
Sp. gr.	3.13	—	2.957	2.946	2.906	2.883	2.766

1. Cinnamon-colored lomonosovite, T. A. Burova, analyst. 2–6. Intermediate compounds. 2. brown, N. E. Kazakova, analyst. 3–4. rose-violet. 5. light yellow. 3–6. I. D. Borneman-Starynkevich, analyst. 7. Murmanite, rose-violet, T. A. Burova, analyst.

Leaching lomonosovite with hot or cold water dissolves Na_3PO_4 from it. Thermal analysis shows a sharp endothermic break at 900° C.

PHYSICAL AND OPTICAL PROPERTIES: Lomonosovite occurs in laminated tabular crystals up to 7×5×0.6 cm. The color varies from dark cinnamon-brown to black, also rose-violet. Streak light rose-cinnamon. Luster on cleavage vitreous to adamantine, on fracture vitreous to greasy. Perfect cleavage in one direction, fracture uneven. The mineral is brittle, hardness 3–4.

Optically negative with alpha = 1.670, beta = 1.750, gamma = 1.778, 2 V 56°. Extinction oblique to cleavage. Universal stage determinations show variable extinction angles of optical directions to cleavage: X ∧ cleavage 61–66°, Y to cleavage 59–65°, Z to cleavage 37–41°. Pleochroism light cinnamon with rose tinge to cinnamon yellow. Fine polysynthetic twinning was observed. The mineral is monoclinic or triclinic.

OCCURRENCE: Not stated. Presumably from Kola Peninsula, U.S.S.R. Lomonosovite occurs in pegmatites in syenite, and is associated with hackmanite, ussingite, lamprophyllite, eudialyte, arfvedsonite, microcline, ramsayite, and aegirite; sometimes chinglusuite, nordite, neptunite, sphalerite, molybdenite, and others.

NAME: For M. V. Lomonosov, 1711–1765, Russian naturalist.

EARL INGERSON

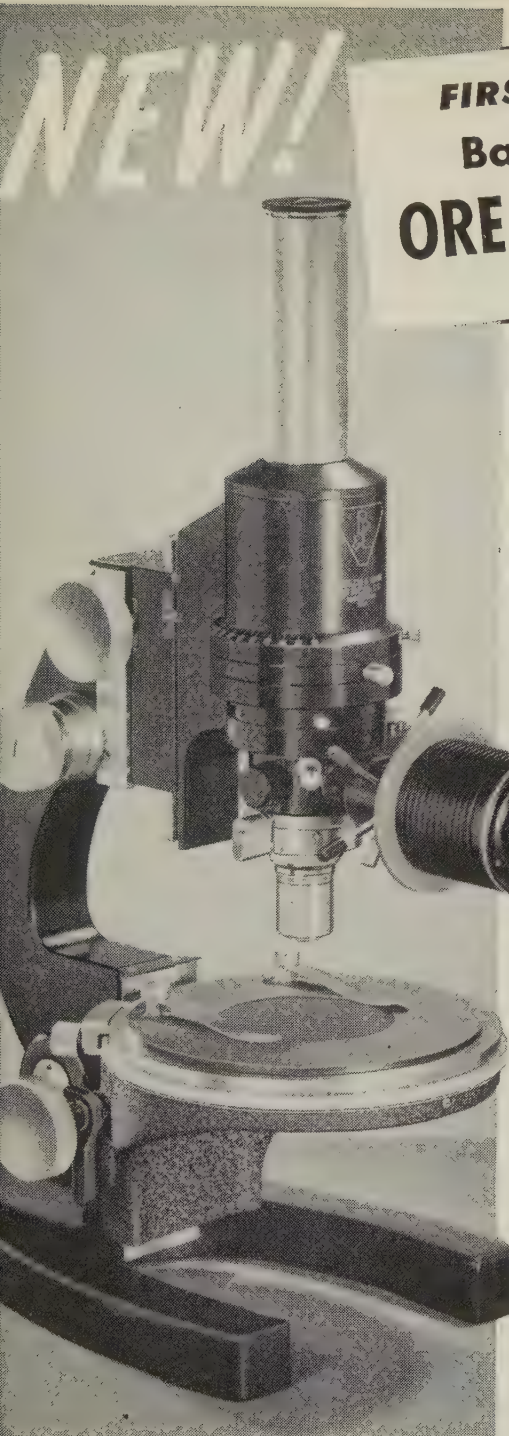

NEW!

FIRST IN AMERICA!

Bausch & Lomb ORE MICROSCOPE (POLAROID)

America's first microscope designed especially for *examining opaque minerals in polarized light* . . . sturdily constructed for a lifetime of hard, practical use.

- **Built-in vertical illuminator with integral light source.** Provision for polarized and non-polarized work.
- **Polarizer on exit face of prism** — provides *complete* extinction over the entire field.
- **Protected analyzer.** Rotatable analyzer is *inside* tube for protection from dust and dirt.
- **Extra-large capacity.** New extra-long slide, focusable by rack and pinion . . . accommodates large specimens up to 4" thick.
- **Special strain-free objectives corrected for use with uncovered specimens.**
- **Focusing stage with friction stage clamp.** Prevents stage drifting under heavy specimens.
- **Standard accurate B&L focusing.** Includes B&L *patented* ball bearing slide fine adjustment.

See FOR YOURSELF WITH A DEMONSTRATION

Prove to yourself the incomparable advantages of the B&L Ore Microscopes over any other methods used to examine opaque ores in polarized light.

WRITE for complete information and a demonstration to Bausch & Lomb Optical Company, 676-W St. Paul St., Rochester 2, N. Y.

The World's Finest Instruments are made in America

Bausch & Lomb *Ore* Microscope

A New Series of

SPENCER POLARIZING MICROSCOPES

with Polaroid Polarizers and Analyzers

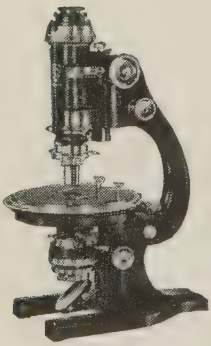

RESEARCH POLARIZING MICROSCOPE No. P37A

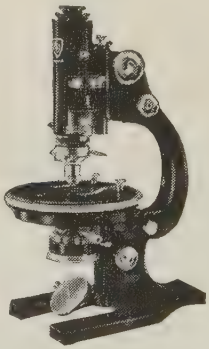

LARGE POLARIZING MICROSCOPE No. P39A

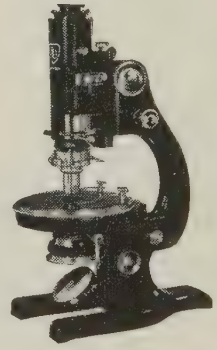

POLARIZING MICROSCOPE No. P41AC

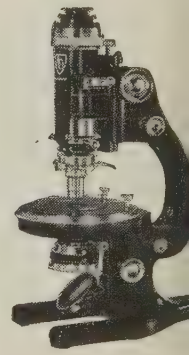

POLARIZING MIC SCOPE No. P40

During the past five years two Spencer Polarizing Microscopes have been regularly equipped with Polaroid polarizers and analyzers. These have proven so successful that we are now offering a complete line of instruments with polaroid elements. This means substantial savings to you, whether you buy the simplest or most elaborate. Experience has shown that performance is outstanding in every respect—durability, resistance to heat, sensitivity of extinction point image contrast, and freedom from residual color. Spencer Polarizing Microscopes with Ahrens prisms are still available. Choose your polarizing microscope from this extensive line of American-made instruments for assurance of finest performance and readily available service. Ask your AO Spencer Distributor to show you the new microscopes with Polaroid elements, or write Dept. L

American Optical COMPANY

INSTRUMENT DIVISION • BUFFALO 15, NEW YORK

Makers of Precision Optical Instruments for over 100 Years

TRANSPARENT SPECIMEN BOXES

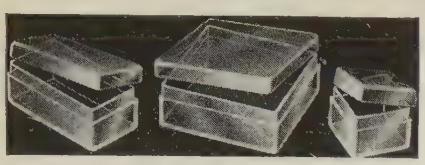

Five Sizes: (Outside Dimensions)
A: 15/16" x 15/16" x 3/4"
B: 1-7/8" x 15/16" x 3/4"
C: 1-7/8" x 1-7/8" x 3/4"
D: 3-1/4" x 2-3/4" x 1-1/4"
E: 6" x 7/8" x 3/4"

Prices: **A: 20** for $1; **100** for $4.60
B: 15 for $1; **100** for $5.60
C: 12 for $1; **100** for $6.60
D: 5 for $1; **100** for $17.50
E: 6 for $1; **100** for $16.00

Assortments:
No. 1: 8 **A**, 4 **B**, 4 **C** $1.00
No. 2: 60 **A**, 20 **B**, 16 **C** $5.00
No. 3: 10 each **A, B, C, D, E**, $5.50
No. 3A: 20 each **A, B, C, D, E** $10.00

Specimen Boxes **A, B,** and **C** are furnished in flat, white cardboard trays that hold 100 A's or 50 B's or 25C's. Convenient for keeping the boxes in order.

FOR
STORING, HANDLING and EXHIBITING SPECIMENS and SMALL OBJECTS
In Convenient, Orderly Arrangement

ADVANTAGES

- Keep specimens dust-free
- Contents are completely visible
- Protect fragile specimens from damage by rough handling

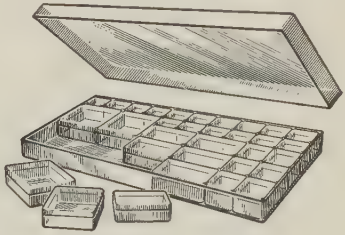

Transparent Boxes in Transparent Cases
For arranging specimens in sets, and for passing the sets around classes or other groups.

Full details on leaflet PB-AM
Write for it

SHILLABER'S

CERTIFIED INDEX OF REFRACTION LIQUIDS

Immersion media for use on the microscope that offer the following **outstanding advantages:**

Range: 1.400 to 1.700—**Intervals:** 0.002 index—**Adjustment:** 0.0002 index (D line, 25° C)
Very inert and non-volatile. Index remains unchanged.
Additional liquids now available in the range 1.71—1.83 Index; Intervals 0.01 Index.
Liquids of higher indices are in preparation.
Just write for latest "Index Data"

(In Preparation)

DENSITY LIQUIDS FOR THE SINK-AND-FLOAT TEST

For determining the specific gravity of minerals, gems and other substances

Write for Leaflet 50-D

R. P. CARGILLE

118 LIBERTY STREET, NEW YORK 6, N.Y.

A New Instrument

Amateur and professional mineralogists will find much of interest in the new Menlo Fluoretor, offering for the first time a lightweight portable ultraviolet source that can be used anywhere, regardless of outside light conditions.

Similar to a large flashlight in design, shape and method of operation, Fluoretor has a patented dark chamber end housing with detachable end caps in which mineral, chemical and a wide range of other substances can be mounted for ultraviolet analysis. 2-pound total weight makes the instrument ideal for on-the-spot examinations of samples in the field, as well as for a variety of indoor uses ranging from laboratory examinations to hobbyists' collection displays.

For maximum utilization, Fluoretor offers both a portable (operating from two standard flashlight batteries) and a 60-cycle a-c power model. Either can be obtained with interchangeable short wave (2537Å) or long wave (3650-63Å) frequency head.

Comprehensive literature is available by writing Menlo Research Laboratory, P.O. Box K522, Menlo Park, Calif. Dealer inquiries are invited.

Central European Minerals

The following Selected Mineral Specimens are additions to our advertisement appearing in the last issue of the American Mineralogist.

NAGYAGITE—Nagyag, Hungary. Hundreds of crystals completely covering one surface of specimen 2¼" x 3". Very rare $15.00.

STIBNITE—Felsobanya, Hungary. A radiating aggregate of thin acicular crystals with a few barite crystals. Size 2⅝"x 3". Price $6.50.

SPHALERITE—Kapnik, Hungary. Choice brilliant crystals on matrix 2" x 2¼" x 3¼". Largest crystal is ⅞". Price $6.00.

MAGNETITE—Moravicza, Hungary. Fine group of sharp dodecahedron crystals up to ⅜" on matrix 1¼" x 2⅛". Price $5.00.

CASSITERITE—Schlaggenwald, Bohemia. Excellent group of sharp and brilliant crystals nearly covering flat surface of specimen 2½" x 4". Price $15.00.

PYRITE—Pribram, Bohemia. Many small crystals of a rare form on matrix 1¾" x 3". Price $2.50.

CHALCOPYRITE—Siegen, Westphalia. Group of many fine sphenoidal crystals on massive chalcopyrite 1¼" x 1¾" x 2½". Price $5.50.

LÖLLINGITE—Reichenstein, Silesia. Serpentine penetrated by lollingite. Size 2½" x 3". Price $2.50.

TETRAHEDRITE—Kapnik, Hungary. Many sharp and brilliant tetrahedrite crystals with sphalerite crystals on crystallized quartz 3" x 3½". Price $5.00.

BOULANGERITE—Pribam, Bohemia. Massive gray nearly pure 2⅛" x 2¾". Price $2.00.

SCHWATZITE—Brixlegg, Austrian Tyrol. Group of sharp crystals up to ½" with barite on matrix 1⅝" x 2¾". Very rare. Price $10.00.

MIMETITE—Johann-Georgenstadt, Saxony. Group of small brownish crystals on rock 1⅜" x 2½". Price $3.00.

PYROMORPHITE—Ems, Hessen-Nassau. A stalactite of pyromorphite crystals up to 5/16" x ⅜". Sharp brownish crystals. Length of specimen 3⅜", diameter ⅞". Price $10.00.

CERUSSITE—Ems, Hessen-Nassau. Solid mass of long interlaced crystals. Size 2½" x 3¾". Price $4.00.

WULFENITE—Bleiberg, Carinthia. Group of honey-yellow crystals completely covering surface of specimen 3½" x 4⅞". Price $10.00.

WOLFRAMITE—Zinnwald, Bohemia. A very good terminated crystal 1⅝" x 2" x 1". Price $6.00

SCHEELITE—Zinnwald, Bohemia. Group of brownish crystals on smoky quartz. Specimen size 1½" x 2¼" x 1⅜". Choice specimen. Price $7.50.

BARITE—Felsobanya, Rumania. Choice group of grayish small crystals about ½" in size completely covering face of specimen 3" x 6¼". Price $6.50.

EPIDOTE—Knappenwald, Untersulzbachthal, Salzsburg. A flat group of transparent crystals 2¼" x 2" x ⅜", some crystals on one side are terminated. Price $7.50.

EMERALD—Habachthal, Salzburg. Crystal 9/16" x 5/16" of good color in shist 1" x 1⅞". Price $5.00.

AXINITE—Bourg d'Oisans, France. Many fine brown brilliant terminated crystals up to ½" on rock 1¾" x 2⅞". Price $10.00.

KYANITE—Tessin, Switzerland. Kyanite crystals of blue color up to 3/16" x 1¼" with some staurolite in rock 2⅝" x 3⅝". Price $5.00.

GARNET var. Grossularite—Dognaczka, Hungary. Group of intergrown crystals of greenish color. Largest crystal ⅝" x ⅞". Specimen size 1¼" x 1¾". Price $2.25.

NEPHELITE—Fichtelgebirge, Bohemia. Many six sided prisms on rock, longest crystal ⅜". Not showy but still a very fine specimen. Size 2¼" x 3". Price $5.00.

HYALITE—Waltsch, Bohemia. Colorless transparent globular masses on matrix. Size 2¼" x 2½". Price $4.50.

SCHORTMANN'S MINERALS

6 and 10 McKinley Avenue **Easthampton, Massachusetts**

CURRENT AND CHOICE SELECTIONS

BREWSTERITE. *Strontian, Scotland.* Small prismatic crystals in rock: 2 x 2", $2.00; 2 x 3 to 3 x 3", $3.50

CYRTOLITE. *Hybla, Ontario, Canada.* Partly xled and massive with feldspar: 2 x 3" to 2½ x 3", $4.00, $5.00; 3½ x 4", $10.00

GAHNITE. *Bosost, Spain.* Greenish blue octahedral crystals and masses in quartz: 1 x 2" to 2 x 2", $3.00, $3.50, $4.00; 2 x 3", $7.50

GERSDORFFITE. *Mitterberg, Salzburg.* Massive with chalcopyrite etc.: 2 x 3", $3.00

GEOCRONITE. *Bayerland Mine, Palatinate, Germany.* Massive with quartz: 3½ x 4½", $25.00

IDOCRASE. *Crestmore, California.* Partly xled and massive with crestmoreite: 2 x 2", $.50; 2 x 3", $.80; 3 x 4", $2.25

JORDANITE. *Wiesloch, Baden.* Massive with sphalerite, polished specimens showing fine colloform structure: 1¼ x 2½", $4.00; 1¾ x 2", $5.00

LOELLINGITE. *Near Hüttenberg, Carinthia.* Xline with bismuth in siderite; polished: 2¼ x 3¼", $3.50

MICROLITE. *Harding Mine, Taos, New Mexico.* Yellow-brown xline in lepidolite with spodumene: 2 x 2" to 2 x 3", $1.00, $1.50, $2.00

PEARCEITE. *Golden Manitou, Ontario.* Massive with tetrahedrite and pyrite: 2 x 2", $10.00

PHLOGOPITE. *Ontario.* A large xl: 1⅞ x 4 x 3½", $7.50

PHLOGOPITE. *Quebec.* Xls in blue apatite: 3¼ x 5½", $4.50. Thick crystal plates with hexagonal outline, 2½ to 3" diameter: $.75 each

PSEUDOBROOKITE. *Jumilla, Spain.* Partly xled, black in rock: 1 x 2" to 2 x 2", $1.50, $2.00, $2.50, $3.00; 2 x 3", $3.50, $4.00, $5.00

SAFFLORITE. *Cobalt, Ontario.* Massive with native silver, stephanite, etc.: 2¾ x 4", $6.00

SCAPOLITE. Marmora, Ontario. Attractive blue polished specimens: 2 x 3½", $1.50; 3½ x 4", $2.50

SCAPOLITE (Wilsonite). *Templeton, Quebec.* Blue-lavender, polished: 3 x 3½", $2.50

STANNITE. *Albert Canyon, British Columbia.* Massive with pyrite in rock: 2 x 2", $1.50; 2½ x 3½", $2.00; 2½ x 5", $3.50; 3 x 4½", $4.50

ULLMANITE. *Lölling, Carinthia.* Xline with bismuth in siderite: 2¼ x 3¼", $2.00; 2 x 3½", $3.00

XANTHOPHYLLITE. *Crestmore, California.* Xl plates in rock: 2 x 3", $.75, $1.00; 2½ x 3½" to 3 x 4", $1.50, $2.00

ZIRCON. *Brudnell Twp., Ontario.* Large xls in feldspar: 3 x 4", $5.00

NEW CATALOGS AND PRICE LISTS

FM 3 *Fine Mineral Specimen Catalog*
U 7 *Uranium and Thorium Minerals*
S8 *Minerals for Cutting and Polishing*
MH 5 *Collections of Minerals and Rocks*
Meteorite Lists

GEORGE BANTA PUBLISHING COMPANY, MENASHA, WISCONSIN